International PhD Program in Neuropharmacology
XXVI Cycle

Implications of dopamine D3 receptor for glaucoma: in-silico and in-vivo studies

PhD thesis

Chiara Bianca Maria Platania

Coordinator: Prof. Salvatore Salomone

Tutor: Prof. Claudio Bucolo

Department of Clinical and Molecular Biomedicine

Section of Pharmacology and Biochemistry.

University of Catania - Medical School

December 2013

TABLE OF CONTENTS

ACKNOWLEDGEMENTS

LIST OF ABBREVIATIONS

IOP	Intraocular Pressure
TM	Trabecular Meshwork
GPCRs	G protein Coupled Receptors
hD_x	human Dopamine D_x receptor
D_{2L}	Dopamine D_2 receptor long isoform
D_{2S}	Dopamine D_2 receptor short isoform
wt	wild-type
$5HT_{xy}$	Serotonin $5HT_{xy}$ receptor
$D_3^{-/-}$	D_3 receptor gene knockout
AH	Aqueous Humor
POAG	Primary Open Angle Glaucoma
RGCs	Retinal Gaglion Cells
PACG	Primary Angle Closure Glaucoma
AQPs	Aquaporins
CA	Carbonic Anhydrase
ATP	Adenosin Triphosphate
ADP	Adenosin Diphosphate
ECM	Extracellular Matrix
NICE	National Institute for Health and Clinical Excellence
cAMP	cyclic Adenosin MonoPhospate
CAI	Carbonic Anhydrase Inhibitor
BBB	Blood Brain Barrier
PG	Prostaglandin
EP	Prostaglandin E receptor
M_x	Muscarinic M_x receptor
siRNA	Small Interference RNA
11-β HSD1	11-β hydroxysteroid dehydrogenase-1
NPE	Non-Pigmented Epithelial cells
A_x	Adenosin A_x receptor
MMP	Matrix Metallic Proteinase
AEA	Anandamide
FAAH	Fatty Acid Amide Hydrolase

CB_x	Cannabinoid CB_x receptor
PEA	Palmitoyl ethanolamide
PPARP-α	Peroxisome Proliferator Activated Receptor-alpha
Gs	G stimulatory protein
Gi	G inhibitory protein
DEX	Dexamethasone
PBS	Phosphate Buffered Saline
IUPHAR	International Union of Basic and Clinical Pharmacology
FDA	Food and Drug Administration
NCE	New Chemical Entities
FP	Prostaglandin F receptor
MW	Molecular Weight
3D	Three Dimentional
H_x	Histamine H_x receptor
x-OR	x-Opiod Receptor
NTSR	Neurotensin Receptor
PAR	Protease Activated Receptor
ECL	Extracellular Loop
ICL	Intracellular Loop
$S1P_1$	Sphingosine 1-phospate receptor
R&D	Research and Development
FG-MD	Fragmente Guided Molecular Dynamics
MD	Molecular Dynamics
IR	Infrared
NMR	Nuclear Magnetic Resonance
CHARMM	Chemistry at Harvard Macromolecular Mechanics
VdW	Van der Waals
oop	out of plane movement
GB	Generalized Born
CPU	Computing Processing Unit
CUDA	Computed Unified Device Architecture
GPU	Graphic Processing Unit
MM/GBSA	Molecular Mechanics/Generalized Born Solvent Accessible surface area
MM/PBSA	Molecular Mechanics/Poisson Boltzmann Solvent Accessible surface area

ABSTRACT

Glaucoma is a progressive optic neuropathy and it is considered by the World Health Organization to be the cause of 12% of visual impairment and 2% of blindness. Glaucoma is characterized by alterations of optic disc and visual field. High intraocular pressure (IOP) is the main risk factor of glaucoma. The pathogenesis of glaucoma is still evanescent, and unfortunately the disease becomes symptomatic when irreversible and severe damage has occurred at the optic nerve head. IOP reduction represents the first step in the management of glaucoma which is eventually followed by laser surgery of the trabecular meshwork (TM) and glaucoma-filtering surgery.

Currently, there are five main classes of approved ocular hypotensive drugs: beta-blockers, carbonic anhydrase inhibitors, prostaglandin analogs, sympathomimetics and miotics. However, there is still the need to have more potent medications available for this disease, and pharmacological management of IOP is one of the most interesting and challenging endeavors facing the ocular pharmacology scientists.

In the panorama of pharmacological targets for regulation of IOP, there are some interesting G protein coupled receptors (GPCRs) such as dopaminergic receptors. The work of the present thesis has been focused on GPCRs and in particular on dopamine D_3 receptor as pharmacological target for ocular hypotensive drugs. Cabergoline, bromocriptine, cianergoline and legotrile, classical D_2 receptor agonists, have been shown to decrease intraocular pressure. D_3 receptor belongs to the D_2 class of dopaminergic receptors, along with D_2 and D_4 receptor. It shares high sequence homology and identity with D_2 receptor and several efforts have been carried out in order to design selective ligands for either D_3 or D_2 subtype. Drug design and discovery, based on structure based approach, need the knowledge of the tertiary structure of the target protein. In 2010 the x-ray structure of human D_3 receptor (mutated hD_3-lysozime chimera) was solved, then this structure was used to carry out the homology modeling of wild-type (wt) hD_3 and hD_{2L} receptors. The homology models of these receptors were not able to discriminate selective ligands by a molecular docking study, thus these structures have been subjected to optimization by means of molecular dynamics in a water-membrane environment. After optimization the structures differentiated in the binding pockets and have been validated, strengthen the validity and reliability of the *in silico* approach. A similar computational approach was carried out in order to study the structure differences between the D_3

receptors and $5HT_{1A}$, $5HT_{2A-C}$ receptors, known to be involved in regulation of intraocular pressure.

The role of D_3 receptor activation by cabergoline in lowering IOP was confirmed in C57BL/6J wt and $D_3^{-/-}$ mice, using a pharmacological approach along with D_3 gene deletion. Animals were pre-treated with U99194A, D_3 selective antagonist, that antagonized the effects of cabergoline. Ocular hypertension was induced in mice, implanting subcutaneously an osmotic micropump delivering dexamethasone. Cabergoline was not effective in ocular hypertensive $D_3^{-/-}$ mice, whereas exerted a greater and longer hypotensive effect in ocular hypertensive wt mice, in comparison to normotensive animals. The *in silico* approach, validated for D_3 and D_{2L} receptors, has been used to model and optimize the structures of $5HT_{1A}$, $5HT_{2A-B-C}$ receptors which are other putative ocular targets of cabergoline. *In silico* results showed that cabergoline binds in a similar way into pockets of D_3 and $5HT_{2A-C}$ and it has higher affinity for D_3 receptor in comparison to serotonergic receptors, according to experimental affinity data. Moreover docking revealed that binding of cabergoline into D_3 and $5HT_{1A}$ receptors is associated with a better desolvation energy in comparison to $5HT_{2A-C}$ binding.

The structure-based computational approach hereby adopted was able to build, refine, and validate structure models of homologous dopaminergic and serotonergic receptors that may be of interest for structure-based drug discovery of ligands, with dopaminergic selectivity or with multi-pharmacological profile, potentially useful to treat optic neuropathies such as glaucoma.

Finally, the present work represents an excellent example of successful integration of two different approaches to biomedical research, *in silico* and *in vivo*, which are not in contrast but complementary.

GENERAL INTRODUCTION

GLAUCOMA

Glaucoma refers to a series of progressive optic neuropathies that involve optic disc degeneration and visual field aberration, with or without ocular hypertensions. Ocular hypertension in glaucomatous patients is related to an imbalance between aqueous humor (AH) production and drainage [1]. The most common form of glaucoma is the primary open angle glaucoma (POAG), that is an optic neuropathy characterized by optic disc damage and partial loss of visual acuity, associated to retinal ganglion cells (RGCs) death and atrophy of optic nerve [2]. The progression of POAG leads to irreversible blindness. Gene association studies have been carried out and more than 20 genetic loci have been reported for POAG; up to now only three have been found to have a causal relationship with the disease (myocillin, optineurin and WDR36) [3]. POAG is associated to increased IOP. However there are about 20-52% of glaucomatous patients with normal IOP and those patients develop damage at the optic nerve head similar to POAG patients. Ocular hypertension (> 21 mmHg), can arise asymptomatically and patients develop symptomatic visual field loss when damage at optic nerve head is irreversible. Progression of optic disc damage leads to irreversible blindness. Up to know the only therapeutic approach in glaucoma therapy is aimed at decreasing the IOP, also in normotensive glaucomatous patients [4].

Glaucoma could be classified in primary and secondary glaucoma. The former is related to glaucoma forms not correlated to previous and concomitant ocular disease. Primary glaucoma has most probably genetic etiology and it is often bilateral. On the contrary secondary glaucoma is associated to previous ocular or systemic diseases, trauma or iatrogenic causes.

Glaucoma can be classified into major categories according to the appearance and obstruction of the drainage pathway at the iridocorneal angle. In POAG, despite normal clinical appearance the outflow of AH is restricted, possibly due to pathologic changes at the TM (Fig. 1A). In the primary angle-closure glaucoma (PACG) the block of drainage of AH is related to the contact of the iris at the TM, causing its permanent obstruction (Fig. 1B). PACG is often characterized by a rapid increasing of IOP, along with eye pain.

Two potential pathogenetic mechanisms of glaucoma have been postulated. Mechanic hypothesis: high levels of IOP could lead to mechanic compression of fibers at the optic

nerve head and lamina cribosa where they pass. The axons of RGCs are grouped at the optic nerve head, and death of RGCs leads to visual field loss.

Vascular hypothesis: a presumed perfusion deficit at optic disc could lead to papillar atrophy leading to optic nerve head damage. The assumption of vascular deficit has not been demonstrated by validated scientific results; however it is an hypothesis able to explain normotensive glaucoma, although a perfusion deficit could be explained by an imbalance between AH production/outflow.

Aqueous Humor Dynamics

In healthy eye the flow of AH against resistance generates an average intraocular pressure of approximately 15 mmHg. IOP is necessary to inflate the eye and maintain the proper shape and then optical properties of the globe [5]. High intraocular pressure values are the main risk factor of glaucoma. Epidemiological studies have shown that per each 1 mmHg increase of IOP, the risk of incidence of glaucoma increases of 12% [6]. Up to now long term lowering of IOP is the only strategy to counteract RGCs death, than optic nerve head damage and visual field loss.

Increasing of IOP is due to imbalance between AH production and AH drainage. The ocular sites involved in the production of AH are the processes of ciliary bodies, that have a glomerular structure, due to basal and inner interdigitations. The epithelium of the ciliary processes has two layers: an inner non-pigmented layer in contact with AH in the posterior chamber, and the external pigmented epithelium in contact with the ciliary process stroma; those two epithelial layers have the apical surfaces opposite to each other. Non-pigmented epithelium is the continuation of retina, whereas the pigmented epithelium is a continuation of retinal pigmented epithelium. Both sympathetic and parasympathetic nerves supply the ciliary body. Production of AH is regulated by vascular contraction-dilatation and by neurovegetative inputs from the sympathetic and parasympathetic systems. Three mechanisms are involved in AH production: diffusion, ultrafiltration and active secretion. Diffusion occurs when solutes, especially lipid soluble molecules, are transported through the lipid portion of tissues between capillaries and posterior chamber. Ultrafiltration is related to the flow of water and water soluble molecules through fenestrated ciliary capillary endothelia into the ciliary stroma. Diffusion and ultrafiltration are responsible of accumulation of plasma ultrafiltrate in the stroma behind tight junction of non-pigmented ciliary epithelium.

The active secretion of AH from ciliary bodies is related to active transport of Na^+, Cl^- and HCO_3^-, than water passively passes the blood-water barrier of ciliary bodies. Proteins responsible of rapid bulk water flux are Aquaporins (AQPs) and in particular AQP1 and AQP4 [7]. The carbonic anhydrase (CA) is the enzyme responsible for secretion of hydrogen carbonate, and Na^+/K^+ pump leads to secretion of Na^+. Na^+-K^+ ATPase is devoted to hydrolysis of ATP (adenosine triphospate) to ADP (adenosine disphosphate) providing energy for active transport of solutes. Na^+-K^+ ATPase can be inhibited by different molecules [8, 9], and this enzyme has been of particular interest for pharmacological studies on aqueous humor production. Furthermore the chloride ion is secreted through chloride channels.

AH is secreted in the posterior chamber, then it passes in the anterior chamber where there is the TM (Fig. 2A), the prominent outflow facility for AH. The TM is a structure that overpasses the sclera sulcus and converts it into the Schlemm's canal. The TM is a spongy tissue, that consists of connective tissue surrounded by epithelium. TM can be divided in three components: uveal meshwork, corneoscleral meshwork and juxtacanalicular meshwork, ordered from innermost to outermost part. Three systems innervate TM: the sympathetic from superior sympathetic ganglion, the parasynmpathetic innervations from ciliary ganglion and sensory nerves that originate from trigeminal ganglion. The AH passes all TM parts and is collected in the Schlemm's canal, which is connected to episcleral and conjunctival veins through external collector canals. Fluid movements take place under a pressure gradient from the TM to Schlemm's canal and through its inner wall. This flux appears to be related to a passive pressure-dependent transcellular mechanism, associated with paracellular routes such as giant vacuoles and pores [10]. After exiting from Schlemm's Canal, AH enters in aqueous veins, mixes with blood in episcleral veins where pressure is 8-10 mmHg; considering that normal pressure of AH conventional drainage system is 3-4 mmHg, average normal IOP is 15 mmHg. In humans 75% of the AH outflow resistance is localized at TM and in particular at juxtacanalicular portion [11]. The role of the extracellular matrix (ECM) on AH drainage has been investigated. ECM is constituted by glycosaminoglycans that hydrate TM leading to obstruction; catabolic enzymes depolymerize glycosaminoglycans preventing the excessive TM hydratation. Such effects of lysosomal enzymes is inhibited by corticosteroids, explicating a possible mechanism of steroid-induced glaucoma [12, 13]. AH outflow through the conventional route is influenced by two contractile structures, the iris and ciliary muscle innervated by cholinergic nerves. Contraction of such structures results in spreading of TM and dilation

of Schlemm's canal resulting in increased outflow, on the contrary relaxation of such structures leads to decreased outflow [14].

The TM is assisted in AH outflow by an unconventional route (Fig. 2B), the uveo-scleral pathway through the uveal meshwork and ciliary muscle. That unconventional pathway accounts to a variable percentage of AH excretion, likely age related [15, 16]. Ciliary muscle contraction influences the uveo-scleral outflow, which is increased by prostaglandin F2α by decreasing the flow resistance of the interstitial spaces in the ciliary muscle [17].

Pharmacological treatments of glaucoma

The described AH inflow and outflow facilities are the pharmacological targets of ocular hypotensive drugs. Up to know there are five classes of IOP lowering approved drugs; beta-blockers, carbonic anhydrase inhibitors, prostaglandin analogs, sympathomimetics and miotics [18]. The first two drug classes can be named as "inflow" and the letter three can be named "outflow" drugs. The UK National Institute for Health and Clinical Excellence (NICE) has published a guideline for glaucoma treatment (guideline CG85), in which algorithms for treatment of glaucoma are stated; beta-blockers and prostaglandin analogs are advised for first-line and second line-treatment of glaucoma, whereas the remaining drug classes are mostly used as second-line drugs.

Beta-blockers are used in clinics since 30 years and timolol is the most used drug belonging to this class. Timolol antagonizes β-adrenergic receptors of iris-ciliary body system inhibiting the synthesis of the second messanger cAMP due to adrenergic stimulation. The elevation of cAMP leads to AH production. Timolol is effective at the iris-cilary body, where there is an endogenous adrenergic stimulation; TM lacks of this adrenergic tone even if there are expressed β-adrenergic receptors. Timolol is not a selective beta-blocker, and the role of either β_1 or β_2 receptors is still evanescent; because of a β_2 agonist (solbutamol) increases AH production. Several beta-blockers have been approved for treatment of glaucoma: timolol, betaxolol, levobunol and carteolol. Beta-blockers are associated to adverse effects, involving respiratory (increased severity of bronchial occlusive disease) and cardio-vascular systems (arrhythmia, hypotension); thus the anamnesis of patients is important before treatment with beta-blockers.

Carbonic anhydrase inhibitors (CAI) are effective at epithelial cells of ciliary processes, inhibiting the release of HCO_3^- in the posterior chamber and then production of AH. The first CAI used in clinics to treat glaucoma is acetazolamide as oral medication.

Acetazolamide as ocular hypotensive drug has been, in the fifties, an advance in treatment of glaucoma relied at that time mostly on pilocarpine and cholinesterase inhibitors. However carbonic anhydrases are ubiquitous enzymes and several adverse effects arose in glaucomatous patients treated with acetazolamide, such as metabolic and respiratory acidosis, paraesthesias, hypokalemia, hyperuricemia, liver failure and respiratory failure. Thus several efforts were carried out to design new CAI as eye drops. Effective topical CAI must be highly active at CA enzyme, should be amphifilic in order to pass the cornea and be formulated as eye drops [19]. Drug design of new CAI led to dorzolamide, a thienothiopyran-2-sulfonamide. Dorzolamide has shown a low $K_i=0.3$ nM, inhibiting the 98% of CA. Dorzolamide is effective in decresing IOP of about 26% with a prolonged action (12%). Secondary effects of dorzolamide, compared to acetazolamide, are negligible.

Sympathomimetics ocular hypotensive drugs are α_2-adrenergic and non-selective adrenergic agonists, activating presynaptic adrenergic receptors in the ciliary body and inhibiting the release of noradrenaline that stimulate AH secretion. Sympathomimetics have shown not only to block the inflow of AH, but also to increase the uveo-scleral outflow. Clonidine was the first sympathomimetic drug effective in decreasing the IOP, but due to its high lipophilicity it crosses the blood-brain barrier (BBB) acting at vasomotor center, then inducing systemic hypotension and bradycardia. Apraclonidine is less lipophilic, it does not pass the BBB and does not lead to systemic side effects. It is absorbed through the conjunctival-scleral pathway and it is effective in decreasing IOP. Brimonidine is another α_2-adrenergic agonist approved as ocular hypotensive drug [20]. Dipivefrin is a non-selective adrenergic agonist used in treatment of glaucoma and it is the prodrug of epinephrine.

Prostaglandin (PG) analogs are first-line, along with beta-blockers, drugs for treatment of ocular hypertension. PG analogs increase primary the uveo-scleral outflow, even though effects on TM have been reported. The uveo-scleral outflow is increased due to less resistance by means of remodeling of the ECM within the ciliary muscle and sclera. This effect of PG is mediated by activation of the GPCRs EP_2 and EP_4 activating the synthesis of cAMP by stimulation of phosphoinositide turnover. It was reported in isolated TM a relaxant activity of EP_2 agonists due to coupled activation of Ca^{2+} -activated K^+ channels. The current PG analogs approved in USA and EU are latanoprost, bimatoprost, travoprost and tafuprost, which are $PGF_{2\alpha}$ analogs [18]. Topical treatment with PG analogs is not

associated to systemic side effects. PG analogs side effects are mostly local and not severe: changes in eye color and eyelid skin, stinging, blurred vision, eye redness, itching, burning. Pilocarpine has been used since 100 year for the treatment of glaucoma; it is a miotic or parasympathomimetic drug. It is an alkaloid extracted from plants belonging to *Pilocarpus specie*. Pilocarpine mimics acetylcholine activating muscarinic receptors of ocular parasympathetic nerve. Pilocarpine leads to myosis by activation of muscarinic M_1 and M_3 receptors, it induces increasing of Ca^{2+} levels and contraction of ciliary muscle thus leading to opening of the TM and to increased AH outflow. Due to the miotic effect of pilocarpine, treated patients report blurring of the vision. Moreover continuous treatments can lead to systemic side effects such as nausea, bradycardia and hypotension.

It is worth to be mentioned an experimental pharmacological approach for the treatment of glaucoma, in particular of normotensive glaucoma, focused on neuroprotection. In fact normotensive glaucomatous patients have optic nerve damage and atrophy comparable to ocular hypertensive patients. Thus it has been proposed a neurodegenerative etiology of glaucoma, assuming that RGCs death could be related to glutamate excitotoxicity. Thus NMDA noncompetitive antagonists, memantine [21] and bis-7-tacrine[22], have been studied in order to assess their properties as neuroprotectors at RGCs. Although phase III clinical trial results assessed the inefficacy of memantine in glaucoma treatment, the therapeutic application of neuroprotectors compounds should not be abandoned [23]. Considering neuroprotection as a potential endpoint in glaucoma, several studies about the role of autophagy modulation on RGCs death have been carried out. It is still not clear if promotion of authophagy might prevent RGCs death, however this field is worthy to be explored [24].

Pharmacologic perspectives in treatment of glaucoma

Even thought there are five approved classes of drugs for treatment of glaucoma, the pharmacological management of the disease is still a challenge. New pharmacological perspectives are facing the possibility to becoming ocular hypotensive treatments.

Gene therapy, by means of small interference RNA (siRNA), have been studied to silence β_2-receptors. Treatment with siRNA appears to be promising even if the drug delivery of such small polynucleotides is challenging. SYL040012 is a small siRNA able to interfere with the transduction of β_2-receptor gene, potentially reducing IOP by means of β_2-receptor knockdown [25].

Within the GPCRs pharmacological targets for treatment of glaucoma the melatonin receptor deserves to be mentioned. Melatonin receptors have been found to be expressed in the ciliary body, and several melatonin analogs have been studied and have showed ocular hypotensive effects [26, 27]. Furthermore the pharmacological effects of melatonin has been confirmed by treatment of melatonin receptor 1 knockout mice, insensitive to melatonin effects [28].

Another promising "inflow" drug target is the hydroxysteroid dehydrogenase-1 (11β-HSD1), this enzyme is localized in the ciliary body, in particular in the non-pigmented epithelial cells (NPE). 11β-HSD1 catalyzes the conversion of cortisone to cortisol, thus increasing the sodium transporting capacity of NPE. Carbenoxolone, inhibitor of 11β-HSD1, has shown to be able to lower IOP in rabbits treated topically [29, 30].

Considering "outflow" drugs, all current approved ocular hypotensive drugs, do not modify directly the structure of TM. Resistance to AH outflow has been identified mainly in TM, which has a spongy structure with interwoven beams of ECM, TM cells and cell layer in the inner wall of Schlemm canal. In glaucoma patients TM is stiffer in comparison to healthy people [31] and the use of drugs altering cytoskeleton of TM has been proposed. In this direction latruculins and rho-associated protein kinase inhibitors have been studied and reduced IOP in animals and humans. Moreover rho-kinase inhibitors have showed improved blood-flow, might helping survival of RGCs [32].

Since TM cells have a role in regulating AH outflow by modulation of their own cell volume and contractility and those function are regulated by NO/CO system, there is an emerging role of these biatomic molecules in regulation of IOP [33, 34]. It has been reported that NO releasing molecules are able to regulate IOP [35], on the contrary also inhibitors of nitric oxide synthase have shown an ocular hypotensive effect in ocular hypertensive animals [36]; thus positive or negative control of IOP by NO is not clear [37]. The potential role of NO donor molecules in lowering IOP, has led to preclinical and clinical studies on prostaglandin analogs able to release NO such as BOL-303259-X [38]. Considering the role of CO, induction of heme-oxygenase has shown a IOP lowering effect [39] and a CO releasing molecule has shown an ocular hypotensive activity, thus CO might facilitate AH outflow or block its production.

Studies report the involvement of GPCRs in modulation of TM outflow facility. Adenosin receptors have been identified as pharmacological target for IOP modulation and a A_2 receptor agonist OPA-6566 is currently in development. OPA-6566 lowers IOP by increasing outflow through TM [40]. Also a A_1 receptor agonist has shown to decrease

IOP, through activation of matrix metalloproteinases (MMP) leading to a remodeling of TM [41, 42]. The role of A_3 subtype appears different, since A_3 knockout mice have lower IOP than wild-type due to decreasing AH inflow [43].

The role of cannabinoids in decreasing IOP, is controversial. Cannabinoids are able to decrease IOP, however due to cannabinoids systemic effects efforts to alternative pharmacologic strategies have been carried out. Anandamide (AEA) an endocannabinoid, is transported to cells then is hydrolyzed by fatty acid amide hydrolase (FAAH), that is expressed in TM tissue [44, 45]. Thus FAAH inhibitors have been studied for their potential modulation of IOP, and they have showed ocular hypotensive effects most likely prolonging AEA activity [46, 47]. Several CB_1 and CB_2 agonists have been tested and showed IOP decreasing effects in animals and humans. Also palmitoyl-ethanolamide (PEA) that competitively binds to FAAH showed an ocular hypotensive activity blocking the degradation of AEA [48]. Recently Kumar et al [49] demonstrated that PEA acts in a peculiar way, increasing AH outflow through GPR55, a cannabinoid related receptor, and through activation of peroxisome proliferator activated receptor-alpha (PPARP-α).

Serotonergic and dopaminergic receptors as pharmacological targets in modulation of IOP are the objectives of the present work. Serotonergic receptors are a large family of GPCRs ($5HT_{1A-F}$, $5HT_{2A-C}$, $5HT_4$, $5HT_{5A-B}$, $5HT_6$, $5HT_7$) and a ligand-gated ion channel, the $5HT_3$ receptor. Several serotonergic receptor subtypes are expressed in ocular tissue: iris-ciliary body, ciliary epithelium, ciliary muscle and TM [50]. Moreover serotonin has been found in AH of humans. The serotonin receptor subtypes that seem to be strictly involved in the regulation of IOP, $5HT_1$ and $5HT_2$ subfamilies, are characterizing their self as interesting targets. In particular extensive pharmacological studies suggested that $5HT_{2A}$ activation has a crucial role in lowering IOP, by means of activation of phospholipase C and releasing of diacylglicerol and inositol-3-phosphate than increasing of free intracellular Ca^{2+} [51]. A series of $5HT_{2A}$ agonists have shown IOP lowering effects [52]; even though ketanserine, $5HT_{2A}$ receptor antagonist, decreases IOP in glaucomatous patients [53]. For this reason further studies, about the role of $5HT_{2A}$ in IOP modulation, are needed. $5HT_{2A}$ agonists and antagonists have been proposed for IOP reduction, but some obstacles in development arose, possibly pertaining efficacy, adverse effects or lack of selectivity of those compounds. Swedish Orphan Biovitrum completed a phase IIa clinical trial in 2008 on BVT.28949, a $5HT_{2A}$ antagonist showing an ocular hypotensive activity (10%), however no further development is reported [54].

Within the pharmacological targets hereby analyzed only three of them are GPCRs that bind small molecules. Adenosine receptors diverge significantly from serotonergic and dopaminergic receptors, which are both aminergic. Dopaminergic receptors are a family of GPCRs characterized by two subfamilies of receptors: D_1-like (D_1 and D_5) coupled to Gs (stimulatory) proteins and D_2-like (D_2, D_3 and D_4) coupled to Gi proteins (inhibitory). The pioneering study, about D_2-like receptors as pharmacological targets of glaucoma and in particular D_3 receptor, is the work of Chu and collaborators. Chu and co-workers [55] used a pharmacological approach to identify D_3 receptor and its role in lowering IOP. Topical 7-OH-DPAT, a selective D_3 receptor agonist was able to decrease IOP in rabbits, and a D_3 selective antagonist U99194A reverted this effect. The suggested location of D_3 receptor in the eye, are sympathetic fibers afferent to ciliary body, thus activation of D_3 receptor might block AH inflow. Moreover, ibopamine, D_1 receptor agonist, increases AH inflow, and activation of D_3 receptor leads to decreased IOP. The role of D_3 receptor as potential pharmacological target of ocular hypotensive drugs has been confirmed by means of pharmacological approaches along with gene deletion study, using $D_3^{-/-}$ mice. Bucolo et al. [56] have treated wt and $D_3^{-/-}$ mice, either normotensive and steroid-induced ocular hypertensive, with 7-OH-DPAT that exerts its IOP lowering effects only in wt mice. The effects of 7-OH-DPAT have been counteracted by the pretreatment with U99194A. Since all dopaminergic receptors have been identified in ciliary body of mice, it could be stated that inhibition of D_3 receptor blocks AH production. In the present work of thesis a study with a similar experimental paradigm was carried out in order to explain cabergoline lowering IOP effect. The ocular hypotensive effect of cabergoline has been claimed to the activation of $5HT_{2A}$ receptor [51]. However, cabergoline, along with other ergot derivatives with IOP lowering activity, is a mixed serotonergic and dopaminergic agonist. Cabergoline has been used, in the present work, as a pharmacological tool in order to confirm the role of D_3 receptor in modulation of intraocular pressure, at least in the glaucoma model hereby used.

Animal models of glaucoma

Research animal models have helped in understanding causes of diseases and in particular the discovery and development of new drugs. Animal models, sometimes do not mimic all features of a disease, although even one mimicked feature is useful to find a drug target and to develop new drugs.

Glaucoma is a complex disease and as written before its etiology is still unknown. Several animal models of glaucoma have been reported [57], including a wide variety of species with spontaneous or induced features of glaucoma [58, 59]. These include large animals such as monkeys, dogs, cats and pigs, with disadvantages of breeding and management. Small animals such rodents are used as animal model of glaucoma [60] and relative advantages exceed disadvantages. Rodent models of POAG are reported below.

Steroid-induced glaucoma is reported in humans and it is associated to ocular hypertension [61, 62]. A rat model of glaucoma, induced by topical application of dexamethasone (DEX), was developed to study the expression of myocilin. After two weeks of DEX treatment IOP increased but not significant changes in mRNA levels of myocilin, one causative gene of glaucoma in human [63], have been found. Thus increasing of IOP in steroid-induced glaucoma could be not related to myocilin [64], at least in the described animal model. Rats, in contrast to other non-primate models, have anatomical features of anterior chamber similar to the human especially regarding the AH outflow facility [65-67]. Retinal and optic nerve damage in ocular hypertensive rats resembles damage in POAG patients. However it was found that some glaucoma medications do not have identical effects to those observed in humans [68]. Rats, as well mice, are easy to maintain in laboratory, can be manipulated genetically and be used in large numbers.

A mouse strain expressing the Tyr423His myocilin mutation, corresponding to the human Tyr437His point mutation, was developed to study POAG [69, 70]. At 18 months of age, the myocilin mice model demonstrated loss of 20% of RGCs in peripheral retina, axonal degeneration in the optic nerve and detachment of endothelial cells of the TM. Myocilin mutant mice show a moderate but persistent increasing of IOP, 1-2 mmHg higher than normal. Another transgenic mouse model of glaucoma has been reported: mice with a mutation in the α1 subunit of collagen type I develop POAG [71, 72]. In this model mice have progressive optic nerve axonal loss and gradual elevation of IOP, thus IOP modulation can be related to fibrillar collagen turnover.

The steroid-induced ocular hypertension in mice, used in the present work, was first reported by Whitlock et al. [73]. Osmotic micropumps filled with either DEX (water soluble cyclodextrin-DEX complex) or PBS as control, have been implanted in B6.129 hybrid mice. Administration of DEX for four weeks resulted in increased IOP in comparison to baseline and PBS treated mice. This animal model of glaucoma was also used to induce ocular hypertension in C57BL/6J wt and $D_3^{-/-}$ mice by Bucolo et. al. [56]. Implantation of osmotic micropumps allows delivery of DEX at constant concentration, 0.09 mg per day. The continuation of administration of DEX is crucial to maintain stable ocular pressure. Main risks for implanted animals are immune-depression and infections. A maximum of 50% of IOP increase, in comparison to baseline and PBS treated animal, was reached. Ocular hypertension in that animal model is mainly related to impairment of AH outflow facility, even if the related molecular mechanism is still unknown.

Figure 1. Schematic rapresentetion of POAG (A) and PACG (B).
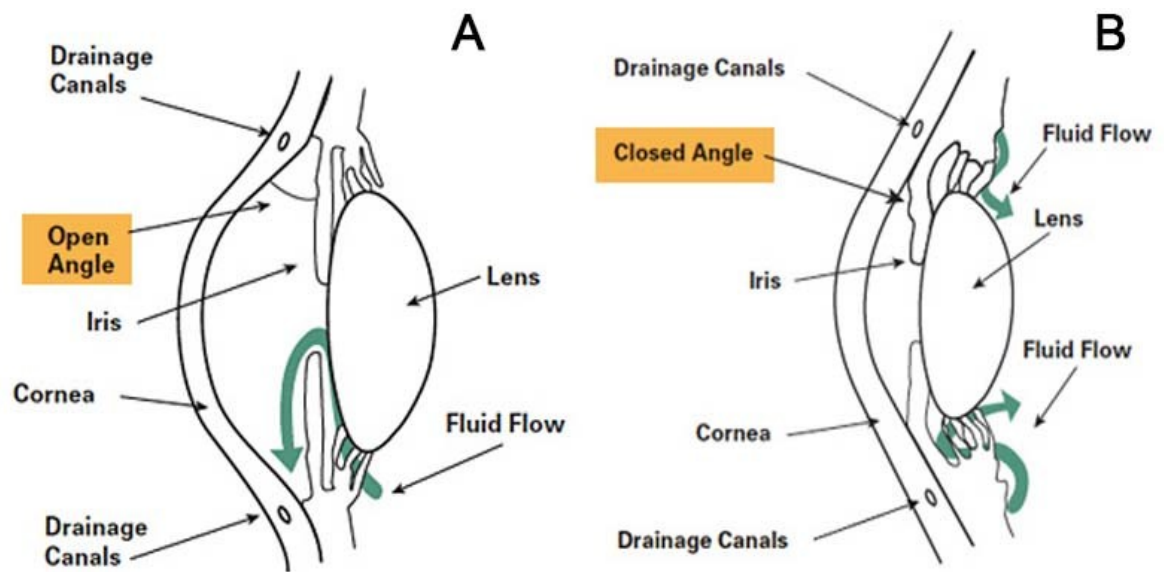
Fig. 2 Conventional (A) and unconventional (B) root of aqueous humor outflow.
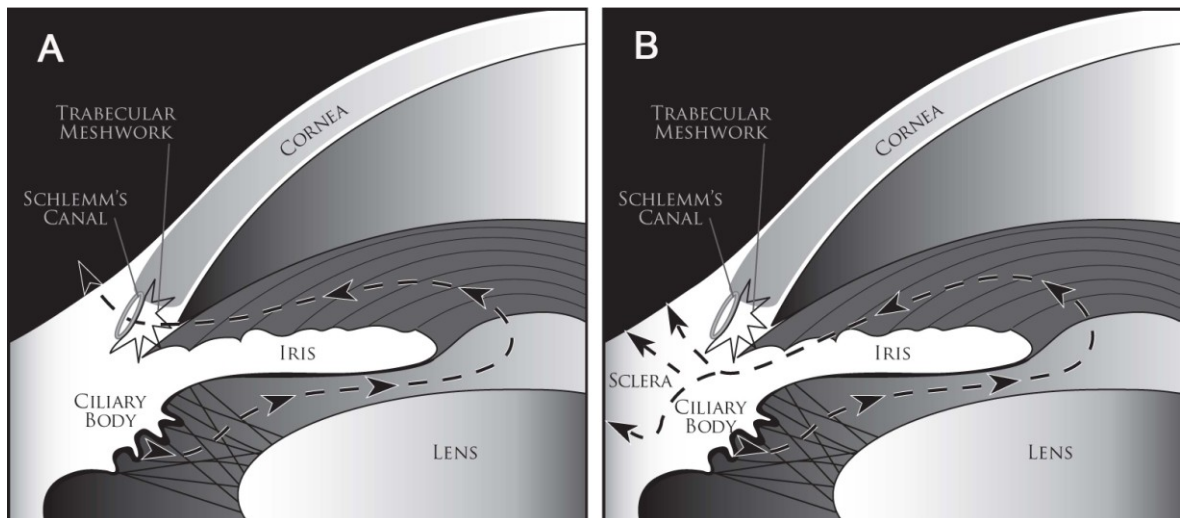
Goel M. et al. 2010

G PROTEIN COUPLED RECEPTORS

G Protein Coupled receptors are integral membrane proteins, with seven trasmembrane helices bundle embedded in the lipid bilayer. In human genome more than 800 genes have been identified encoding GPCRs [74]. In accordance to International Union of Basic and Clinical Pharmacology (IUPHAR), GPCRs are classified in four main classes (excluding sensory GPCRs): (1) class A rhodopsin-like; (2) class B secretin-like, (3) class C metabotropic glutamate/pheromone, (4) and frizzled receptors. Up to now such GPCRs classes are accounted to be pharmacological targets of about 30-50% of approved drugs [75-78]. The potential of GPCRs as pharmacological targets is huge as reported by Garland in the 2013 [79]. Garland has arisen an issue: about 400 drugs exert their effect through no more than 100 receptors, accounting for less than 30% of those expressed in human genome; thus a lot of target/pharmacology combination are still hidden.

Analyzing the new Food and Drug Administration (FDA) approved drugs in the last three years 2011-2013, 19% of approved new chemical entities (NCE) target GPCRs. Within these 17 NCE, four account for new activity/target combination and the remaining for a drug action improvement on known mechanism. One of these 17 approved drugs is tafluprost, which is new ocular hypotensive drug targeting the prostaglandin F (FP) receptor. Looking at drugs targeting aminergic receptors, two of them have been approved: lorcaserin a $5HT_{2C}$ agonist for treatment of obesity showing a 100-fold and 17-fold selectivity over $5HT_{2B}$ and $5HT_{2A}$ receptor and mirabegron a selective β_3 adrenergic receptor agonist for treatment of overactive bladder. Analysis of last approved drugs, making attention to drug molecular weight (MW), shows that 80% of those drugs targeting GPCRs are small molecules. 20% of molecules with high MW account for peptides; opening new potential studies in drug discovery of such molecules targeting GPCRs, taking also in account the challenges regarding drug stability and delivery issues. The taking home message is that GPCRs, with known or unknown (orphan) functions, are an important source for drug discovery of NCE but also for the repositioning of shelved drugs.

GPCRs functions and structure

GPCRs are membrane proteins that share the seven transmembrane helices bundle as main structural feature. GPCRs respond to variety of extracellular signals: photons, ions, small organic molecules and peptides. After the action of those signals on GPCRs, the receptor undergoes to a conformational transition, causing the activation of cytosolic signaling networks. GPCRs are conventionally viewed to transmit signals trough activation of G heterotrimeric proteins (Fig. 3). There are encoded 21 α, 6 β, 12γ subunits, the assembly of which characterize four kinds of G proteins; (1) $G_{\alpha}s$ proteins which upon activation stimulate cAMP production, (2) $G_{\alpha}i$ which inhibit cAMP production, (3) $G_{\alpha}q/11$ which leads to intracellular calcium mobilization, (4) $G_{\alpha}12/13$ which activates monomeric GPTase RhoA. Some GPCRs are coupled with just one G protein, but other receptors couple to more than one G, depending i.e. from localization, leading to various physiological functions. Alternative signaling pathways of GPCRs have been identified to be exploited in the drug discovery process, such as the β-arrestin signaling. Agonist binding to a receptor promotes both G protein activation but also sensitization and internalization. Receptor sensitization arises from phosphorilation of intracellular site of GPCRs, leading to increased affinity for β-arrestins, than to block of later receptor activation and to subsequent promotion of receptor internalization. β-arrestin signaling had been characterized as negative regulator of GPCRs, but now it has been studied for peculiar signal pathways such as MAP and Src kinases activation, transcriptional regulation and receptor transactivation [80-83]. Thus there is the emerging research field on discovery and development of biased agonists. Biased agonists differentiate themselves from other ligands, activating a subset of signal pathways of the receptor, that can be useful either for activation of clinically beneficial effects or inhibition of side effects. Recently some structural features have been identified to have a role in the biased signaling of GPCRs. A functional and structural approach was carried out to elucidate the behavior of ergotamine, which acts as biased agonist on 5HT$_{2B}$ receptor but not at 5HT$_{1B}$ receptor, identifying the conformational changes at VII helix crucial for β-arrestin signaling [84].

This result highlights the scientific contribution of structural studies on GPCRs. In the past of 12 years, more than 75 x-ray structures of 18 different classes of GPCRs have been solved in complex with several ligands [85]. The availability of such 3D structures, provides an unprecedented opportunity to study deeply the structural and functional

features of GPCRs, a protein family characterized by a great heterogeneity even if the overall structure is conserved.

Research now is helped by structural data in addressing questions about: molecular signature of GPCRs, fold and molecular changes that undergo upon receptor activation. Moreover the knowledge of receptor structure is fundamental in the drug discovery and development process that takes advantage of structure-based drug design approaches. So far, high-resolution structure of GPCRs have been solved for the following class A GPCRs: rhodopsin, β_1/β_2 adrenoreceptors, muscarinic $M_{2,3}$ receptors, H_1 histaminergic receptor, dopamine D_3 receptor, $5HT_{1B}$ and $5HT_{2B}$ receptors, adenosine A_{2A}, CXCR4 chemokine receptor, opiod receptors (nociceptin receptor, κ-OR, μ-OR and δ-OR), neurotensin receptor NTSR1, protease activated receptor PAR1, and the lipid activated GPCR sphingosine-1 phosphate $S1P_1$ receptor. Within these structures an important turning point is the crystal structure of β_2-adrenoreceptor in complex with heterotrimeric G protein [86].

The structure of a GPCR can be divided into three parts. The extracellular domain that consists of the N-terminus (often not solved due to its flexibility), and three extracellular loops (ECL). The transmembrane region that includes the orthosteric binding site. The third part is characterized by the intracellular part of a GPCR, consisting of intracellular loops (ICL); the ICL3 is generally longer than the other ICLs and binds to the effectors G proteins.

Sequence analysis shows that N-terminus and ECLs sequences are not highly conserved. At a structural analysis, the class A rhodopsin-like is characterized by two types of receptors: the one with occluded binding pocket that binds hydrophobic ligands, the other with open binding pocket typical of receptors activated by hydrophilic ligands. The ECL2 is involved in the receptor activation and can be folded as helix or sheets. Molecular dynamics simulations suggest that ECL2 is involved in the first stage of ligand recognition and selectivity [87], moreover pharmacological studies have identified the role of ECL2 in binding kinetics [88]. GPCRs have another conserved structural feature, disulfide bridges, that contribute to structural stability. The disulfide bridge involving cysteine residues of the III helix and of ECL2 is conserved, with exception of $S1P_1$ receptor. Furthermore an accessory disulfide bridge within the ECL3 has been found in the crystal structure of D_3, $5HT_{1B}$ and $5HT_{2B}$ receptors. This accessory disulfide bridge seems to influence the overall receptor stability [89], but also the shape of binding pocket [90].

The seven transmembrane helices bundle serves as a link between the ligand binding pocket and the G protein. A comparison between the GPCRs structures solved so far using a network representation [85], has revealed that tertiary contacts in the trasmembrane region are conserved, independent of sequence diversity and receptor conformation (active or inactive). A consensus network of 24 contacts mediated by 36 residues have been identified (Fig. 4), and provide an evolutionarily conserved structural scaffold of non-covalent contacts for the GPCR fold. These tertiary contacts involve the central and cytoplasmatic site of the helices bundle, and are clustered at the interface of helices I-II, III-IV, III-V, and III-VI-VII. Another remarkable feature of GPCRs is to bind ligands with different shape and physical chemical properties. All ligands bind in a pocket, but some of these ligands bind deeply in that cavity. Despite the diversity of ligands that bind to GPCRs, residues within 4 Å of the ligands are similar. Topologically equivalent residues of III, VI and VII helices bind ligands, characterizing themselves as consensus contacts with ligands across the class A of GPCRs. In the present thesis (Chapter I and II) analyzing D_3, D_{2L}, $5HT_{2A-C}$ receptors; the binding mode of agonists involves also hydrophilic residues in the V helix, which seems to have a role in the affinity of compounds within these homologous receptors [90, 91]. In the consensus network of contacts two interaction patterns between residues 3.36-6.48 and 6.51-7.36 belong to the binding pocket (Fig 4). The described consensus network [85] can be useful for improvement of techniques for homology modeling of GPCRs.

Residues in the intracellular region and the cytoplasmatic part of helices bundle are involved in binding with signaling effectors. Moreover some conserved residues in the ICL2 have been identified to have a role in the activation of GPCRs, such as the conserved motif D(E)RY in several receptors [84, 92-94]. Other structural motifs have been identified to have a role in receptor activation, such as NPXXY at the VII helix, and P-I-F motif localized at the interface between the extracellular and intracellular part of helices bundle [84].

Significant differences, in those mentioned structural motifs, have been found between the x-ray structure of $5HT_{2B}$ receptor in complex with ergotamine, and the simulated receptor in the unbound state (Chapter II). The simulated $5HT_{2B}$ receptor, reported in the present work, have been found to have partially inactivated conformation [91].

The described molecular features, the growing literature and x-ray structures of GPCRs will help to fulfill the need for new targets and new drugs [79]. Tools such as structure-based drug research and discovery (R&D) might help to understand molecular features of

drug efficacy and selectivity and also to carry out high throughput screening of compounds in order to identify new hits and leads [95]. Moreover the knowledge of the structure of a GPCRs, either x-ray or modeled structure could help in the elucidation of the pharmacodynamic profile of multi-target ligands, i.e. trying to predict side effects [96].

Molecular modeling of GPCRs

The progress in crystallization techniques has been associated to the advances in computational (*in-silico*) techniques such as: structural modeling and molecular dynamics simulations. Computational approaches are important for GPCRs characterization. There is a small ratio between the number of x-ray structures and the genes that encodes for GPCRs, since there is still a lack of information. The comparative modeling of GPCRs structures has an important role in fulfillment of this gap.

Comparative modeling is defined as a computational approach that generates a predicted structure of a target molecule, such as a GPCR, with unknown structure. Comparative modeling is a knowledge-based method; in the present thesis two different comparative modeling approaches have been used, homology modeling and threading methods. Homology modeling is based on the assumption that the three dimensional structure of a protein depends on its sequence; moreover the overall structure of proteins is more conserved than their sequences [97]. This assumption is confirmed by experimental data; GPCRs are classified in different classes, families and sub-families of receptors, which diverge in sequences but not in the overall fold. With homology modeling it is possible to predict the structure of a "target protein", building the 3D coordinates of its atoms using as reference the structure of a "template protein", which is high homologous to the target. The reliability of an homology model depends on the homology and sequence identity shared by the target and template protein. The percentage identity cut-off, for large proteins with more than 150 residues, is about 40%. Inside a GPCR family such as dopaminergic GPCRs, the identity shared by D_1 and D_3 receptors is 30% and homology is 47%. Within aminergic GPCRs these values are redundant. Although the percentage identity is below the suggested cut-off, the homology modeling of GPCRs is still an useful and validated approach. An example of software, that carry out homology modeling predictions, is MODELLER [98], moreover in the field of *in-silico* methods several web-servers have been developed and provide access to modeling software, such as the Swiss-Model web server [99]. Another strategy that can be aimed to obtain comparative modeling of protein is the treading method or fold-recognition approach. Threading is useful when non high

homologous templates are identified for a target. Threading methods employ multiple template proteins, and the main difference in comparison to homology modeling is that prediction is carried out by placing each amino acid of target primary structure to a position in the template structure, evaluating iteratively the fitness of target in the template. The fitness is based on a scoring function built on an established structure template database; the scoring function takes into account several knowledge-based structural restraints derived from experimental data. Threading methods are provided by software such as RAPTOR [100] but also web-servers such as HHpred [101] and I-Tasser [102]. Zhang and collaborators have provided an efficient threading pipeline for modeling of GPCRs, the G Protein Coupled Receptor Research Database (GPCRRD), which in addition to treading method performs conformational search of receptors and a Molecular Dynamics Fragment Guided simulation (FG-MD) [103]. Either homology modeling and threading provide useful predicted structural data of proteins with unknown structure. Several caveats affect those prediction approaches, such warnings are related to structure energy optimization. Comparative modeling approaches do not carry out extensive energy optimization of proteins, with some exceptions such as GPCRRD. However GPCRs are membrane proteins, thus the role of membrane-protein environment should be taken into account.

In the present thesis it is presented a computational approach that along with comparative modeling either homology modeling [90] and threading [91] was used to carry out the structural optimization of GPCRs, by means of molecular dynamics simulations in an explicit water-membrane environment. Molecular dynamics (MD) is a simulation technique that relies on physical chemistry laws. A molecule, atoms connected by bonds, is treated in MD as a set of beads connected by springs; during an MD the movement of such set of beads and springs is simulated by numerical integration of the Newton Law of motion (eq. 1).

$$m_i \frac{\partial^2 r_i}{\partial t_i^2} = F_i = -\nabla_i V(r_1, r_2, ..., r_n) \quad \text{i=1,N} \quad (1)$$

In equation (1), m is the mass and r are the coordinates of the i atom. The force F_i experienced by the i particle is the derivative of potential energy. This potential energy is described in MD by a mathematical function called *force field*. The force field is characterized by a sum of contributes that accounts for bound, no-bound and cross-terms energies that govern the degrees of freedom of the simulated system.

$$E = E_{bound} + E_{no-bound} + E_{crossterms} \quad (2)$$

$$E_{bond} = E_{stretching} + E_{bending} + E_{torsion} + E_{oop} \quad (3)$$

$$E_{no\text{-}bound} = E_{Coulomb} + E_{Lennard\text{-}Jones} \quad (4)$$

$$E_{crossterms} = E_{bending\text{-}bending} + E_{bending\text{-}stretching} +$$
$$+ E_{torsion\text{-}stretching} + E_{torsion\text{-}stretching} + ... \quad (5)$$

The physical reliability of MD is stated by the force field and its parameters, that are derived by *ab inizio* quantum chemical calculations but also by experimental data such as: Infrared (IR), Raman and Nuclear Magnetic Resonance (NMR) spectroscopy. In fact IR, Raman and NMR techniques measure energies respectively related to the stretching, rotational and torsional degrees of freedom of molecules. Several force field have been implemented in MD software, but CHARMM it is worth to be mentioned. CHARMM (Chemistry at Harvard Macromolecular Mechanics) force field and the homonymous implementing software have been developed by the "2013 Nobel Prize for chemistry" Martin Karplus and his collaborators [104]. The CHARMM forcefield is peculiar in comparison to other force fields, such as AMBER, since it describes the out-of-plane "oop" motions of bounds (eq. 6). Furthermore in CHARMM the Van Der Walls term includes the description of hydrogen bond (eq. 7), where sw is a function that describes the geometrical properties of hydroben bond.

$$E_{pot_{(oop)}} = K_{\chi}(\chi - \chi_0)^2 \quad (6)$$

$$E_{VdW+Hbond} = \sum \left(\frac{A_{ij}}{r_{ij}^{12}} - \frac{b_{ij}}{r_{ij}^{6}} \right) sw(r_{ij}^2, r_{on}^2, r_{off}^2) \quad (7)$$

MD allows the inclusion of solvent in the simulation; since water is fundamental for folding and function of proteins several explicit water models are described by force fields parameters, such as TIP3P and SPC/E. Also an implicit water model is used in MD in order to speed simulations; the Generalized Born (GB) model where solvent is treated as continuum medium. GB is useful for simulation of small peptides but this approximate solution lacks of reliability when simulating proteins bigger than 30 amino acids. Moreover implicit water models do not account for solvent effects such as viscosity, hydrophobic effect and water-molecule hydrogen bonds. Since biomolecules are charged, ions can be added to the simulation system in order to reach neutralization. Moreover molecule structure is influenced by the ionic strength, then in the simulation of biological

molecules ions are added up to 150 mM concentration in order to resemble the physiologic condition.

Several kind of physical ensembles can be simulated:
- microcanonical ensemble NVE, where particle number N, volume V and energy E are constant;
- canonical ensemble NVT, where T stands for constant temperature;
- isothermal isobaric ensemble NPT, where P stands for constant pressure; a variation of this ensemble is NPγT or NPAT, where γ stands for costant surface tension of lipid bilayer and A for constant area of membrane.

The principal steps of MD simulation of a GPCR are:
- building of simulation box, i.e a GPCRsembedded in a lipid bilayer, often 100x100 Å or bigger lipid leaflet,
- primary equilibration steps such as lipid melting, water-ions equilibration, lipid-water-ions equilibration around the protein kept fixed with harmonic constraints,
- equilibration of the whole system, with small integration time-step (1 fs),
- MD production run with 2 fs integration time-step.

MD is a statistical method; in statistical mechanics the average of observables are defined as average ensemble, thus the average of a huge number of simultaneous replicas of the analyzed system. Just one replica is simulated in MD and it is statistically reliable because of the ergodic principle: "the average system is equal to the time average of the system" (eq.8); it means that a system that is free to evolve in a time span, explores all possible allowed energetic states.

$$<A>_{ensemble} = <A>_{time} \qquad (eq.\ 8)$$

The time span or time-scale depends on which molecular event would be observed with MD. During a classical MD simulation, the most CPU (Computing Processing Unit) intensive task is the evaluation of non-bonded or non-covalent terms of force field. In Big O notation, common molecular dynamics simulations scale by $O(n^2)$ if all pair-wise electrostatic and Van der Waals interactions are accounted explicitly. This computational cost can be reduced by employing electrostatics methods such as Particle Mesh Ewald ($O(n\log(n))$), or good spherical cutoff techniques ($O(n)$). Another factor that impacts total CPU time required by a simulation is the size of the integration time step. This is the time length between two recurrent evaluations of the potential or integration of motion. The time step must be chosen small enough to avoid discretization errors (i.e. smaller than the fastest vibrational frequency in the system). Typical time steps for classical MD are in the

order of 1 fs (1E-15 s). This value may be extended by using algorithms such as SHAKE, which fixes the vibrations of the fastest atoms (e.g. hydrogen bound to carbon). Up to now MD simulations could be scaled-up (speeded up) not only by distribution of calculation on large number of CPU, up to 64 threads, but also by using MD software that support CUDA (Computed Unified Device Architecture) acceleration. With CUDA acceleration calculation of non-bond interactions could be speeded up by distributing the calculation also on GPU (Graphic Processing Units). Thus hardware development is going to pursue to MD the ability to carry out longer simulations in less time. Molecular dynamics time-scale depends from molecule dimensions and structure; moreover the simulation time extension depends on which molecular event is studied. In example simulation of protein folding may require from 30 ns to μs of simulation, protein aggregation requires μs [105]. Looking at GPCRs long time-scale all-atom MD, up to 15 μs for each trajectory, have been carried out to perform the analysis of β_2-adrenergic receptor activation [106] and analyze the allosteric binding at M_2 muscarinic receptor [107]. Such long time-scale all-atom MD simulation of GPCRs have been carried out on a special purpose computer, Anton, running the software Desmond, in order to perform acceleration of classical molecular dynamics [108].

In the present thesis, short time-scale (3 ns) simulation have been carried out in order to optimize the structural models of D_3, D_{2L} dopaminergic receptors [90] and $5HT_{1A}$, $5HT_{2A-C}$ serotonergic receptors [91]. Three ns of molecular dynamics simulation have been enough to reach a relative conformational minimum for both D_3 and D_{2L} receptors, which differentiated in structure and have been validated for discrimination of selective agonists. Also the serotonergic receptors reached a relative minimum within 3 ns of simulation, and prediction of binding of cabergoline are comparable to the experimental binding of ergotamine at crystallized human $5HT_{2B}$ receptor.

The binding of compounds have been studied by molecular docking. Docking is frequently used to predict the binding orientation of small molecules to potential protein targets in order to predict affinity and activity of compounds. Docking could play an important role in the rational design of drugs and considerable efforts have been directed towards improved docking methods. Molecular docking can be thought of as a problem of lock-and-key; where the key in the ligand which is active toward the receptor (lock). The lock-and-key vision is quite rigid, because ligand and receptor are flexible. For this reason the ligand-receptor binding could be described as a hand that wears a glove (hand-in-glove). In fact during the binding process, ligand and protein adjust their conformations to achieve an

overall "best-fit" and these kind of conformational adjustments resulting in binding are referred as "induced-fit". Molecular docking, simulating the molecular recognition process, aims to achieve an optimized conformation at least of the ligand. This conformation called "pose" is the relative orientation between protein and ligand, characterized by the best interaction energy. Two approaches are popular within molecular docking software. The matching technique that describe the protein and the ligand as complementary surfaces. In the second approach ligand-protein pairwise interaction energies are calculated iteratively; the most validated approach is the semi-flexible docking where ligand is flexible and receptor atoms are kept fixed. Input information of docking are protein structure and a set of potential ligands. The success of a docking program depends on two components: the search algorithm and the scoring function. The search space consists of all possible orientations and conformation of the protein paired with the ligand. However up to now it is hard to exhaustively explore the search space of the whole system, than the search space is in practice limited to the ligand. A variety of conformational search strategies have been applied to the ligand and to the receptor: systematic or stochastic torsional searches about rotable bonds, molecular dynamics simulations and genetic algorithms. The scoring function takes a pose as input and returns a number indexing the likelihood that the pose represents a favorable binding interaction. Existing scoring functions can be divided into three main classes: force field-based methods, empirical score functions and knowledge-based methods [109]. Docking software fail often to predict absolute values of binding energy, but could be successful in prediction of the trend of binding energy of congeneric class of compounds [90]. This capability is useful in order to identify hit or lead compounds. Sometimes there is the need of rescoring methods, in example by rescoring of poses with another scoring function. Rescoring could be atime expensive approach but can help to obtain reliable results. The evaluation of binding energy in terms of prediction of binding free energy has been shown to be successful by means of time expensive calculations such as MM/GB(PB)SA [Molecular Mechanics/Generalized Born (Poisson Boltzmann) Solvent Accessible surface area] [110, 111]. This kind of calculations are very predictive of drug affinity, however those are not yet extensively available for virtual screening studies in terms of codes and hardware. Application of MM-GBSA scoring or re-scoring to GPCRs is straightforward, because of receptor encounters to conformational changes upon binding and interaction with lipid bilayer should be taken into account. This consideration implies, i.e. in virtual screening, the use of multiple conformations of receptor obtained from MD, with more or less approximations [112].

D₂-like receptors

The dopaminergic system is characterized by two subfamilies of receptors, D_1-like (D_1, D_5) and D_2-like (D_3, D_2, D_4); that respectively are coupled to Gs and Gi proteins. D_2 and D_3 receptors are highly homologous, whereas D4 receptor is phylogenetically distant from the other D_2 like receptors (Fig.5). Several efforts have been carried out to model selective ligands toward either D_3 or D_2 receptor [113-119]; recently also D_4 receptor [120, 121] has been investigated by means of ligand or structure-based in silico approaches.

Since the D_3 receptor x-ray structure was solved [122] important information have been revealed in comparison to previous structural knowledge. An interesting study was published after the releasing of dopamine D_3 receptor structure, published by Carlsson et al. in 2011 and entitle "Ligand discovery from a dopamine D_3 receptor homology model and crystal structure". In that paper it is highlighted that the screening on the homology model of D_3 receptor carried out before releasing of D_3 receptor structure has led to unbiased results since hit rates of virtual screening on homology models (23%) was comparable to the one (20%) carried on crystal structure of D_3 receptor. The main bias of these two virtual screening studies was found to be related to the binding at the allosteric binding pocket, which is more open in the homology modeling in comparison to the x-ray structure [95]. Differences in the allosteric binding pocket between D_3 and D_2 receptors have been claimed by Chien et al. [122] to influence the selectivity either at D_3 or D_2 receptors, possibly due to different electrostatic properties of the two cavities. In chapter I of the present thesis it is showed that upon molecular dynamics simulation there is an evolution of binding pockets of D_3 and D_2 receptors, and the whole pocket of D_2 receptor became bigger than D_3, possibly due to the lack of the accessory disulfide bridge within the 3ECL [90]. Recently, an interesting update about the role of allosteric pocket in D_2-like receptor and the 1ECL have been reported by Michino et al. 2013 [123]. In this publication it is reported that a single glycine residue, in the 1ECL of D_3 receptor, influences 1ECL flexibility and II helix movement upon ligand binding. Moreover it has been recognized a high energy hydration site in the allosteric binding pocket of D_3 receptor, thus compounds that are able to displace such high energy water molecules have high affinity for D_3 receptor. Those calculations have been carried out with Water-Map [124].

Starting from latest literature about structural features of dopaminergic D_2-like receptors, medicinal chemists must move toward evaluation of NCE or drugs for repositioning that could interact with the allosteric binding pocket of D_3 receptor.

In chapter II it is reported an analysis of structural features between D_3 receptor and several serotoninergic receptors: $5HT_{1A}$, $5HT_{2A-C}$ [91]. Ergot derivatives ocular hypotensive drugs such as lisuride, cabergoline, cianergoline and bromocriptine are reported to be serotonergic and dopaminergic agonists. Moreover multi-pharmacological profiles are also accounted to antipsychotics that bind with high affinity to $5HT_{2A}$ and D_2 receptors such as iloperidone and risperidone [125]. Up to date few modeling studies have compared the structural features of binding of mixed serotonergic and dopaminergic ligands at D_2-like and serotonergic receptors [96, 126, 127]. The *in silico* study reported in chapter II is the first that shows an extensive comparative modeling study on D_3 receptors and four homologous serotonergic receptors. In that study it is reported that cabergoline has a conservative binding mode at D_3 and $5HT_{2A-C}$. Furthermore affinity of this compound is higher for D_3 and $5HT_{1A}$ receptors in comparison to $5HT_{2A-C}$, due to the better desolvation energy associated to the predicted complexes cabergoline/ D_3 and $5HT_{1A}$.

Recently an interesting paper suggested new perspective studies for drug development of biased agonists active on D_3 receptor. D_3 receptor, but not D_2 receptor, undergoes to fast pharmacological sequestration and desensitization which is GRK-independent [128]. The molecular mechanism of pharmacological sequestration (Fig. 6), upon agonist action, seems to be related to a D_3 receptor conformation that forbids the binding of hydrophilic agonists, but allows the binding of hydrophobic compounds. β-arrestin binding through Gβγ interaction regulates such pharmacological sequestration. Pharmacological sequestration and desensitization of D_3 receptors are related to each other; 7-OH-DPAT>quinpirole>dopamine pharmacological sequestration pattern resembles the sensitization induced by those compounds. However sensitization characterizes a long term modification of D_3, since it is maintained after five washes; whereas pharmacological sequestration is reverted in the middle of one wash. It could be stated that pharmacological sequestration is the event the precedes the sensitization. This highlight on the novel results about biased signal of D_3 receptor, open research on D_2-like receptors to R&D of biased agonists.
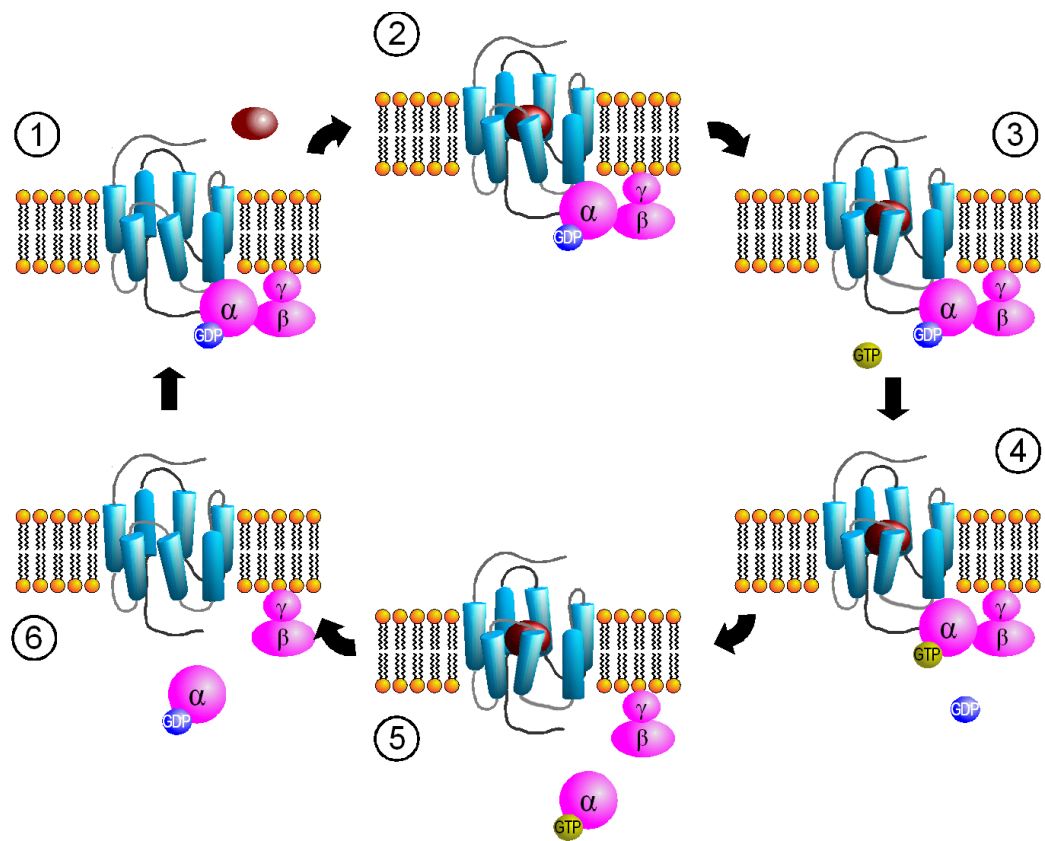
Figure 3. GPCRs activation cycle

Figure 4. Consensus network of contacts in aminergic GPCRs

Contact	Beta1-AR	Beta2-AR	*Beta2-AR	Dopamine-R	Histamine-R	Muscarinic2-R	Muscarinic3-R
BW	2VT4	2RH1	3SN6	3PBL	3RZE	3UON	4DAJ
1.46:7.47	I55--A337	I47--G320	I47--G320	I43--A377	T41--T462	T37--T434	T81--T537
1.49:7.50	G58--P340	G50--P323	G50--P323	G46--P380	L44--P465	G40--P437	G84--P540
1.50:2.47	N59--A84	N51--A76	N51--A76	N47--A72	N45--S70	N41--A66	N85--A110
1.50:2.50	N59--D87	N51--D79	N51--D79	N47--D75	N45--D73	N41--D69	N85--D113
1.50:7.46	N59--S336	N51--S319	N51--S319	N47--S376	N45--S461	N41--S433	N85!!S536
1.53:2.47	V62--A84	V54--A76	V54--A76	V50--A72	V48--S70	V44--A66	V88--A110
1.57:2.44	I66--T81	I58--T73	I58--T73	V54--V69	V52--V67	I48--F63	F92--L107
2.42:3.46	F79--I135	F71--I127	F71--I127	L67--I124	Y65--L121	F61--I117	F105--I161
2.43:7.53	I80--Y343	I72--Y326	I72--Y326	V68--Y383	I66--Y468	L62--Y440	L106--Y543
2.50:7.46	D87--S336	D79--S319	D79--S319	D75--S376	D73--S461	D69--S433	D113--S536
3.34:4.53	L123--S169	L115--S161	L115--S161	M112--A161	V109--S155	V105--S151	V149--S195
3.34:4.57	L123!!S173	L115--S165	L115--S165	M112--S165	V109--V159	V105--W155	V149--W199
3.36:6.48	V125--W303	V117--W286	V117--W286	C114--W342	S111--W428	S107--W400	S151--W503
3.38:4.50	A127--W166	A119--W158	A119--W158	A116--W158	A113--W152	A109--W148	A153--W192
3.38:4.53	A127--S169	A119--S161	A119--S161	A116--A161	A113--S155	A109--S151	A153--S195
3.40:6.44	I129--F299	I121--F282	I121--F282	I118--F338	I115--F424	V111--F396	V155--F499
3.44:5.54	C133--M223	C125--M215	C125--M215	C122--T204	F119--M206	L115--M202	L159--M246
3.47:5.57	A136--V226	A128--V218	A128--V218	S125--V207	C122--F209	S118--L205	S162--L249
3.51:5.57	Y140--V226	Y132--V218	Y132--V218	Y129--V207	Y126--F209	Y122--L205	Y166--L249
3.51:5.60	Y140--R229	Y132--R221	Y132--R221	Y129--R210	Y126--K212	Y122--H208	Y166--R252
5.54:6.41	M223--M296	M215--M279	M215--M279	T204--L335	M206--M421	M202--L393	M246--L496
6.47:7.45	C302--N335	C285--N318	C285--N318	C341--N375	C427--N460	T399--N432	T502--N535
6.51:7.38	F306--F328	F289--L311	F289--L311	F345--T368	Y431--T453	Y403--G425	Y506--G528
6.51:7.39	F306--N329	F289--N312	F289--N312	F345--T369	Y431--I454	Y403--Y426	Y506--Y529

BW stands for Ballesteros Weinstein definition of residues.

Venkatakrishnan et. al. 2013

Figure 5. Phylogenetic three of dopaminergic system.

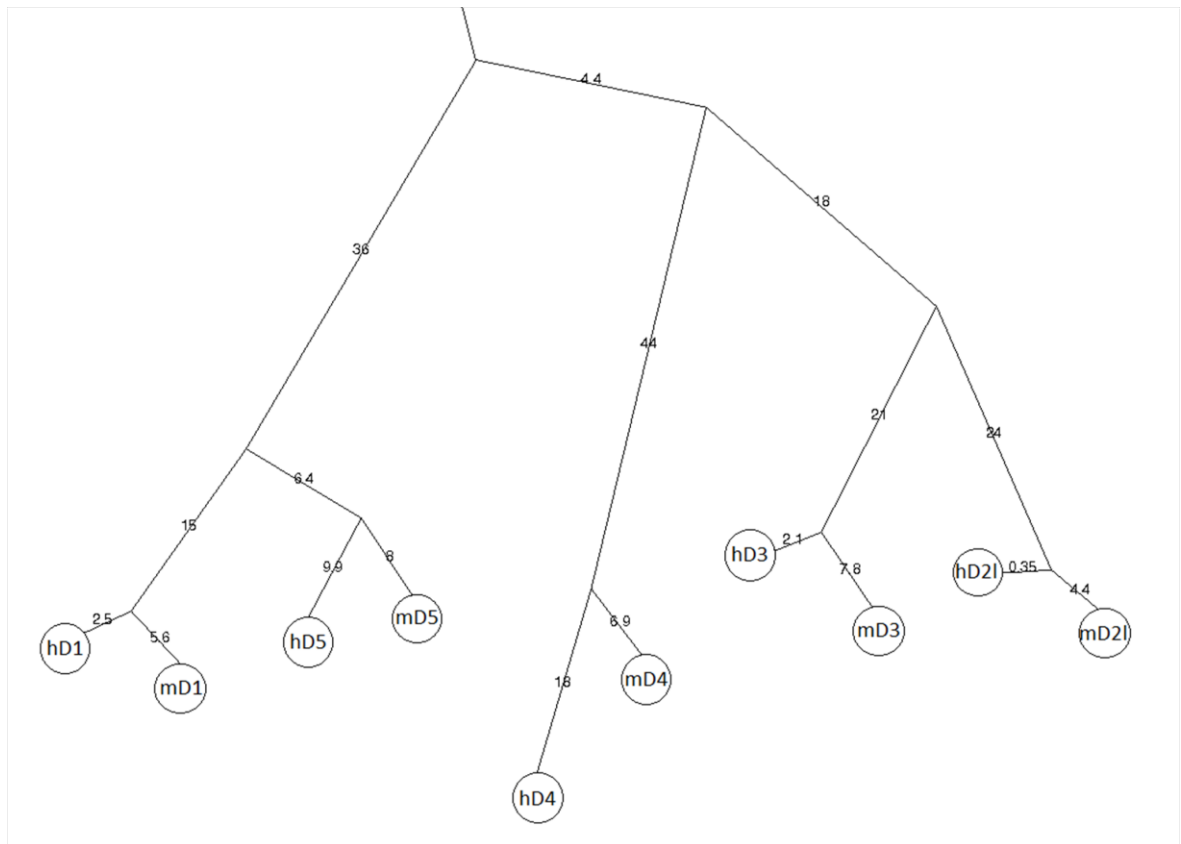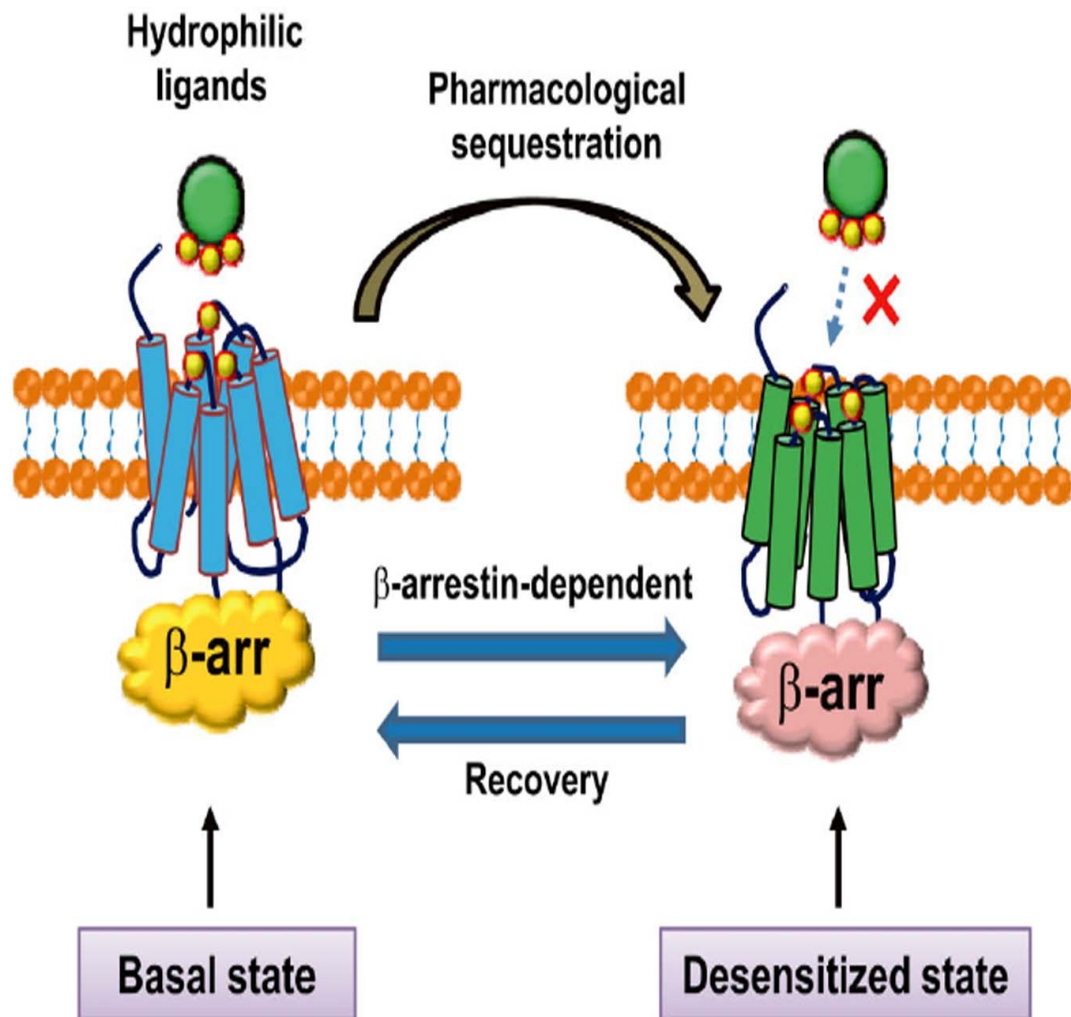Comparison between human and murine isoforms.

Figure 6. Biased signal of D$_3$ receptor

CHAPTER I

HOMOLOGY MODELING OF DOPAMINE D_2 AND D_3 RECEPTORS: MOLECULAR DYNAMICS REFINEMENT AND DOCKING EVALUATION

Chiara Bianca Maria Platania, Salvatore Salomone, Gian Marco Leggio, Filippo Drago, Claudio Bucolo

Department of Clinical and Molecular Biomedicine, Section of Pharmacology and Biochemistry, Catania University, Catania, Italy.

Abstract

Dopamine (DA) receptors, a class of G-protein coupled receptors (GPCRs), have been targeted for drug development for the treatment of neurological, psychiatric and ocular disorders. The lack of structural information about GPCRs and their ligand complexes has prompted the development of homology models of these proteins aimed at structure-based drug design. Crystal structure of human dopamine D_3 (hD_3) receptor has been recently solved. Based on the hD_3 receptor crystal structure we generated dopamine D_2 and D_3 receptor models and refined them with molecular dynamics (MD) protocol. Refined structures, obtained from the MD simulations in membrane environment, were subsequently used in molecular docking studies in order to investigate potential sites of interaction. The structure of hD_3 and hD_{2L} receptors was differentiated by means of MD simulations and D_3 selective ligands were discriminated, in terms of binding energy, by docking calculation. Robust correlation of computed and experimental K_i was obtained for hD_3 and hD_{2L} receptor ligands. In conclusion, the present computational approach seems suitable to build and refine structure models of homologous dopamine receptors that may be of value for structure-based drug discovery of selective dopaminergic ligands.

Introduction

The dopaminergic systems in the central nervous system (CNS) have been extensively studied over the past 50 years [1]. Dopamine exerts its action through five distinct G-protein coupled receptors (D_{1-5} receptors), grouped in two classes, D_1-like and D_2-like receptors, that differ in their signal transduction, binding profile and physiological effects [1]. D_1-like receptors (D_1 and D_5) are principally coupled to stimulatory G_s-proteins and

enhance the activity of adenylyl cyclase (AC), whereas D_2-like receptors (D_2, D_3, and D_4) are primarily coupled to inhibitory G_i-proteins and suppress the activity of AC [1].

Alternative splicing of D_2 receptor mRNA leads to generation of two isoforms: D_2 short (D_{2S}) and D_2 long (D_{2L}), which have been associated (though not exclusively) with presynaptic and postsynaptic populations of D_2 receptors, respectively [2]. The difference between these two splicing isoforms is represented by 29 amino acid residues in the III intracellular loop (3ICL), involved in the G protein coupling. The D_{2S} is mainly considered as a presynaptic receptor, whereas, the D_{2L} as a postsynaptic receptor [2], like the D_3 [3]. However, it has been suggested that D_3, in addition to the classical postsynaptic location, is also localized in the presynapse, where it modulates dopamine release and synthesis [4], [5]. D_2 and D_3 receptors display a high degree of sequence homology and share the putative binding site for dopamine and synthetic ligands at the interface of transmembrane helices [6]. D_2 and D_3 receptors also share the signal-transduction mechanism, though under certain conditions the latter may exert a weaker stimulation of effectors like AC [7], [8]. Several pathological conditions such as schizophrenia, Parkinson's disease, Tourette's syndrome, and hyperprolactinemia have been linked to a dysregulation of dopaminergic transmission [1]. Furthermore, D_2 and D_3 receptor have been implicated as potential target for drug development in ocular diseases such as glaucoma [9], [10], [11], [12], [13], [14], [15]. D_2-like receptors represent the most relevant class in the pathophysiology of neurological and psychiatric disorders. However, while D_2 receptor is considered the principal target to control the positive symptoms of schizophrenia, none of antipsychotics approved so far discriminates D_2 from D_3 receptors; on the other hand, the functional significance of D_4 receptor largely remains to be defined.

Human dopamine D_2 receptor (hD_2) and hD_3 are highly homologous [16], sharing 78% of sequence identity in the transmembrane domains [17], [18], including the binding site [19]. This sequence identity has introduced difficulties in the design of selective ligands. However, in the past two decades, medicinal chemists have succeeded, by using ligand-based approaches, in developing selective agonists such as aminotetralins: 7-hydroxy-2-dipropylaminotetralin (7-OH-DPAT) [20], trans-7-hydroxy-2-[N-propyl-N(3′-iodo-2′-propenyl)amino]tetratalin(7-OH-PIPAT) [21], [22] and rotigotine [23], [24]. Because the pharmacokinetic profile of 7-OH-DPAT was unsatisfactory, a bioisosteric replacement of the hydroxyphenyl group was carried out [25], leading to ligands selective for D_3 over D_2 subtype: quinpirole and pramipexole [26]. More recently a compound with the pyrazole moiety of quinpirole, FAUC 329, was found to selectively activate D_3 receptor [K_i = 4.3

nM] over D_2 receptor and it has a partial agonist activity (52% compared to quinpirole) [27]. Other drug design studies were carried out successfully by Lopez et al [28] who reported benzolactam derivatives with distinct selectivity against D_3 and D_2 receptors; functionalized benzolactam compounds were reported to have D_3 dopaminergic agonism [29]. Recently, Tschammer et al [30] synthesized heterocyclic dopamine surrogates, among which one compound (biphenylcarboamide (S)-5a) has a very high affinity (27 pM) at the D_3 receptor and high selectivity over D_2 subtype.

The crystal structure of hD_3 has been solved [31] and identified as a powerful tool for structure-based drug discovery of selective dopaminergic D_2-like ligands [32]. This crystallized receptor is a hD_3-lysozyme chimera, where the 3ICL is replaced by the lysozime protein; moreover, the receptor bears the mutation Leu119Trp in order to increase the thermal stability of the system. Recently, the determination of the crystal structure of hD_3 receptor and subsequent efforts in molecular modeling led to successful prediction of the pose of eticlopride in complex with a refined homology model of D_3 receptor [33]. Kortagere et al [34] analyzed in 2011 the binding mode of preferential D_3 ligands by means of site-directed mutagenesis and homology modeling studies (template structure 2RH1); these authors identified Ser 192 of V helix as an important site of interaction for the activation of D_3 receptor. Ser 192 belongs to a cluster of three serine residues (Ser 192, Ser 193, Ser 196); thus we have carefully looked at these residues, and their homologous (Ser 193, Ser 194, Ser 197) in hD_{2L} subtype, in our docking protocol. The subtype selectivity of D_2-like ligands had been also studied before, by Wang et al [35], in the absence of structural information on D_3 and D_2 receptors, by a mixed structure-based (homology modeling using β_2-adrenergic and rhodopsin receptors, molecular dynamics of haloperidol-receptor complexes) and ligand-based approach (3D-QSAR). These authors, however, did not carry out docking calculations. No study published so far has used a total structure-based approach for modeling ligand interactions with the hD_3 and hD_{2L}. In the present study we aimed at building and validating homology models of hD_3 and hD_{2L} receptors using the hD_3 receptor structure (3PBL) as template. Furthermore, in order to better discriminate their structural difference as well as selective ligands, we have carried out a structural optimization by molecular dynamics (MD) simulations of these two receptors for 3 ns in an explicit palmitoyl-oleoyl-phosphatidyl-choline (POPC) bilayer, that mimics the plasma membrane lipid environment, reaching a structural differentiation of these homologous receptors. The short-term MD simulations were adequate to obtain optimized structures of hD_3 and hD_{2L} receptors, because of the high homology and

sequence identity between target and template proteins. We have validated these optimized structures using a total structure-based approach by molecular docking calculations that are extremely influenced by the reliability of receptor structure. The validation of optimized structure models was successful, giving good correlation between experimental and predicted K_i of agonists.

Methods

Homology Modeling

The retrieved (Swiss-Prot) protein sequences of hD_3 and hD_{2L} receptors are respectively: P35462.2 and P14416.2. Homology models of hD_3 and hD_{2L} receptors were obtained by the Automated Modeling tool of Swiss Model web service http://swissmodel.expasy.org/[36], [37] using the crystal structure of the human D_3 dopaminergic receptor-lysozyme chimera (Protein Data Bank-code 3PBL) in complex with the antagonist eticlopride as template. N-terminals of receptors were not modeled, because we focused on the binding pocket. Moreover the structure of N-terminal of hD3 was not solved by Chien et al [26]. The terminal residues Tyr 32 in hD3 and Tyr 37 in hD_{2L} were blocked in the homology models by acetylation. The hD_3 model was validated by docking eticlopride in the binding pocket. The model validation was carried out using two different molecular docking software (the docking protocol is reported in the Docking section): Autodock Vina (Vina) and Autodock 4.2 (AD4.2).

Molecular Dynamics

Homology models of dopaminergic receptors were embedded in a pre-equilibrated POPC bilayer. Then, the systems were hydrated with TIP3P water molecules, and neutralized adding NaCl up to 150 mM. CHARMM 27 parameters were assigned to all molecules. Disulfide bridges of hD_3 were parameterized by involving the following residues: Cys 103-Cys 181 connecting the III helix with the II extracellular loop (2ECL) and Cys 355-Cys 358 in the 3ECL. In the hD_{2L} model we parameterized the conserved disulfide bridge between the III helix and 2ECL involving the Cys 109-Cys 187 residues. The system preparation processes (building of bilayer, embedding of the proteins into the membrane, hydration and neutralization) were done using VMD v1.8.7 [38]. Before MD simulations the systems were equilibrated as follows: i) MD of lipid tails for 50 ps (time-step = 1 fs) while protein, water, ions and lipid head groups were kept fixed; ii) equilibration for 100

ps (time-step = 1fs) of water-ions-lipids, while proteins were kept fixed by applying harmonic constraints; iii) 500 ps (time step = 1 fs) of system equilibration, with no constraints applied to molecules. After the described steps of equilibration, 3 ns of MD simulation were carried out with time-step of 2 fs, collecting trajectory data every 10 ps. The SHAKE algorithm, which constraints the hydrogen-heavy atom bonds.was applied. Equilibration steps and simulations were carried out using NAMD v2.7 [39]. Langevin dynamics and piston were used to maintain constant temperature (300 K) and pressure (1 atm) during simulation. The area per lipid was maintained constant, after the equilibration steps (NPAT ensemble). The particle number of systems was 83242 for hD_3-lipids-water-ions and 83429 for hD_{2L} in membrane. Periodic Boundary Conditions (PBC) and Particle Mesh Ewalds (PME) method [40] were used to treat long-term electrostatics (time-step of 4 fs). The cut-off at 10 Å was applied to Van der Waals and coulombic interactions and switching functions started at 9 Å. First stage minimization was performed using the steepest descent algorithm whereas the conjugate gradient was used during production runs.

Docking and Virtual Screening

We carried out two different molecular docking studies using Vina and AD4.2 software. Vina [41] is an accurate algorithm faster than AD4.2; for this reason it was used for docking calculation of a large group of D_2-like ligands and for virtual screening study. AD 4.2 [42] provided the best prediction of pose of eticlopride in the hD_3 homology model, thus we have chosen it for accurate docking calculation such as prediction of K_i of well-known D_2-like agonists docked into the refined homology models of hD_3 and hD_{2L} receptors. File preparation for AD4.2 docking calculations was carried out using the AutodockTool (ADT), a free graphics user interface (GUI) of MGL-tools.

The search space for all docking calculations included the orthosteric binding pocket individuated by eticlopride in 3PBL, the allosteric binding pocket reported by Chien et al [31] and the extracellular domain of receptors. An high exhaustiveness, 32, was used in Vina calculation because the search space applied to hD_3 and hD_{2L} receptor is relatively wide. In calculations carried out with AD4.2 we chose, as search algorithm, the time-consuming Lamarkian genetic algorithm (GA), that generated the best docking results for eticlopride in hD_3 homology model. Hundred iterations of GA with 2,500,000 energy evaluations per run were carried out. Population size was set to 150 and a maximum of 27,000 generations per run was carried out, followed by automatic clusterization of poses.

Top scored (lowest energy) and more populated poses with orthosteric binding, as reported by Kortagere et al [34],were selected for analysis of ligand-protein interactions using the GUI ADT. AD 4.2 uses a semi-empirical free energy function and a charge-based method for desolvation contributes; the free energy function was calibrated using a set of 188 structurally known ligand-complexes with experimentally determined binding constants [43]. The binding energy of ligand poses (Kcal/mol) is the sum of intermolecular energy, internal energy of the ligand and torsional free energy minus the unbound-system energy (see in Supporting Information S1 about the calculation of K_i from AD4.2 binding energy values and Supporting Information S2 for ligand poses and optimized structure of receptors).

Ligand Dataset

Structure files of ligands were retrieved from PubChem [44], ZINC database [45], and, when not available there, from PRODRG web service (http://davapc1.bioch.dundee.ac.uk/prodrg/), as.mol2 files [46]. Whenever a conversion of file format was necessary it was done by Open Babel [47]. Protonation state of ligands was assigned at pH = 7.4. Three replicas of dockings were carried before and after MD simulations in order to assess the structure differentiation of homology model simulated in membrane. The following ligands were used in fast docking calculations with Vina: r-7-OH-DPAT, s-7-OH-DPAT, r-7-OH-PIPAT, s-7-OH-PIPAT, bromocriptine, lergotrile, lisuride, pergolide, cianergoline, cabergoline, SDZ-GLC-756, PD128907, pramipexole, rotigotine, ropinirole, eticlopride, U99194A, Ru24213, GR103691, r-GSK89472, s-GSK89472, s-nafadotride, NGB2904, PG01037, PNU177864, SB-269-652, S33084, SB277011A, S14297, S17777 and compounds of the USC series from Ortega et al [29] (USC-A401, USC-B401, USC-H401, USC-I401, USC-K401, USC-M401). The D_3 agonists, represented in Figure 1, r-7-OH-DPAT, r-7-OH-PIPAT, pramipexole, ropinirole, rotigotine, quinpirole, dopamine, PD128907 and cis-8-OH-PBZI (cis-8-hydroxy-3-(n-propyl)1,2,3a.4,5,9b-hexahydro-1H-benz[e]indole) were docked with AD4.2 into the hD_3 and hD_{2L} receptors optimized by MD; the predicted K_i values were correlated to the experimental ones. Eighty nine compounds, retrieved from ZINC database, were used to build a small focused drug-like database of ligands (according to the Lipinski's rule of five and similar at 70% to pramipexole); they were docked with Vina into hD_3 and hD_{2L} refined receptors. Structural alignments of proteins and figures were done with the molecular visualization software Open PyMOL. All software utilized in our study were open source

or under free of charge academic license. Computational hours were provided by the GRID service "Consorzio Cometa" [http://www.consorzio-cometa.it/].

Results

Homology Modeling

We built the homology models of hD_3 and hD_{2L} receptors. Two disulfide bridges were modeled in hD_3 receptor according to the crystal structure 3PBL [31], the canonical one that connect the 2ECL with the III helix and the disulfide bridge in the 3ECL involving residues Cys 355 and Cys 358. In hD_{2L} receptor only the conserved disulfide bridge was modeled, because we considered that a single residue of distance between the two conserved cysteine residues (Cys 399 and Cys 401) may lead to unstable disulfide bond. Validation for the hD_3 model, by docking eticlopride with Vina and AD4.2 was performed. Both software were able to reproduce the eticlopride conformation in the binding pocket; AD4.2 gave the lowest root mean square deviation (RMSD, 0.4 Å) and better reproduced the internal H-bonds (Figure 2A), compared to VINA (Figure 2B), that gave 0.6 Å RMSD for re-docked eticlopride. We have evaluated the similarity of hD_3 and hD_{2L} homology models by means of structural alignment. The tridimensional alignment revealed that the two homology models did not differ in transmembrane core structure (Figure 3A), as expected from their high sequence identity; furthermore, RMSD between the two aligned GPCRs was very low (0.033 Å). We have, further, analyzed the structural similarity and capacity of discrimination of active D_2-like ligands by fast docking calculations, with the Vina docking software. The structure similarity was reflected by the high correlation (R^2 = 0.91, Figure 3C) of predicted binding energy of D_2-like ligands docked into the homology models of hD_3 and hD_{2L}. Thus, these two homology models do not seem useful, without a structural refinement, for virtual screening directed at the recognition of selective ligands.

Molecular Dynamics

We have simulated for 3 ns the hD_3 and hD_{2L} homology models in a water-membrane environment that reproduces the biological milieu where these two GPCRs are located, to further discriminate their structural difference. By reporting the RMSD of protein structure from the starting homology model, both receptors differentiate in structure and reach a relative stable conformational minimum roughly after 1.25 ns (Figure 4). Total energy (E_{tot}) and potential energy (E_p) of systems are constant during the MD simulation

(Supporting Information S1) and energy values of D_3 receptor are slightly lower compared to the energy of D_{2L} subtype. We stopped simulations at 3 ns because we reached stable local minima and distinct conformations for hD_3 and hD_{2L} receptors. Longer simulations (over 30 ns) might reveal other local minima and further characterize the conformational space of these receptors; this goal, however, is beyond the aim of our study. GPCRs are in equilibrium between active and inactive conformation, and, as far as the inactive conformation is concerned, a structural marker, the "ionic lock" was described in several studies [48], [49], [50], [51] and was also revealed in the crystal structure of eticlopride-hD_3 complex (3PBL) [31]. This ionic lock involves, four conserved residues, Arg128-Asp127-Glu324-Tyr138 in hD_3 (Figure 5A), and Arg132-Asp131-Glu368-Tyr142 in hD_{2L} receptor (Figure 5B), respectively. The salt-bridges that constitute the ionic lock are retained during the 3 ns of simulation. We can assume that the conformation of receptors, that reached the relative minimum, describes the inactive state. The superimposition of the simulated hD_3 and hD_{2L} receptors confirmed the structural deviation of receptors in membrane, as the RMSD was 1.63 Å (Figure 3B). The differentiation of the two homologous receptors was further strengthen by the lower correlation ($R^2 = 0.74$) of binding energies of D_2-like ligands docked, with VINA, into hD_3 and hD_{2L} optimized structures (Figure 3D). We have measured the Cα deviation of residues belonging to the orthosteric binding pocket of receptors in order to further characterize the structural modification of hD_3 and hD_{2L} induced by the membrane environment. The deviations of these residues, comparing the initial homology models with the refined structures are reported in Table 1. The residues of binding pocket of hD_{2L} receptor deviated from starting model more than residues of hD_3 subtype (Table 1). The V helix of hD_{2L} receptor had the greater deviation than other helices after the simulation (Supporting Information S1), involving the extracellular and intracellular side (transversal to the plane of the membrane). The VI and VII helices deviated mostly in the extracellular side and the greater deviation is shown for the VII helix (Supporting Information S1). Within the seven helices of hD_{2L} receptor, only IV helix had a major transversal deviation and a sensible deviation along the z-axis of membrane (Supporting Information S1). Furthermore, the binding pocket of hD_3 receptor was also remodeled in membrane, because there were major structural deviations involving the residues of V helix (Ser 192, Ser 193, Ser 196), VI helix (His 349) and VII helix (Tyr 375) (Table 1 and Supporting Information S1). We further characterized the binding pocket of hD_3 and hD_{2L}, before and after refining with MD simulations, by using the web service fpocket http://fpocket.sourceforge.net/ [52].

Fpocket generates clusters of spheres to describe each pocket of a given protein; in Figure 6 we have assigned different colors to pockets of hD_3 and hD_{2L} receptors, before and after optimization. Before simulation in membrane, the binding pockets of the two receptors were very similar in shape and dimension. After simulation, the pocket of hD_3 became smaller than that of hD_{2L} and divided in three pockets (Figure 6C); the one in blue includes the orthosteric and the allosteric pockets, the one in magenta is surrounded by the extracellular loops, and the deepest and smallest pocket is colored in red. In docking calculations, we did not find poses in the red pocket, that was occupied by water molecules during MD simulation (data not shown). The pocket of hD_{2L} after simulation became bigger than that of D_3 subtype (Figure 6B and 6D). The hD_{2L} receptor after simulation shows a big pocket (orange spheres) and a smaller pocket (magenta) located along the big one, between the III and IV helices. After simulation the red pocket of hD_{2L} appears included within the orange one (Figure 6B and 6D). The optimized structures of hD_3 and hD_{2L} used for analysis and docking calculations were extracted randomly from one of the last frames of simulations that characterize the relative conformational equilibrium, by considering as equivalent frames belonging to the same local minimum. To confirm this assumption we randomly selected one additional frame from each local minimum of the hD_3 and hD_{2L} MD simulations. These two additional frames resulted equivalent to the previous, because, when carrying out docking of pramipexole superimposable results were obtained both in terms of binding energy (Table 2, values in brackets) and poses (data not shown). We did not carried out a clusterization of trajectories because we have reached one local minimum in each simulation. Furthermore, as reported by Yap et al [53] clusterization of GPCR trajectories, is not useful for selecting the representative structure to be used in docking calculation.

Docking

We validated the optimized structures of hD_3 and hD_{2L} receptors by docking D_3–preferring receptor agonists into receptor binding pockets using AD 4.2 docking software, which provided the best result of eticlopride pose prediction in the hD_3 homology model. Binding energy of agonists docked in hD_3 and hD_{2L} receptors correlates with their higher affinity for the D_3 subtype (Table 2), consistent with more polar contacts of ligands docked into D_3 receptor compared to ligands docked into the D_{2L} subtype (Table 3). The experimental pK_i values (retrieved from http://pdsp.med.unc.edu/free access database) of agonists were compared with the predicted values (Figure 7, see also Supporting Information S1)

obtaining a good correlation as indicated by Pearson coefficients relative to hD_3 and hD_{2L} receptors equal to 0.88 and 0.83 respectively ($p<0.005$). Linear regression coefficients however were low (Figure 7), due to the limitations of AD4.2 in predicting absolute values of K_i, as reported by Lape et al [54] and by Yap et al [55]. Another explanation to the mentioned issue might be related to the heterogeneity in K_i determination assays. Quinpirole was not included in the regression analysis because it was an outlier, even though its predicted binding energies for hD_3 and hD_{2L} correlate with the higher affinity toward the D_3 subtype. Quinpirole is a bioisoster of DPAT, among other ligands included in the regression model (Figure 1), with a tricyclic structure where the hydroxyphenyl group is substituted with a pyrazolic group. On the contrary, PD-128907, a tricyclic compound with the hydroxyphenyl group, fits in the regression model of pK_i for hD_3 and hD_{2L} receptor. Another tricyclic compound included in the regression model is cis-8-OH-PBZI (PBZI), which retains the position of hydroxyl and amine groups of 7-OH-DPAT. The affinity of PBZI was determined for D_{2S}, D_3 and D_4 receptors but not for D_{2L} receptor, therefore we did not include it in the regression model for hD_{2L} receptor. Recently, PBZI was found to not induce tolerance and slow response termination, in comparison to known agonists such as 7-OH-DPAT and pramipexole [56]. Comparing the tricyclic structures of PD-128907, PBZI and quinpirole, this latter might behave as an outlier in the chemical space, due to the substitution of the hydroxyphenyl moiety with the pyrazol condensed group.

Virtual Screening

Pramipexole is a selective D_3 agonist ($D_2/D_3 = 75.5$) indicated in the treatment of early-stage Parkinson disease. This agonist was chosen as reference for building a small ligands database (89 molecules), where drug-like compounds are 70% similar to pramipexole. We carried out a virtual screening by docking these ligands into the refined hD_3 and hD_{2L} models. The top scored compound is a novel selective D_2-like agonist synthesized by Ghosh et al [57] (-)-(S)-N6-Propyl-N6-(2-(4-(4-(pyridin-4-yl)phenyl)piperazin-1-yl)-ethyl)-4,5,6,7-tetrahydrobenzo[d]-thiazole-2,6-diamine,deposited in the ZINC database with the name ZINC45254546. This compound is reported to have high affinity towards hD_3 subtype ($D_{2L}/D_3 = 56.5$) (Table 4). ZINC45254546 (Figure 1) is an hybrid compound bearing a pramipexole moiety and a piperazin(4-phenyl(4pyridyl)) antioxidant group. This compound was re-docked with AD4.2, into hD_3 and hD_{2L} receptors. As shown in Figure 8, polar contacts involved aspartate and threonine residues in III helix and the cluster of

serine residues in V helix that interact with the pramipexole group. The analysis of pose of ZINC45254546 did not show the H-bond with Asp114 in hD_{2L}, which may explain its lower affinity toward the D_{2L} subtype. The piperazin(4-phenyl(4pyridyl)) group interacted with part of the 2ECL in hD_3 subtype and with residues of II and VII helices in hD_{2L} receptor, that characterize the allosteric pocket. The top 30 compounds (ZINC-db code), docked into hD_3 and hD_{2L} receptors, are reported in Supporting Information S1.

Discussion

In the present study we have successfully modeled and optimized the structure of two high homologous GPCRs, the hD_3 and hD_{2L} receptors. The homology modeling is a powerful tool in the prediction of protein structure. The strength of this methodology is related to the sequence identity shared between the target and the template protein: the highest sequence identity determines the best structure model. We built and validated the homology models of hD_3 and hD_{2L} receptor using the x-ray structure of hD_3 receptor, a lysozyme-chimera protein. The high sequence identity shared by these two receptors did not allow us to differentiate their homology models that were therefore unsuitable for prediction of binding energies and subtype selectivity of D_2-like ligands. The high structure similarity of hD_3 and hD_{2L} arises from the energy minimization process, and represents a weakness in the homology modeling approach. Usually, in homology modeling, the energy optimization of the modeled protein structure is performed by energy minimization *in vacuo*, with some exceptions such as the GPCRRD server http:/zhanglab.ccmb.umich.edu/GPCRRD/. GPCRRD carries out a pipeline of structural optimizations of homology models, with a final MD simulation: Fragment-Guided Molecular Dynamics (FD-MD), which takes into account knowledge-based (H-bonds and positional restraints) and physics-based atomic potentials (AMBER99 forcefield) [58], [59]. So far protein-lipid and protein-water explicit interactions, based on empirical physics-based atomic potentials, are not taken into account by homology modeling software. Thus, we attempted to optimize the structure of the hD_3 and hD_{2L} models by MD in an explicit water-membrane environment, reaching a local conformational minimum within 3 ns. The MD simulations led to structural adaptation and differentiation of the two receptors in membrane, enabling the prediction of trends of pK_i values and the modeling of ligand-protein interactions of D_3-preferring receptor agonists. Moreover, the refined models were useful in the identification, by a virtual screening approach, of an agonist (ZINC45254546) referred to be selective for D_3 over D_2 [57]. Our results are consistent

with the findings of Chien et al [26]; the hD_3 homology model we built was validated by docking eticlopride and by obtaining with AD 4.2 a pose highly similar to the one in the x-ray structure 3PBL. Because the ionic lock, a marker of inactive state described in 3PBL, was retained during MD simulations in both hD_3 and hD_{2L} receptors, we can assume that refined models represent an inactive state of the receptors. Moreover, we modeled both disulfide bridges solved in 3PBL in hD_3 model and we modeled just one disulfide bridge, the canonical one, in hD_{2L}. We made this choice because the conserved cysteine residues in the 3ECL, Cys 399 and Cys 401, are separated just by one residue Asp 400, leading to a high constrained loop in the case a disulfide bridge is formed. The lack of the accessory disulfide bridge in the 3ECL might have influenced the dynamics of hD_{2L} receptor, leading to the swelling of its binding pocket, in comparison to the hD_3 which is restrained by two disulfide bridges. Wang et al [60] have predicted the structural differences of hD_3 and hD_2 receptors. The homology models of these GPCRs were built in complex with haloperidol (previously aligned to the β_2-adrenergic inverse agonist s-carazolol), using the crystal structure of β_2-adrenergic receptor (2RH1); the complexes were subsequently simulated in a POPC bilayer for 1.5 ns. Haloperidol in complex with simulated D_3 and D_2 receptors was also used to carry out 3D-QSAR studies using 163 compounds. These authors [35] concluded that the higher affinity of bigger ligands for D_3 receptor over D_2 subtype is related to the shape of binding pocket, which is shallower in D_2 receptor. We found that the binding pocket of hD_3 receptor, after adapting in the membrane environment, significantly deviates from the initial homology model, becoming smaller and partitioned. The binding pocket of hD_3 in membrane environment is also smaller than the one of hD_{2L} receptor. We carried out docking calculations rather than 3D-QSAR (ligand-based method) because we considered our refined models highly predictive due to the crystal structure of hD_3 receptor, used as template for homology modeling. Docking calculations (structure-based method) are strictly related to the reliability of the receptor structure, and we obtained a good correlation of experimental and computed K_i values for agonists docked into hD_3 and hD_{2L} binding sites. Although the prediction of absolute K_i values is a difficult task, AD 4.2 was a powerful tool in order to validate homology model of hD_3 receptor (eticlopride re-docking) as well as to validate the refined models by MD simulations. In fact, the predicted trend of K_i values is well correlated (high Pearson coefficients) with the experimental trend. This correlation was carried out with aminotetraline derivatives, a congeneric chemical class that does not include quinpirole. This latter is a preferential D_3 agonist, but behaved as an outlier in the chemical space of docked ligands, due to the tricyclic structure

and the pyrazole moiety. Neverthless, our optimized models were able to predict the affinity of quinpirole higher for D_3 than for D_{2L} receptor. In conclusion, the computational approach, totally structure-based, adopted in the present study is able to build and refine structure models of homologous dopamine receptors that may be of interest for structure-based drug discovery of selective dopaminergic ligands, potentially useful to treat neurological, psychiatric and ocular disorders.

Author Contributions

Conceived and designed the experiments: CBMP CB GML. Performed the experiments: CBMP. Analyzed the data: CBMP CB SS. Contributed reagents/materials/analysis tools: CBMP CB. Wrote the paper: CBMP CB GML SS FD.

References

1. Beaulieu JM, Gainetdinov RR (2011) The physiology, signaling, and pharmacology of dopamine receptors. Pharmacological reviews 63: 182–217.

2. Lindgren N, Usiello A, Goiny M, Haycock J, Erbs E, et al. (2003) Distinct roles of dopamine D2L and D2S receptor isoforms in the regulation of protein phosphorylation at presynaptic and postsynaptic sites. Proc Natl Acad Sci U S A 100: 4305–4309.

3. Landwehrmeyer B, Mengod G, Palacios JM (1993) Dopamine D3 receptor mRNA and binding sites in human brain. Brain Res Mol Brain Res 18: 187–192.

4. Diaz J, Pilon C, Le Foll B, Gros C, Triller A, et al. (2000) Dopamine D3 receptors expressed by all mesencephalic dopamine neurons. J Neurosci 20: 8677–8684.

5. Chen PC, Lao CL, Chen JC (2009) The D(3) dopamine receptor inhibits dopamine release in PC-12/hD3 cells by autoreceptor signaling via PP-2B, CK1, and Cdk-5. J Neurochem 110: 1180–1190.

6. Ballesteros JA, Shi L, Javitch JA (2001) Structural mimicry in G protein-coupled receptors: implications of the high-resolution structure of rhodopsin for structure-function analysis of rhodopsin-like receptors. Mol Pharmacol 60: 1–19.

7. Neve KA, Seamans JK, Trantham-Davidson H (2004) Dopamine receptor signaling. J Recept Signal Transduct Res 24: 165–205.

8. Sokoloff P, Diaz J, Le Foll B, Guillin O, Leriche L, et al. (2006) The dopamine D3 receptor: a therapeutic target for the treatment of neuropsychiatric disorders. CNS Neurol Disord Drug Targets 5: 25–43.

9. Potter DE, Ogidigben MJ, Chu TC (1998) Lisuride acts at multiple sites to induce ocular hypotension and mydriasis. Pharmacology 57: 249–260.

10. Ogidigben M, Chu TC, Potter DE (1993) Ocular hypotensive action of a dopaminergic (DA2) agonist, 2,10,11-trihydroxy-N-n-propylnoraporphine. The Journal of pharmacology and experimental therapeutics 267: 822–827.

11. Potter DE, Shumate DJ (1987) Cianergoline lowers intraocular pressure in rabbits and monkeys and inhibits contraction of the cat nictitans by suppressing sympathetic neuronal function. Journal of ocular pharmacology 3: 309–321.

12. Mekki QA, Hassan SM, Turner P (1983) Bromocriptine lowers intraocular pressure without affecting blood pressure. Lancet 1: 1250–1251.

13. Geyer O, Robinson D, Lazar M (1987) Hypotensive effect of bromocriptine in glaucomatous eyes. Journal of ocular pharmacology 3: 291–294.

14. Chu E, Chu TC, Potter DE (2000) Mechanisms and sites of ocular action of 7-hydroxy-2-dipropylaminotetralin: a dopamine(3) receptor agonist. J Pharmacol Exp Ther 293: 710–716.

15. Bucolo C, Leggio GM, Maltese A, Castorina A, D'Agata V, et al. (2011) Dopamine-3 receptor modulates intraocular pressure: implications for glaucoma. Biochem Pharmacol 83: 680–686.

16. Sibley DR, Monsma FJ Jr (1992) Molecular biology of dopamine receptors. Trends Pharmacol Sci 13: 61–69.

17. Levant B (1997) The D3 dopamine receptor: neurobiology and potential clinical relevance. Pharmacol Rev 49: 231–252.

18. Sokoloff P, Giros B, Martres MP, Bouthenet ML, Schwartz JC (1990) Molecular cloning and characterization of a novel dopamine receptor (D3) as a target for neuroleptics. Nature 347: 146–151.

19. Shi L, Javitch JA (2002) The binding site of aminergic G protein-coupled receptors: the transmembrane segments and second extracellular loop. Annu Rev Pharmacol Toxicol 42: 437–467.

20. Malmberg A, Nordvall G, Johansson AM, Mohell N, Hacksell U (1994) Molecular basis for the binding of 2-aminotetralins to human dopamine D2A and D3 receptors. Mol Pharmacol 46: 299–312.

21. Chumpradit S, Kung MP, Kung HF (1993) Synthesis and optical resolution of (R)- and (S)-trans-7-Hydroxy-2-[N-propyl-N-(3′-iodo-2′-propenyl)amino]tetralin:a new D3 dopamine receptor ligand. J Med Chem 36: 4308–4312.

22. Chumpradit S, Kung MP, Vessotskie J, Foulon C, Mu M, et al. (1994) Iodinated 2-aminotetralins and 3-amino-1-benzopyrans: ligands for dopamine D2 and D3 receptors. J Med Chem 37: 4245–4250.

23. Martin PL, Kelly M, Cusack NJ (1993) (-)-2-(N-propyl-N-2-thienylethylamino)-5-hydroxytetralin(N-0923), a selective D2 dopamine receptor agonist demonstrates the presence of D2 dopamine receptors in the mouse vas deferens but not in the rat vas deferens. J Pharmacol Exp Ther 267: 1342–1348.

24. Reynolds NA, Wellington K, Easthope SE (2005) Rotigotine: in Parkinson's disease. CNS drugs 19: 973–981.

25. Glase SA, Corbin AE, Pugsley TA, Heffner TG, Wise LD (1995) Synthesis and dopaminergic activity of pyridine analogs of 5-hydroxy-2-(di-n-propylamino)tetralin. J Med Chem 38: 3132–3137.

26. Mierau J, Schneider FJ, Ensinger HA, Chio CL, Lajiness ME, et al. (1995) Pramipexole binding and activation of cloned and expressed dopamine D2, D3 and D4 receptors. Eur J Pharmacol 290: 29–36.

27. Bettinetti L, Schlotter K, Hubner H, Gmeiner P (2002) Interactive SAR studies: rational discovery of super-potent and highly selective dopamine D3 receptor antagonists and partial agonists. J Med Chem 45: 4594–4597.

28. Lopez L, Selent J, Ortega R, Masaguer CF, Dominguez E, et al. (2010) Synthesis, 3D-QSAR, and structural modeling of benzolactam derivatives with binding affinity for the D(2) and D(3) receptors. ChemMedChem 5: 1300–1317.

29. Ortega R, Hubner H, Gmeiner P, Masaguer CF (2011) Aromatic ring functionalization of benzolactam derivatives: new potent dopamine D3 receptor ligands. Bioorganic & medicinal chemistry letters 21: 2670–2674.

30. Tschammer N, Elsner J, Goetz A, Ehrlich K, Schuster S, et al. (2011) Highly potent 5-aminotetrahydropyrazolopyridines: enantioselective dopamine D3 receptor binding, functional selectivity, and analysis of receptor-ligand interactions. J Med Chem 54: 2477–2491.

31. Chien EY, Liu W, Zhao Q, Katritch V, Han GW, et al. (2010) Structure of the human dopamine D3 receptor in complex with a D2/D3 selective antagonist. Science 330: 1091–1095.

32. Carlsson J, Coleman RG, Setola V, Irwin JJ, Fan H, et al. (2011) Ligand discovery from a dopamine D3 receptor homology model and crystal structure. Nat Chem Biol 7: 769–778.

33. Obiol-Pardo C, Lopez L, Pastor M, Selent J (2011) Progress in the structural prediction of G protein-coupled receptors: D3 receptor in complex with eticlopride. Proteins 79: 1695–1703.

34. Kortagere S, Cheng SY, Antonio T, Zhen J, Reith ME, et al. (2011) Interaction of novel hybrid compounds with the D3 dopamine receptor: Site-directed mutagenesis and homology modeling studies. Biochemical pharmacology 81: 157–163.

35. Wang Q, Mach RH, Luedtke RR, Reichert DE (2010) Subtype selectivity of dopamine receptor ligands: insights from structure and ligand-based methods. Journal of chemical information and modeling 50: 1970–1985.

36. Arnold K, Bordoli L, Kopp J, Schwede T (2006) The SWISS-MODEL workspace: a web-based environment for protein structure homology modelling. Bioinformatics 22: 195–201.

37. Kiefer F, Arnold K, Kunzli M, Bordoli L, Schwede T (2009) The SWISS-MODEL Repository and associated resources. Nucleic Acids Res 37: D387–392.

38. Humphrey W, Dalke A, Schulten K (1996) VMD: visual molecular dynamics. J Mol Graph 14: 33–38, 27–38.

39. Phillips JC, Braun R, Wang W, Gumbart J, Tajkhorshid E, et al. (2005) Scalable molecular dynamics with NAMD. J Comput Chem 26: 1781–1802.

40. Darden T YD, Pedersen L (1993) Particle mesh Ewald: An N [center-dot] log(N) method for Ewald sums in large systems. J Chem Phys 98: 10089–10092.

41. Trott O, Olson AJ (2010) AutoDock Vina: improving the speed and accuracy of docking with a new scoring function, efficient optimization, and multithreading. J Comput Chem 31: 455–461.

42. Morris GM, Goodsell DS, Huey R, Olson AJ (1996) Distributed automated docking of flexible ligands to proteins: parallel applications of AutoDock 2.4. J Comput Aided Mol Des 10: 293–304.

43. Huey R, Morris GM, Olson AJ, Goodsell DS (2007) A semiempirical free energy force field with charge-based desolvation. J Comput Chem 28: 1145–1152.

44. Sayers EW, Barrett T, Benson DA, Bolton E, Bryant SH, et al. (2012) Database resources of the National Center for Biotechnology Information. Nucleic Acids Res 40: D13–25.

45. Irwin JJ, Shoichet BK (2005) ZINC–a free database of commercially available compounds for virtual screening. J Chem Inf Model 45: 177–182.

46. Schuttelkopf AW, van Aalten DM (2004) PRODRG: a tool for high-throughput crystallography of protein-ligand complexes. Acta Crystallogr D Biol Crystallogr 60: 1355–1363.

47. O'Boyle NM, Banck M, James CA, Morley C, Vandermeersch T, et al. (2011) Open Babel: An open chemical toolbox. J Cheminform 3: 33.

48. Ballesteros JA, Jensen AD, Liapakis G, Rasmussen SG, Shi L, et al. (2001) Activation of the beta 2-adrenergic receptor involves disruption of an ionic lock between the cytoplasmic ends of transmembrane segments 3 and 6. The Journal of biological chemistry 276: 29171–29177.

49. Okada T, Sugihara M, Bondar AN, Elstner M, Entel P, et al. (2004) The retinal conformation and its environment in rhodopsin in light of a new 2.2 A crystal structure. Journal of molecular biology 342: 571–583.

50. Palczewski K, Kumasaka T, Hori T, Behnke CA, Motoshima H, et al. (2000) Crystal structure of rhodopsin: A G protein-coupled receptor. Science 289: 739–745.

51. Vogel R, Mahalingam M, Ludeke S, Huber T, Siebert F, et al. (2008) Functional role of the "ionic lock"–an interhelical hydrogen-bond network in family A heptahelical receptors. Journal of molecular biology 380: 648–655.

52. Le Guilloux V, Schmidtke P, Tuffery P (2009) Fpocket: an open source platform for ligand pocket detection. BMC bioinformatics 10: 168.

53. Yap BK, Buckle MJ, Doughty SW (2012) Homology modeling of the human 5-HT(1A), 5-HT (2A), D1, and D2 receptors: model refinement with molecular dynamics simulations and docking evaluation. Journal of molecular modeling.

54. Lape M, Elam C, Paula S (2010) Comparison of current docking tools for the simulation of inhibitor binding by the transmembrane domain of the sarco/endoplasmic reticulum calcium ATPase. Biophys Chem 150: 88–97.

55. Yap BK, Buckle MJ, Doughty SW (2012) Homology modeling of the human 5-HT(1A), 5-HT (2A), D1, and D2 receptors: model refinement with molecular dynamics simulations and docking evaluation. J Mol Model.

56. Kuzhikandathil EV, Kortagere S (2012) Identification and Characterization of a Novel Class of Atypical Dopamine Receptor Agonists. Pharmaceutical research.

57. Ghosh B, Antonio T, Zhen J, Kharkar P, Reith ME, et al. (2010) Development of (S)-N6-(2-(4-(isoquinolin-1-yl)piperazin -1-yl)ethyl)-N6-propyl-4,5,6,7-tetrahydrobenzo[d]-thiazole-2,6-diamine and its analogue as a D3 receptor preferring agonist: potent in vivo activity in Parkinson's disease animal models. J Med Chem 53: 1023–1037.

58. Zhang J, Zhang Y (2010) GPCRRD: G protein-coupled receptor spatial restraint database for 3D structure modeling and function annotation. Bioinformatics 26: 3004–3005.

59. Zhang J, Liang Y, Zhang Y (2011) Atomic-level protein structure refinement using fragment-guided molecular dynamics conformation sampling. Structure 19: 1784–1795.

60. Wang Q, Mach RH, Luedtke RR, Reichert DE (2010) Subtype selectivity of dopamine receptor ligands: insights from structure and ligand-based methods. J Chem Inf Model 50: 1970–1985.

61. Millan MJ, Newman-Tancredi A, Audinot V, Cussac D, Lejeune F, et al. (2000) Agonist and antagonist actions of yohimbine as compared to fluparoxan at alpha(2)-adrenergic receptors (AR)s, serotonin (5-HT)(1A), 5-HT(1B), 5-HT(1D) and dopamine

D(2) and D(3) receptors. Significance for the modulation of frontocortical monoaminergic transmission and depressive states. Synapse 35: 79–95.

62. Millan MJ, Maiofiss L, Cussac D, Audinot V, Boutin JA, et al. (2002) Differential actions of antiparkinson agents at multiple classes of monoaminergic receptor. I. A multivariate analysis of the binding profiles of 14 drugs at 21 native and cloned human receptor subtypes. The Journal of pharmacology and experimental therapeutics 303: 791– 804.

63. Scheller D, Ullmer C, Berkels R, Gwarek M, Lubbert H (2009) The in vitro receptor profile of rotigotine: a new agent for the treatment of Parkinson's disease. Naunyn-Schmiedeberg's archives of pharmacology 379: 73–86.

64. Sokoloff P, Andrieux M, Besancon R, Pilon C, Martres MP, et al. (1992) Pharmacology of human dopamine D3 receptor expressed in a mammalian cell line: comparison with D2 receptor. European journal of pharmacology 225: 331–337.

65. Tadori Y, Forbes RA, McQuade RD, Kikuchi T (2011) Functional potencies of dopamine agonists and antagonists at human dopamine D(2) and D(3) receptors. European journal of pharmacology 666: 43–52.

66. Scheideler MA, Martin J, Hohlweg R, Rasmussen JS, Naerum L, et al. (1997) The preferential dopamine D3 receptor agonist cis-8-OH-PBZI induces limbic Fos expression in rat brain. European journal of pharmacology 339: 261–270.

Table 1. Deviations of Cα of residues belonging to the orthosteric binding pocket of optimized receptors in comparison with the starting models.

hD$_3$		hD$_{2L}$	
Residue	Cα deviation (Å)	Residue	Cα deviation (Å)
Asp 110 (III helix)	0.3	Asp 114 (III helix)	1.3
Ser 192 (V helix)	0.9	Ser 193 (V helix)	1.3
Ser 193 (V helix)	0.9	Ser 194 (V helix)	1.0
Ser 196 (V helix)	1.3	Ser 197 (V helix)	3.2
Trp 342 (VI helix)	0.3	Trp 386 (VI helix)	1.5
Phe 345 (VI helix)	0.3	Phe 389 (VI helix)	1.8
Phe 346 (VI helix)	0.3	Phe 390 (VI helix)	0.9
His 349 (VI helix)	0.6	His 393 (VI helix)	1.8
Tyr 375 (VII helix)	1.2	Tyr 416 (VII helix)	0.9

Table 2. Predicted binding energy (Autodock 4.2) of D_3 agonists towards hD_3 and hD_2 receptors. Experimental K_i (exp. K_i) with respective references are also shown.

D_3 agonist [reference]	hD_3 $E_{binding}$ (kcal/mol)	hD_2 $E_{binding}$ (kcal/mol)	hD_3 exp. K_i (nM)	hD_2 exp. K_i (nM)
Dopamine	-6.5	-6.0	32.5[1]	598[1]
r-7-OH-DPAT [61]	-7.7	-6.4	1.58	158
r-7-OH-PIPAT [19]	-8.4	-7.3	2.9[2]	142[2]
Pramipexole [62]	-7.1	-6.6	10.5	790
Pramipexole[3]	(-7.1)	(-6.4)		
Ropinirole [62]	-7.0	-6.4	37.2	933
Rotigotine [63]	-8.4	-7.4	0.71	13.5
Quinpirole [64]	-7.6	-6.6	39	1402
PD 128907 [65]	-7.7	-6.0	3.1	1573
cis-8-OH-PBZI [66]	-7.1	ND	27.4	ND

[1]Average value from PDSP database: http://pdsp.med.unc.edu/indexR.html. [2]The K_i is reported for the racemic 7-OH-PIPAT. [3]Pramipexole re-docked in two other frames of hD_3 and hD_{2L} receptor; see also text.

Table 3. Ligand protein-interaction of D_3–preferring receptor agonists docked with AD4.2.

Ligands	hD$_3$		hD$_{2L}$	
	Hydrogen bonds-polar contacts	Hydrophobic contacts	Hydrogen bonds-polar contacts	Hydrophobic contacts
Dopamine	Asp 110, Thr 115, Ser 192, Ser 196.	Ile 183, Phe 345, His 349.	Asp 114, Ser 194	Val 115, His 393, Phe 389, Phe 390.
r-7-OH-DPAT	Asp 110, Ser 192, Ser 196, Thr 115.	Ile 183, Phe 345, His 349.	Asp 114, , Ser 193.	Val 111, Phe 110, Ile 184, Phe 390.
r-7-OH-PIPAT	Asp 110, Val 111 (C=O of peptide bond), Thr 115, Ser 192.	Val 111, Val 107, Ile 183, Trp 342, Phe 345, His 349.	Asp 114, Val 190 (C=O of peptide bond), Ser 193.	Val 111, Phe 110, Ile 184, Phe 390.
Pramipexole	Asp 110, Thr 115, Ser 192, Ser 196.	Val 111, Trp 342, Phe 345, Thr 369.	Asp 114, Val 190 (C=O of peptide bond), Ser 194.	Phe 110, Val 111, Phe 390, His 393.
Ropinirole	Asp 110, Ser 192	Val 189, Trp 342, Phe 345, His 349, Tyr 373	Asp 114, Ser 193.	Val 111, Phe 110, Val 115, Phe 390, His 393
Rotigotine	Asp 110, Ser 192.	Val 107, Phe 106, Phe 345, Phe 346, His 349	Asp 114	Phe 110, Val 111, Val 115, Ile 184, Phe 390, His 393
Quinpirole	Asp 110, Ser 192	Val 111, Ile 183, Trp 342, Phe 345, Thr 369, Tyr 373.	Asp 114	Val 115, Trp 386, Phe 389, Gly 415, Tyr 416.
PD128907	Asp 110, Ser 192	Val 111, Ile 183, Phe 188, Trp 342, Phe 345, Phe 346, Thr 369, Tyr 373.	Asp 114	Val 111, Phe 389, His 393.
cis-8-OH-PBZI	Asp 110, Ser 192, Ser 196, , Thr 115	Val 111, Ile 183, Trp 342, Phe 346, Tyr 373, Thr 369.	*ND	*ND

*ND = Not Determined

Residues involved in H-Bonds are underlined.

Table 4. Virtual Screening. Top scored compound ZINC45254546.

	hD$_3$	hD$_{2L}$
Vina (Kcal/mol)	-8.7	-8.1
AD4.2 (Kcal/mol)	-8.8	-7.98
Exp. Ki (nM)	4.78	270
H-bonds and Polar contacts	Asp 110, Thr 115, Ser 196, Ser 182,	Ser 197, Ser 193, Thr 119
Hydrophobic interactions	Val 111, Ile 183, Phe 345, Phe 346, His 349, Tyr 365, Pro 362,Thr 369.	Leu 94, Val 91, Val 111, Ile 184, Val 115, Phe 198, Phe 389, Phe 390, His 393, Thr 412, Tyr 416.

Residues involved in H-bonds are underlined

Figure 1. D₂-like agonists

Dopamine

Ropinirole

PD 128,907
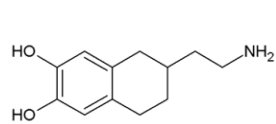
7-OH-DPAT
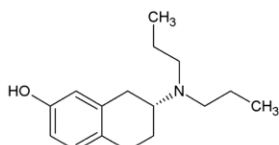
Rotigotine
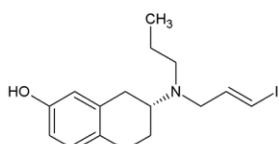
cis-8-OH-PBZI

7-OH-PIPAT
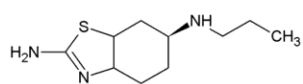
Pramipexole
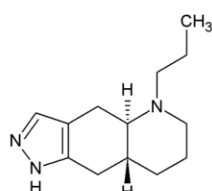
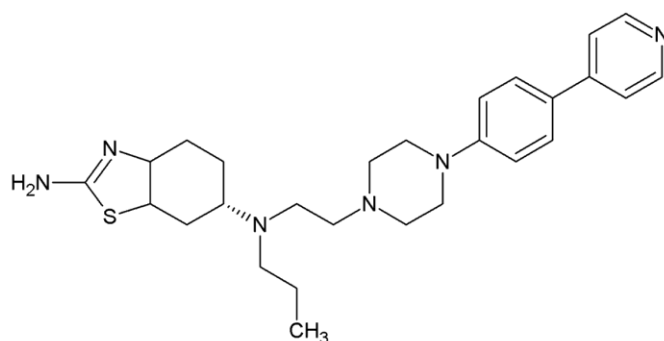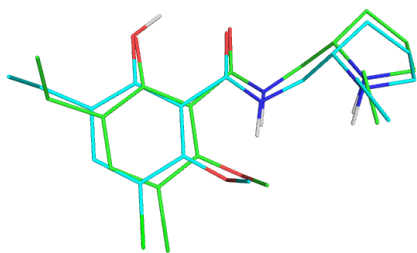Quinpirole
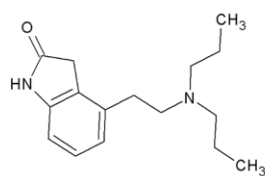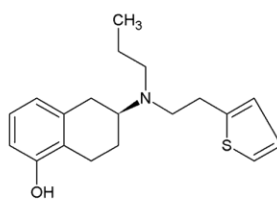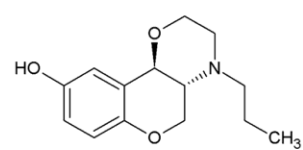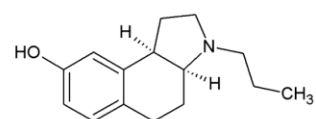
ZINC45254546

Figure 2. Re-docking eticlopride.

Superimposition of eticlopride re-docked with AD4.2 (cyan lines, A) and with Vina (magenta lines, B) toward eticlopride in complex with hD$_3$ in the crystal structure 3PBL (green lines).
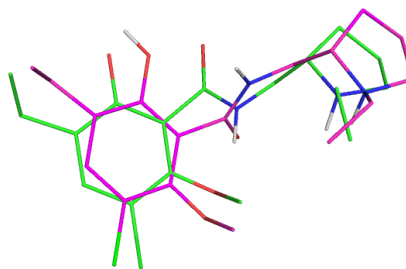
Figure 3. Structure differentiation of hD$_3$ and hD$_{2L}$ receptors simulated in membrane. (A) Superimposition of hD$_3$ (green cartoon) and hD$_2$ (cyan cartoon) homology models before the refinement with simulation in membrane. (B) structural alignment of hD$_3$ (green cartoon) and hD$_2$ (cyan cartoon) receptors after 3 ns of MD simulation in membrane. (C) high correlation of hD$_3$ and hD$_2$ binding energies (Autodock Vina) of D$_2$-like ligands from homology models without MD refinement. (D) low correlation of hD$_3$ and hD$_2$ binding energies (Autodock Vina) of D$_2$-like ligands after MD refinement.
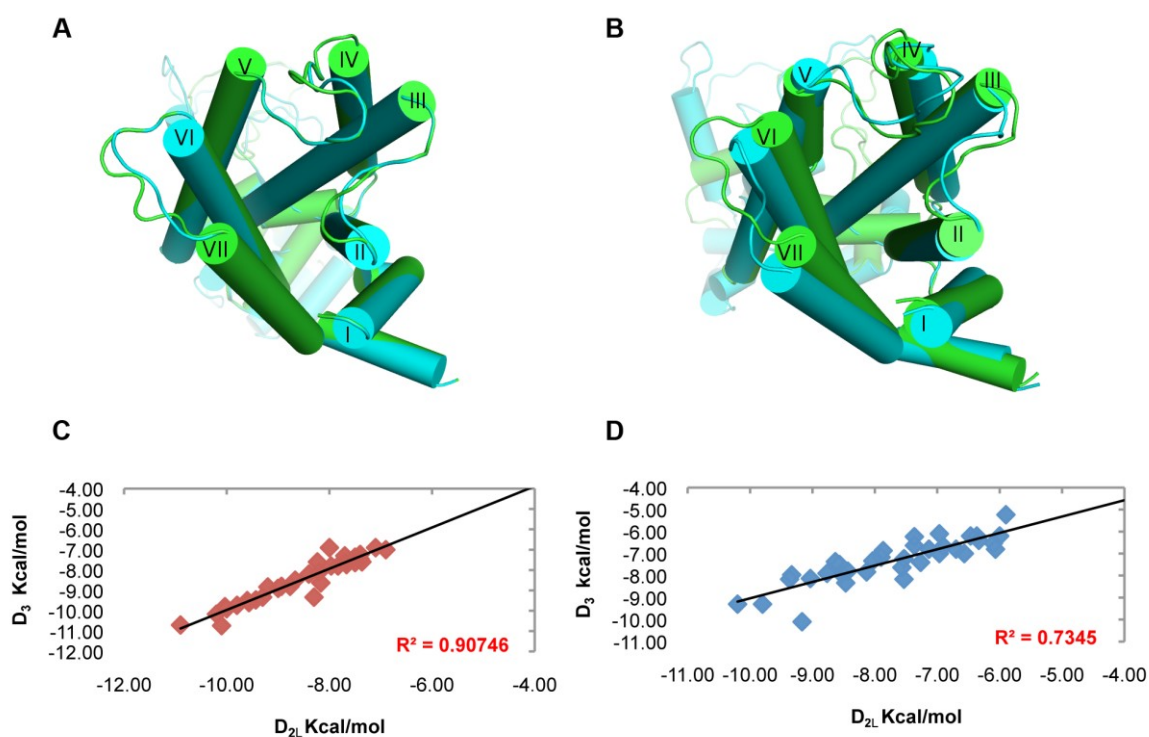
Figure 4. Analysis of Root Mean Square Deviation of Cα atoms during molecular dynamics simulation.

RMSD respect to the starting structures, homology models, of hD_3 (black squares) and hD_{2L} (red circles) receptors.
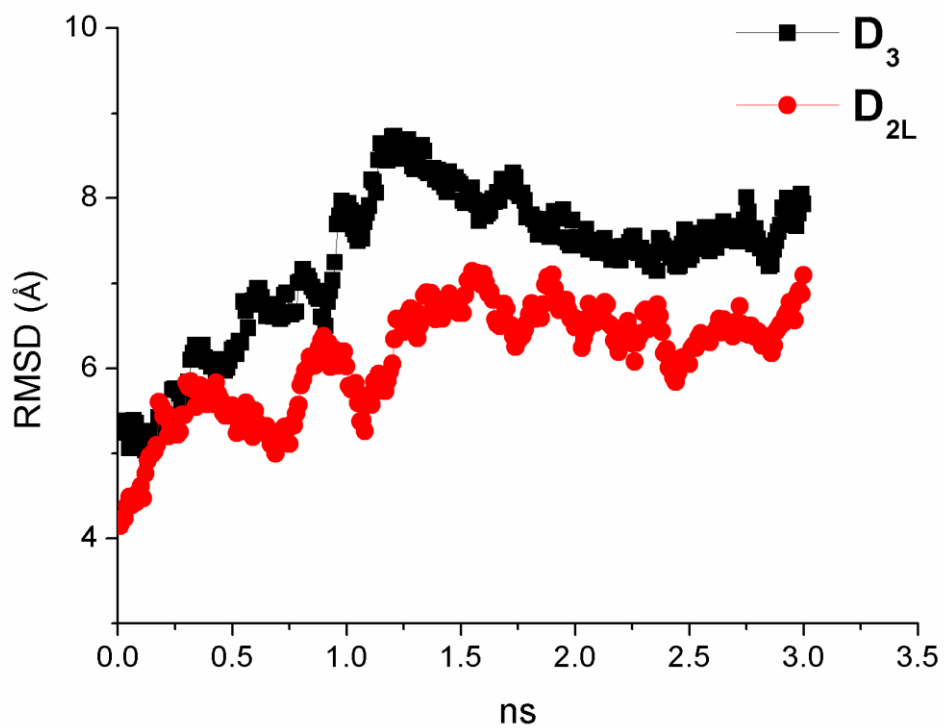
Figure 5. Figure 5. Ionic-lock, structural marker of inactive state of G-protein Coupled Receptors.

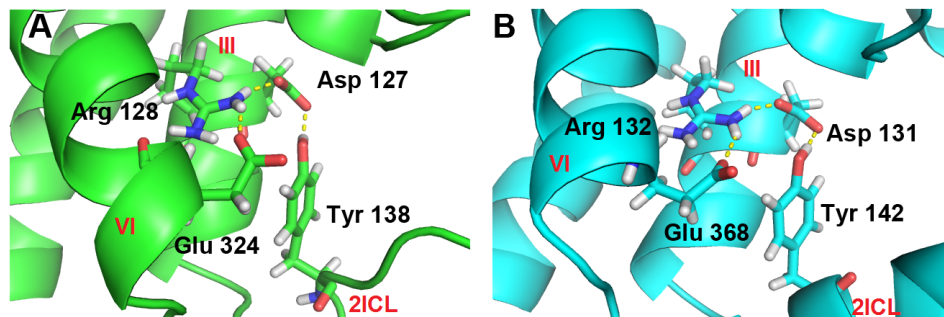(A) hD$_3$ and (B) hD$_{2L}$ receptor.

Figure 6. Evolution of binding pockets of hD$_3$ and hD$_{2L}$ receptor after model refinement.

Pockets generated by Fpocket server are represented as colored clusters of spheres. Left panels represent hD$_3$ (green ribbons) and right panels represent hD$_{2L}$ (cyan ribbons), before (A, B) and after (C, D) MD simulations. The red circles target the orthosteric binding pocket whereas the black circles highlight the allosteric binding pocket.
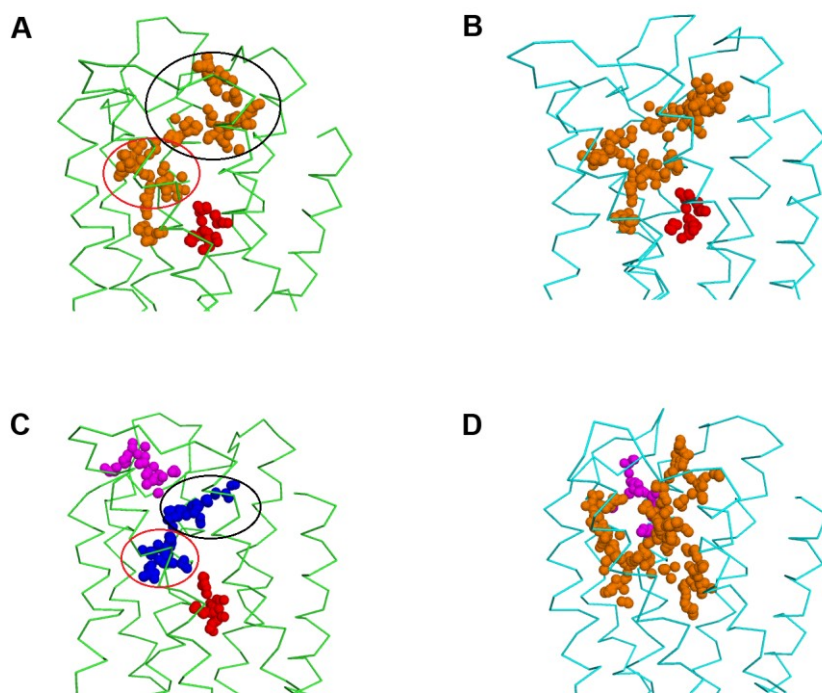
Figure 7. Correlation of predicted pK$_i$ and experimental pK$_i$ values.

Plots of D$_3$ preferring agonists docked toward hD$_3$ (A) and hD$_{2L}$ (B) receptors: a. dopamine; b. 7-OH-DPAT; c. 7-OH-PIPAT; d. pramipexole; e. quinpirole; f. ropinirole; g. rotigotine; h. PD 128,907; i. cis-8-OH-PBZI; j. ZINC45254546.
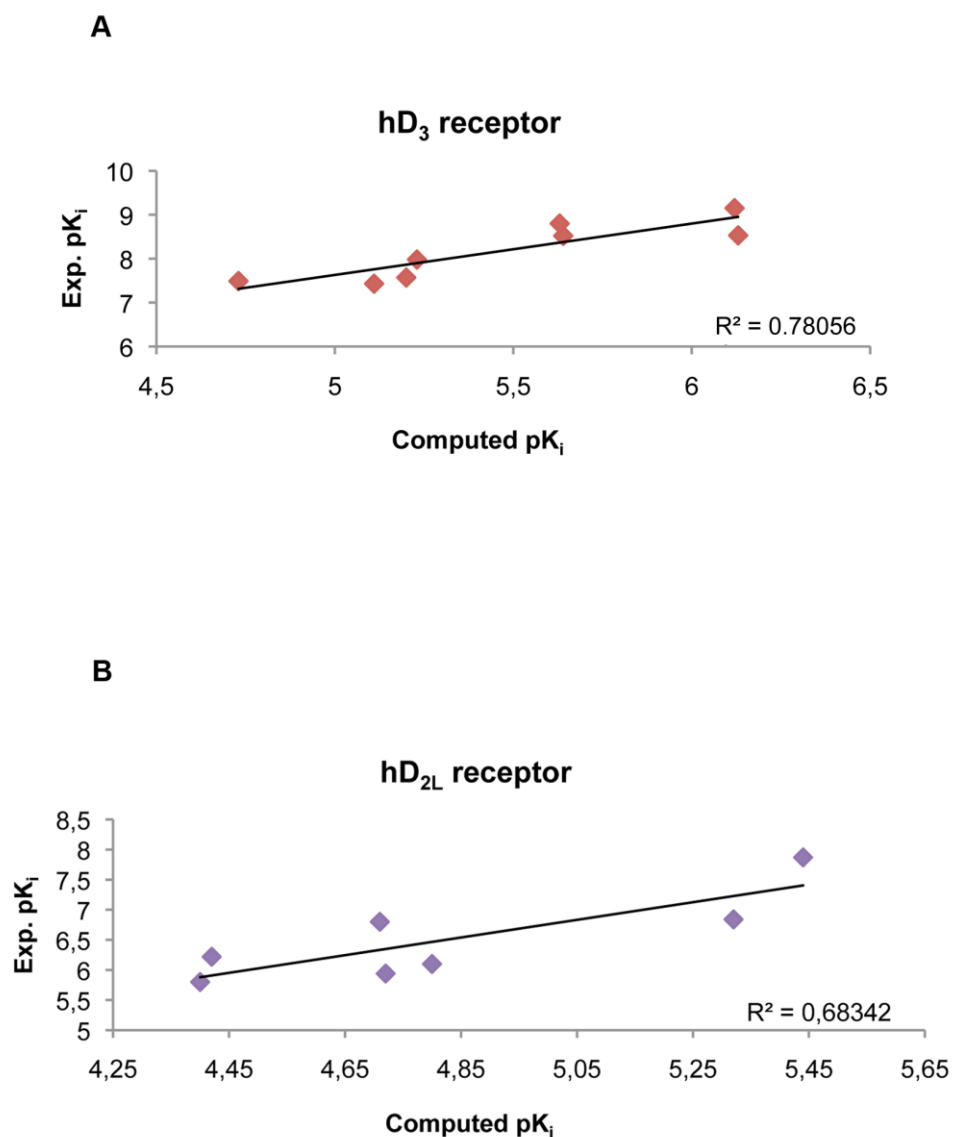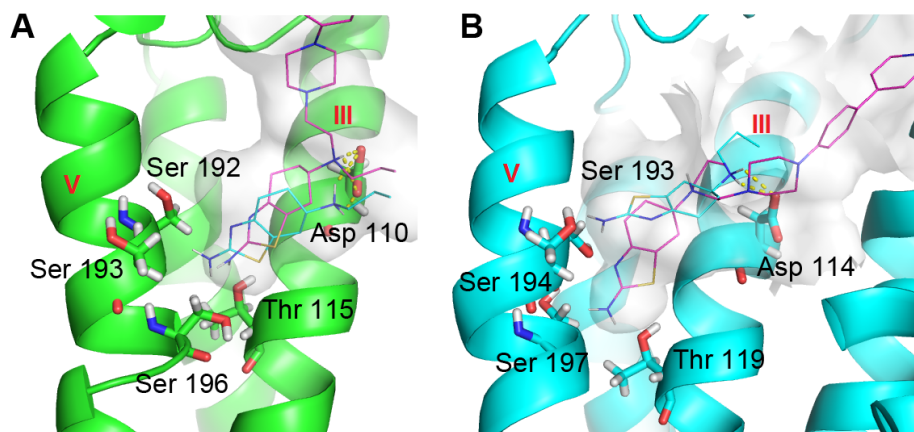
Figure 8. Virtual screening.

Pose of pramipexole (cyan lines) and compound ZINC45254546 (magenta lines, see also text) docked into hD_3 (A) and hD_{2L} (B) optimized receptor structures. H-bonds with Aspartate conserved residues are represented with yellow dashes.

Supporting information S1.

Ki calculation from the Binding Energy of poses generated by Autodock 4.2; source:

http://autodock.scripps.edu/faqs-help/faq/how-autodock-4-converts-binding-energy-kcal-mol-into-ki.

```
// equilibrium:   E  +  I  <=>    EI
// binding:       E  +  I  ->    EI          K(binding),     Kb
// dissociation:    EI     -> E  +  I       K(dissociation), Kd
//
//                        1
//       K(binding) = ---------------
//                     K(dissociation)
// so:
//     ln K(binding) = -ln K(dissociation)
//           ln Kb = -ln Kd
// Ki = dissociation constant of the enzyme-inhibitor complex = Kd
//       [E][I]
// Ki = ------
//        [EI]
// so:
//             ln Kb = -ln Ki
// deltaG(binding)    = -R*T*ln Kb
// deltaG(inhibition) =  R*T*ln Ki
//
// Binding and Inhibition occur in opposite directions, so we
// lose the minus-sign:  deltaG = R*T*lnKi,  _not_  -R*T*lnKi
// => deltaG/(R*T) = lnKi
// => Ki = exp(deltaG/(R*T))
```

Figure S1. Energy plots of systems. Potential energy (E_{pot}) and total energy (E_{tot}), of hD_{2L} and hD_3 receptors.
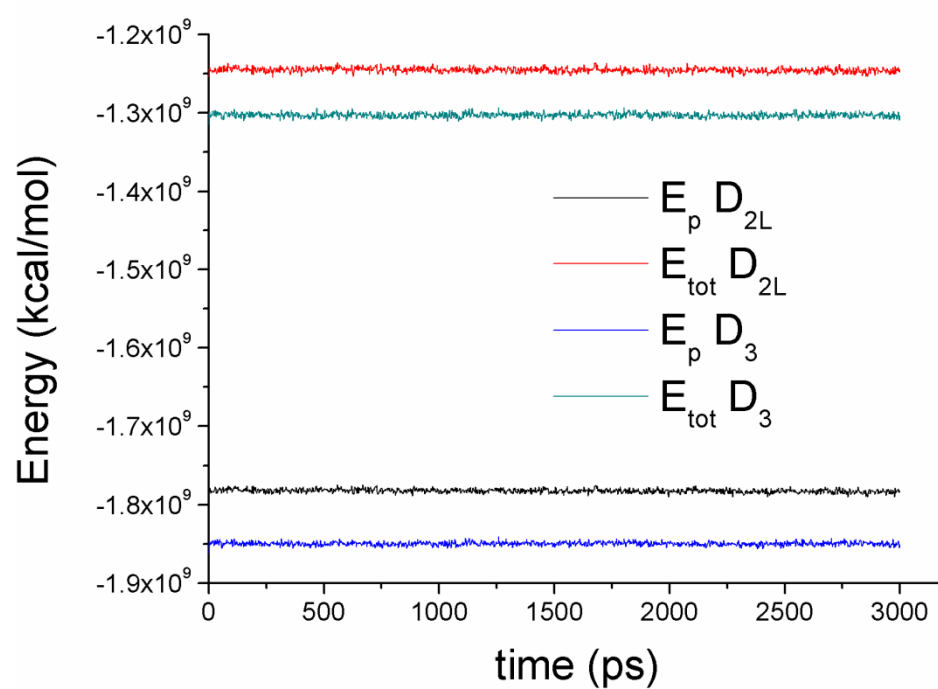
Table S1. Cα deviations of transmembrane helices (TM) of D$_3$ and D$_{2L}$ simulated receptors from the starting models. Cα deviation values were determined by structural alignment of each helix of the model and of the optimized structure.

TM helices	D$_3$-R Cα deviation (Å)	D$_{2L}$-R Cα deviation (Å)
I	0.486	0.688 [*]
II	0.523	0.903 [*]
III	0.501	0.722 [*]
IV	0.491	0.841 [*]
V	0.672	1.213 [*/**]
VI	0.740	0.855 [*/**]
VII	0.685	0.877 [*/**]

[*] Major transversal deviation in the intracellular side.

[**] Major transversal deviation in the extracellular side.

[*/**] Major transversal deviation in the intracellular and extracellular side.

Figure S2. Deviation of helices of optimized hD$_{2L}$ receptor (cyan cartoon) respect the starting model (yellow cartoon). The upper side of the figure corresponds to the extracellular side.
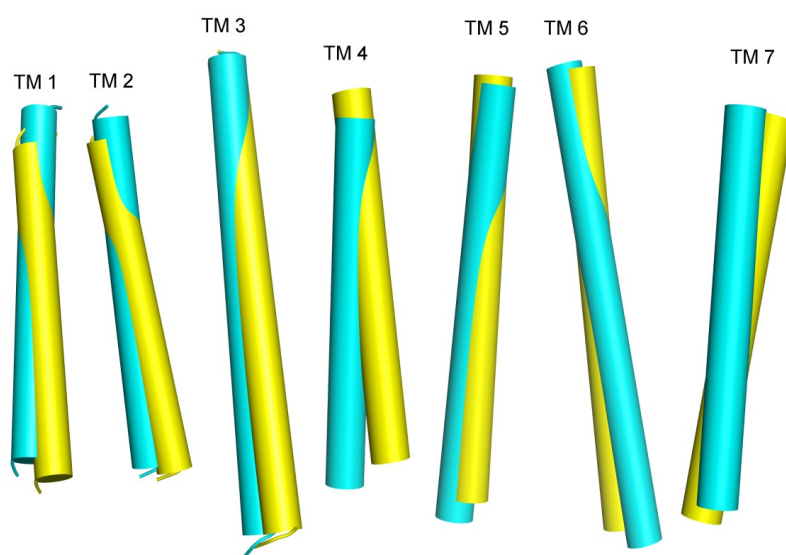
Table S2. Computed pK$_i$ for ligands docked into hD3 and hD2L receptors. Values are reported for ligands inserted in the regressions represented in Figure 7.

D$_3$ agonist	hD$_3$ pK$_i$	hD$_2$ pK$_i$
Dopamine	4.73	4.42
r-7-OH-DPAT	5.63	4.71
r-7-OH-PIPAT	6.13	5.32
Pramipexole [129][128][127]	5.23	4.8
Ropinirole [129][128][127]	5.11	4.72
Rotigotine	6.12	5.44
PD 128907	5.64	4.4
cis-8-OH-PBZI	5.2	ND

Virtual screening results: the 30 top scored compounds (ZINC-db code) docked into hD$_3$ and hD$_{2L}$. The lables _1 and _2 corresponds to different protonation states of ligands.

<u>hD$_3$</u>: ZINC45254546, ZINC11847498, ZINC11847496, ZINC04138713, ZINC04262922, ZINC11847499, ZINC04138711, ZINC11847497, ZINC04262921, ZINC04138712, ZINC65739972_1, ZINC04138714, ZINC65739975_1, ZINC65739975, ZINC65739976_1, ZINC63772249, ZINC29554524, ZINC29554520_1, ZINC65739972, ZINC65739978, ZINC63772250, ZINC65739976, ZINC29554520, ZINC29554520_2, ZINC27555141, ZINC27555141_1, ZINC00553652_1.

<u>hD$_{2L}$</u>: ZINC04138714, ZINC04138712, ZINC45254546, ZINC63772250, ZINC11847497, ZINC04262921, ZINC11847496, ZINC04138711, ZINC04262922, ZINC11847498, ZINC63772249, ZINC29554524, ZINC65739978, ZINC65739978_1, ZINC65739976_1, ZINC29554524_1, ZINC29554520, ZINC11847499, ZINC29554524_2, ZINC04138713, ZINC29554520_2, ZINC29554520_1, ZINC00574128, ZINC65739976, ZINC65739975, ZINC65739975_1, ZINC65739972.

Figure S3. Superimposition of template (3PBL)-homology model- optimized model of hD₃ receptor and hD₂ₗ receptor. The template structure (green cartoon) is the A chain of hD₃ receptor crystal structure (3BPL). The cyan cartoon corresponds to the homology model of hD₃ receptor, the yellow cartoon corresponds to the homology model of hD₂ₗ receptor. The optimized models of hD3 and hD2L receptor are respectively the magenta and orange cartoons.
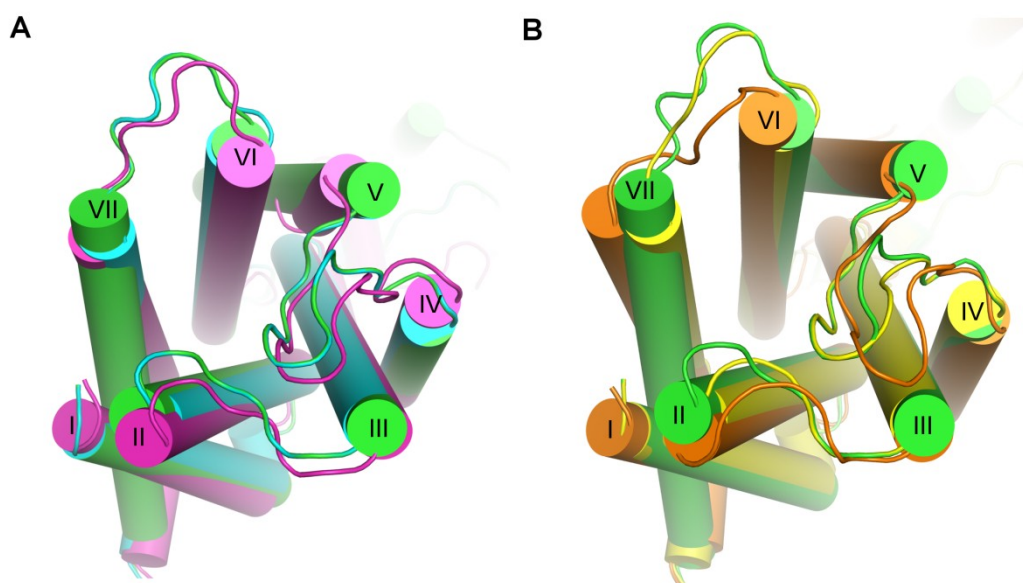
CHAPTER II

Regulation of intraocular pressure in mice: Structural analysis of dopaminergic and serotonergic systems in response to cabergoline

Chiara Bianca Maria Platania[1], Gian Marco Leggio[1], Filippo Drago, Salvatore Salomone, Claudio Bucolo

Department of Clinical and Molecular Biomedicine, Section of Pharmacology and Biochemistry, Catania University, Catania, Italy.

[1] These authors contributed equally to this work

Abstract

Elevated intraocular pressure (IOP) is the main recognized risk factor of glaucoma. To investigate the contribution of dopaminergic and serotonergic systems in IOP regulation, we used cabergoline, a mixed dopamine and serotonin agonist, in C57BL/6J WT and dopamine D_3 receptor knock-out ($D_3R^{-/-}$) mice with normal eye pressure or steroid-induced ocular hypertension. Furthermore, we studied the structural basis of the cabergoline-mediated activation of the dopaminergic and serotonergic systems by molecular modeling. Topical application of cabergoline, significantly decreased, in a dose-dependent manner, the intraocular pressure in WT mice, both in an ocular normotensive group (-9, -5 and -2 mmHg with 5%, 1%, and 0.1%, respectively) and an ocular hypertensive group, with a prolonged effect in this latter group. No change of intraocular pressure was observed after topical application of cabergoline in $D_3R^{-/-}$ mice. We modeled and optimized, with molecular dynamics, structures of hD_3, $h5HT_{1A}$ and $h5HT_{2A-C}$ receptors; thereafter we carried out molecular docking of cabergoline. Docking revealed that binding of cabergoline into D_3 and $5HT_{1A}$ receptors is associated with a better desolvation energy in comparison to $5HT_{2A-C}$ binding. In conclusion, the present study support the hypothesis that dopaminergic system is pivotal to regulate IOP and that D_3R represents an intriguing target in the treatment of glaucoma. Furthermore, the structure-based computational approach adopted in this study is able to build and refine structure models of homologous dopaminergic and serotonergic receptors that may be of interest for structure-based drug discovery of ligands, with dopaminergic selectivity or with multi-pharmacological profile, potentially useful to treat optic neuropathies.

1. Introduction

Elevated intraocular pressure (IOP) is the main recognized risk factor of glaucoma, a progressive optic neuropathy, which is a prominent cause of blindness in industrialized countries. The increase of IOP is due to two principal impaired physiologic mechanisms: dysfunctional outflow of aqueous humor due to abnormalities of the drainage system of the anterior chamber angle of the eye and the limited access of aqueous humor to the drainage system. The first dysfunction leads to the primary open angle glaucoma (POAG), the second one is the cause of the angle closure glaucoma (ACN). POAG represents the most frequent form of glaucoma, and epidemiologic studies demonstrated that the risk of POAG increases by 12% for each increment of 1 mmHg in IOP [1]. National Institute for Health and Care Excellence (NICE, http://guidance.nice.org.uk/CG85/Guidance) recommends a stepwise treatment algorithm for glaucoma, where the initial step is the pharmacological reduction of IOP, followed by laser surgery of the trabecular meshwork and glaucoma-filtering surgery.

We know that several systems are involved in IOP regulation, including adrenergic, cholinergic, purinergic, serotonergic, and dopaminergic [2]. The role of this latter is still unclear, though it represents one of the most intriguing systems implicated in the modulation of IOP both in physiological and pathological conditions. The involvement of the serotonergic and dopaminergic systems in regulation of IOP has been recently investigated in more details using several pharmacological tools and new paradigms [3], [4] and [5]. However, the precise role of the two systems, and in particular the relative magnitude of the effect of each single system in the regulation of IOP is still evanescent.

Some compounds, such as cabergoline, are serotonergic and dopaminergic ligands and are able to decrease IOP with a mechanism that remains uncertain. Cabergoline is an ergot derivative approved for hyperprolactinemia and Parkinson's disease; it is a potent dopamine receptor agonist on D_2 and D_3 subtypes, and it also possesses significant affinity for serotonin receptors such as $5HT_{1A}$, $5HT_{2A-B-C}$ [6] and [7]. Cabergoline has been shown to decrease IOP in different species [3]. To investigate the contribution of dopaminergic and serotonergic systems in ocular hypotensive mechanisms we used cabergoline in wild-type (WT) and dopamine D_3 receptor knock-out mice ($D_3R^{-/-}$) both ocular normotensive and ocular hypertensive. Furthermore, we studied the structural basis of the cabergoline-mediated activation of the dopaminergic and serotonergic systems, by molecular modeling, using the same approach that we previously applied in optimization and validation of structure models of D_3 and D_2 receptors [8].

2. Material and methods

2.1. In vivo studies

2.1.1. Animals

C57BL/6J $D_3R^{-/-}$ and WT littermates (male 8–12 weeks old) mice were used in this work. The animals were fed with standard laboratory food and were allowed free access to water in an air conditioned room with a 12-h light/12-h dark cycle. The experimental procedures were performed during the light cycle. $D_3R^{-/-}$ mice, used in these experiments, were 10th–12th generation of congenic C57BL/6J mice, and generated by a backcrossing strategy as reported by Accili et al. [9]. The genotypes of the dopamine D_3 receptor mutant and WT mice were identified by a PCR method with two pairs of primers flanking either exon 3 of the wild-type dopamine receptor D_3 or the phosphoglycerate kinase 1 gene promoter cassette of the mutated gene [9]. All the animals were treated according to the Association for Research in Vision and Ophthalmology (ARVO) Statement for the Use of Animals in Ophthalmic and Vision Research, and the Directive 2010/63/EU of the European Parliament and of the Council.

2.1.2. IOP measurement

IOP (mmHg) was measured before and after the drug treatment using a Tono-Lab tonometer (Icare, Espoo, Finland). IOP was measured both in the treated and the contralateral eye. Three baseline readings were taken 60, 30 and 0 min before the drug administration. IOP determination was made 30, 60, 120, 180 and 240 min after the topical application of the drug in the right eye. IOPs of animals were measured between 10 a.m. and 12.30 p.m. All measurements, under the same environmental conditions, were made by the same operator blind to treatment.

2.1.3. Treatments

Cabergoline hydrochloride, U99194A maleate, hydroxypropylmethylcellulose (HPMC; viscosity 80–120 cP), and polysorbate 80 were purchased from Sigma-Aldrich (St. Louis, MO, USA). Pharmacological treatments were performed after a baseline IOP measurement, defined as three baseline readings. Fresh aqueous formulation of carbergoline (0.01, 0.1, 1 and 5% w/v) containing 0.5% HPMC, 0.05% polysorbate 80, 0.2% PBS, and 0.75% NaCl, was prepared (pH 7.2) in order to optimize the drug's

residence time [10]. Cabergoline formulations were unilaterally instilled in the right eye in a volume of 10 µl. In each experimental group, animals received either drug or the appropriate vehicle. The animals were randomly assigned to treatment groups ($n = 6$–7) and were used only once.

2.1.4. Animal model of steroid-induced ocular hypertension

Steroid-induced hypertension was done as previously described by Bucolo et al. [5]. Briefly, Alzet micro-osmotic pumps (Model 1004, DURECT Corp., Cupertino, CA, USA) were filled with water-soluble dexamethasone (drug/cyclodextrin complex; cod. n. D2915 Sigma-Aldrich) in sterile PBS or with PBS alone (sham). Dexamethasone (DEX) was formulated at a concentration of 34.5 mg/ml. The flow rate for the micro-osmotic pumps was 0.11 µl per h, which delivers 0.09 mg of DEX per day. Animals were anesthetized with tiletamine hydrochloride and zolazepan hydrochloride (Zoletil 100$^®$, Virbac, Milan, Italy), a small incision was made midline at the base of the scapula to obtain a small subcutaneous pocket along the side of the animal; pumps were placed into the pocket with the flow moderator pointed posterior to the surgical site. Tissue bond adhesive was placed on the surgical wound and allowed to dry. Mice were then single housed and placed on a heating pad to recover. Three baseline readings of IOP were taken in a slot between 8 and 11 a.m. one day prior to the pump implantation surgery, and the day of implantation. Weekly IOP measurements, at the same day and time, were carried out to assess the onset of DEX-induced elevation in IOP. The final IOP was obtained at comparable times during the fourth week following surgery.

2.2. In silico studies

2.2.1. Protein sequence alignment

We retrieved full sequences of the human serotonergic receptors from the Protein-NCBI database (www.ncbi.nlm.nih.gov/protein/), the accession numbers of the analyzed human serotonergic receptors are respectively: $5HT_{1A}$ [NP_000515.2]; $5HT_{1B}$ [NP_000854.1] $5HT_{2A}$ [NP_000612.1]; $5HT_{2B}$ [NP_000858.3] and $5HT_{2C}$ [NP_000859.1]. The accession number of human D_3 receptor is NP_000787.2. Multiple sequence alignment of receptors were carried out with CLUSTAL W [11] using the BLOSUM62 matrix, the alignments were further analyzed with JALVIEW v2.7 [12].

2.2.2. Structure modeling of receptors

The structure models of the human serotonergic receptors were obtained by a threading modeling approach. We used the GPCRRD-ITASSER modeling facility [13] (http://zhanglab.ccmb.med.umich.edu/GPCRRD/) through which the threading method ITASSER is guided by the experimental restrains of GPCR Restrain Database (GPCRRD). The GPCRRD-ITASSER automatic pipeline uses at first the LOMETS threading program in order to identify the putative related template structures in the Protein Data Bank. When significant template alignments are not found, an *ab initio* transmembrane helix folding program is used to build the seven transmembrane bundle from scratch. Meanwhile, GPCRRD is searched for experimental restraints. Then a replica exchange Monte Carlo simulation is carried out to search the conformation space restricted by all the previous steps. The final atomic structure model is rebuilt by fragment guided-molecular dynamics (FG-MD). The output of GPCRRD-ITASSER provides six models per each analyzed protein; we selected the model with the best Ramachandran plot for further refinements. We carried out an *in vacuo* energy minimization (1000 steps of steepest descent algorithm, using NAMD with CHARMM27 force field) of output models in order to model canonical and "accessory" disulfide bridges. The accessory disulfide bridge of serotonergic receptors was individuated by sequence alignment. We created two sets of models, termed: 1_disu receptors with the canonical disulfide bridge, and 2_disu receptors with both canonical and accessory bridges. These models were then optimized by molecular dynamics simulation in a water-membrane environment.

2.2.3. Molecular dynamics refinement

Structure models of receptors were embedded in a palmitoyl-oleoyl phosphatidyl choline (POPC) bilayer, the orientation of each protein was guided by the output of the Orientations of Proteins in Membranes (OPM) database (http://opm.phar.umich.edu/). The systems were hydrated with TIP3P water molecules, and neutralized adding NaCl up to 150 mM. The pre-simulation processes (embedding of the proteins into the membrane, hydration and neutralization) were carried out using VMD v1.8.7 [14]. NAMD v2.7 was used to carry out equilibration steps and MD simulations [15]. Before MD simulations the systems were equilibrated as follows: (a) MD of lipid tails for 50 ps (time-step = 1 fs), while protein, water, ions and lipid head groups were kept fixed; (b) equilibration for 100 ps (time-step = 1 fs) of water-ions-lipids, while coordinates of proteins were fixed by applying harmonic constraints; (c) equilibration for 500 ps (time step = 1 fs) without

constraints. After these three steps, 3 ns MD simulation was done with time-step of 2 fs; trajectory and energy data were collected every 10 ps. The SHAKE algorithm, which constraints the hydrogen-heavy atom bonds, was applied in order to use the time-step of 2 fs. Langevin dynamics and piston were used to maintain constant temperature (300 K) and pressure (1 atm) during simulation. After the equilibration steps, the area per lipid was maintained constant during the MD simulation (NPAT ensemble). The particle number of each system was 83,931 atoms for $5HT_{1A}$, 83,701 atoms for $5HT_{2A}$, 84,296 atoms for $5HT_{2B}$, 84,747 atoms for $5HT_{2C}$. Long-term electrostatics were treated applying Periodic Boundary Conditions (PBC) and Particle Mesh Ewalds (PME) method [8] (time-step =4 fs). The cut-off was applied at 10 Å for the evaluation of Van der Waals and coulombic interactions and the switching functions started at 9 Å. First stage minimization was performed using the steepest descent algorithm whereas the conjugate gradient was used during production runs. All simulations were performed at the FERMI cluster (HPC-CINECA).

2.2.4. Molecular docking of cabergoline and consensus scoring method

AutoDock 4.2 (AD4.2) software provided the best prediction for the pose of eticlopride in the D_3 homology model [8], thus we have chosen it for the accurate docking of cabergoline into the binding pockets of validated D_3 receptor [8] and $5HT_{1A}$, $5HT_{2A-C}$ receptors. File preparation for AD4.2 docking calculations was carried out using the AutoDockTool (ADT), a free graphics user interface (GUI) of MGL-tools. The search space for all docking calculations included the orthosteric binding pocket and the 2ECL of receptors. Input grid maps of search space were created by applying Amber parameters and running the AD4.2 executable Autogrid. We chose Lamarkian genetic algorithm (GA), as search algorithm, running 100 iterations. In each GA run 2,500,000 energy evaluations were carried out. The population size was set to 150; 27,000 generations per run were carried out; poses were then clustered automatically. Poses with top score (lowest energy and more populated poses), orthosteric binding and fundamental salt-bridge (hydrogen bond + coulombic interaction between the protonated amine group and the conserved aspartate residue in the III helix) were further analyzed. AD 4.2 uses a semi-empirical free energy function and a charge-based method for desolvation contributes; the free energy function was calibrated using a set of 188 structurally known ligand-complexes with experimentally determined binding constant [16]. The binding energy of ligand poses (Kcal/mol) represents the sum of intermolecular energy, internal energy and torsional free energy of

the ligand minus the unbound-system energy. Ligand-protein complexes were further rescored with DSX-score [17] (http://pc1664.pharmazie.uni-marburg.de/drugscore/). At variance with AD4.2, DSX-score uses a knowledge-based scoring function that exploits comprehensive crystallographic information and does not rely on affinity data; therefore it can be used for scoring a broad range of ligand-protein complexes [17]. In particular, DSX-score uses statistical pair potentials derived from Cambridge Structural Database (CSD) and from Protein Data Bank (PDB); moreover, associated to PDB potential, Solvent Accessible Surface potential (SAS-potential) is introduced to account for the desolvation effects. PDB statistical pair and SAS potentials were used in this work. Analysis of poses and pictures were done respectively with AutoDock Tools (ADT) and Open Pymol.

2.3. Statistical analysis

For statistical analysis GraphPad (version 6; San Diego, CA, USA) was used. The data were analyzed by one-way analysis of variance (ANOVA) followed by Newman–Keuls or Dunnett *post hoc* test. Values are expressed as mean ± SD. Differences were considered statistically significant when p values were <0.05.

3. Results

3.1. IOP in ocular normotensive WT and $D_3R^{-/-}$ mice

As shown in Fig. 1, topical application of cabergoline caused dose-related ocular hypotension in WT mice. The maximum IOP-lowering effect (−9 and −5 mmHg), obtained with 5% and 1%, occurred at 1 h and a significant hypotensive effect persisted for up to 2 h (Fig. 1A). With 0.1% the maximum IOP-lowering effect (−2 mmHg) occurred at 1 h, but IOP returned at baseline level after 3 h. No significant effect in terms of IOP reduction has been observed with the lowest (0.01%) dose of cabergoline. On the contrary, cabergoline did not cause any detectable modification of IOP in $D_3R^{-/-}$ mice when topically instilled at different concentrations (Fig. 1B); indicating the involvement of dopamine D_3 receptor in the IOP regulation by cabergoline over potential effects through serotonin receptors. To confirm the involvement of D_3 receptor in the mechanism of ocular hypotension, experiments were carried out with U99194A, a selective D_3 antagonist [18]. A topical pretreatment was carried out with 1% U99194A followed (30 min) by a subsequent challenge with cabergoline. The dose of U99194A has been chosen from previous studies [5]. In order to minimize the number of animals we selected the dose (1%) between the

lowest and highest that showed a significant effect on IOP. Pretreatment with U99194A completely antagonized the IOP-lowering effect induced by cabergoline in WT mice (Fig. 1A and C), while no difference were observed in $D_3R^{-/-}$ mice (Fig. 1B and D).

3.2. IOP in ocular hypertensive WT and KO $D_3R^{-/-}$ mice

Dexamethasone elicited a significant ($p<0.01$) increase in terms of IOP after 4 weeks of sustained delivery by micro-osmotic pumps. Topical administration of 1% cabergoline in steroid-induced ocular hypertension caused a decrease in IOP by about 10 mmHg in WT mice (Fig. 1C) with a prolonged effect (up to 4 h) in comparison with ocular normotensive group. On the contrary, topical application of cabergoline in steroid-induced ocular hypertension did not produce any detectable effect on IOP in $D_3R^{-/-}$ mice (Fig. 1D). We used the 1% dose because it was between the lowest and highest doses that showed a significant effect on IOP in ocular normotensive WT mice. Further experiments were performed using selective D_3 antagonist (U99194A). A topical pretreatment was carried out with 1% U99194A followed (30min) by a subsequent challenge with cabergoline in steroid-induced ocular hypertension, in both WT and $D_3R^{-/-}$ mice. Pretreatment with U99194A completely antagonized the IOP-lowering effect induced by cabergoline in WT mice, confirming, also in hypertensive condition, the involvement of dopamine D_3 receptor over serotonin receptors in cabergoline-induced IOP decrease (Fig. 1A and C). No differences in terms of IOP reduction were observed in $D_3R^{-/-}$ mice (Fig. 1B and D).

3.3. Sequence alignments

We built two kinds of phylogenetic trees, using for both the algorithm UPGMA (Unweighted Pair Group Method with Arithmetic Mean) and taking into account for one the percentage of identity (Fig. 2A) and for the other the percentage of homology (Fig. 2B) between receptors. The two dendrograms differ in terms of clustering. The percentage identity tree identify two clusters, one includes $5HT_{1A-B}$ receptors, the other includes the $5HT_{2A-C}$ subfamily and D_3 receptor. The percentage homology tree clusters human D_3 and $5HT_{1A-B}$ receptors in one side, the $5HT_{2A-C}$ receptors subfamily in the other side. Protein sequence alignments (Fig. 2C), including $5HT_{1A}$, $5HT_{2A-C}$ and D_3 receptor, revealed the presence of conserved cysteine residues, corresponding to the accessory disulfide bridge of D_3 receptor. The presence of these residues has led us to model both canonical and accessory disulfide bridges. The conserved cysteine residues are present also in the $5HT_{1B}$ receptor (Fig. 2D).

3.4. Threading models and refinement by molecular dynamics

$5HT_{1A}$ and $5HT_{2A-C}$ structure models were obtained by GPCRRD-ITASSER; the output models with the best Ramachandran plots were chosen for further modeling of disulfide bridges. Two sets of models were created: 1_disu models where only the canonical disulfide bridge, between the 2ECL and the III helix, was modeled; 2_disu models where the canonical and the accessory disulfide bridge, within the 3ECL, were modeled. Both sets were optimized by means of 3 ns molecular dynamics simulation in membrane-water environment. Receptors with two disulfide bridges were more stable, in terms of average RMSD and fluctuations than 1_disu models; thus, as expected, the accessory disulfide bridge led to a more stable receptor conformation (Table 1). We carried out short term MD simulation, because the receptors already equilibrated in membrane within 3 ns, reaching a local minimum for both 1_disu and 2_disu. Because 2_disu models showed better conformational stability than 1_disu models, we carried out docking simulations on receptors with two disulfide bridges. Refined receptor structures were extracted from the last frames of simulation, considering as equivalent frames belonging to the same local minimum.

3.5. Molecular docking of cabergoline

We started our *in silico* study from the best pose of cabergoline docked into the optimized and validated structure of hD_3 receptor [8]. Because cabergoline is a D_3-agonist we speculated that the residues involved in the orthosteric binding [8] and [19] (cluster of serine residues in the V helix and the aspartate residue in the III helix; this last is conserved within all aminergic receptors) could be involved also in the orthosteric binding in serotonergic receptors (Table 2). Docking of cabergoline into the binding pocket of D_3R resulted in a best scored pose similar to those reported for other D_3 agonists [8] and [19]; cabergoline's pose involved the salt bridge between the protonated nitrogen N6 of the tretracyclic ergoline ring system and Asp 110. Furthermore, as for the other agonists, a hydrogen bond donor (HB-D) group (in cabergoline N1-H of ergoline moiety) formed hydrophilic interaction with cluster of serine residues and a threonine residue in the third helix (Thr 115, Fig. 3A). These interactions (orientation and contacts) were similar for the predicted cabergoline binding at $5HT_{2A-C}$ receptors (Table 3, Fig. 3B–D). The major differences between binding of cabergoline into D_3R and into $5HT_{2A-C}$ receptors were the less hydrophilic interactions (Table 3), particularly with the V helix, even though cabergoline retained similar orientation. The binding mode of the ergoline moiety of

cabergoline into the binding pocket of modeled $5HT_{2B}$ receptor closely resembled the binding of ergotamine into the crystal structure of $5HT_{2B}$[20] (Fig. 3D and E) (see also paragraph 3.6). Best scored poses of cabergoline docked into the $5HT_{1A}$ receptor deviated substantially from the best scored poses of the compound docked into the other receptors (Fig. 3F). Despite this fact, the predicted binding mode of cabergoline docked into the $5HT_{1A}$ receptor gave a score that correlated with the experimental Ki of cabergoline for $5HT_{1A}$ receptor. The correlation between the AD4.2 scores (Kcal/mol) and the experimental Ki values was worse (R^2 0.67, Pearson 0.82, $p < 0.05$) than correlation between DSX-scores and experimental Ki values (R^2 0.92, Pearson 0.95, $p < 0.02$), even though R^2 and Pearson correlation coefficients looked reasonably high for both scoring methods (Fig. 4). Table 4 reports the decomposition of total DSX-score for the predicted complexes. Cabergoline had greater experimental affinity for the D_3 and $5HT_{1A}$ in comparison to $5HT_{2A-C}$ receptors; when looking at the SAS score, D_3 and $5HT_{1A}$ had the best scores; thus, the desolvation energy might be an important determinant in the binding affinity of cabergoline.

3.6. Comparison between experimental structure of $5HT_{2B}$ receptor and simulated model

The most recent and relevant update on the structure of serotonergic receptors are the crystal structures of $5HT_{2B}$ (PDB: 4IB4) and $5HT_{1B}$ (PDB: 4IAQ, PDB: 4IAR) receptors in complex with the agonists ergotamine and dihydroergotamine [20] and [21]. We started our study before the publication of those structures. We used the threading method for modeling serotonergic receptor structures because homology model method, that is based on the choice of a single template structure, generated models having no good Ramachandran plots (data not shown). Thereafter models have been optimized by means of molecular dynamics simulation, embedding receptors into a lipid bilayer, trying to mimic the physiologic milieu of GPCRs; in particular all receptors have been simulated in absence of ligands. Comparing the crystallized $5HT_{2B}$ receptor in complex with ergotamine (PDB: 4IB4) with the simulated model (RMSD of α carbon atoms 1.96 Å), differences have been found involving mainly the extracellular part of seven helices bundle and in particular the 2ECL (Fig. 5C) rather than the whole receptor (Fig. 5A) and its intracellular site (Fig. 5B). This could be explained at first by the fact that $5HT_{2B}$ receptor in 4IB4 binds the agonist ergotamine, whereas the simulated model is in the unbound state. The tripeptide moiety of ergotamine interacts tightly with the 2ECL and the Lys 211 is pointing out of the binding pocket (Fig. 3E and Fig. 5E). On the contrary, the 2ECL loop in the

unbound simulated $5HT_{2B}$ receptor points toward the binding pocket and in particular Lys 211 is near the conserved Asp 135, forming a network of interactions with Glu 196 and Arg 213 residues (Fig. 5D). Thus binding of ergotamine might lead to displacement, from the entrance of the binding pocket, of the 2ECL which is therefore stabilized by the binding of the tripeptide moiety with Met 218, Leu 347, Val 348, Leu 362 and Lys 211 (Fig. 3E). Cabergoline, which has a small peptide group, docked into the optimized model of $5HT_{2B}$ receptor (Fig. 3D) lacks this interaction, except the side chain of Lys 211 (Table 3). Since ergotamine has higher affinity for $5HT_{2B}$ receptor (1.3 nM) [22] than cabergoline (9.4 nM) [3], this could be explained considering that the peptide group of cabergoline, in comparison to ergotamine, may lead to less displacement and stabilization of the 2ECL upon binding. Moreover, we have looked at conserved structural motifs (P-I-F, D(E)/RY and NPxxY) in GPCR involved in receptor activation and we have found several differences comparing the 4IB4 structure and the simulated $5HT_{2B}$ model (Fig. 5F–H). Considering the relative position of those residues in the unbound $5HT_{2B}$ model, we can assume that our model is in a partially inactivated conformation, prone to the binding.

4. Discussion

The present study demonstrated that the dopaminergic system, particularly D_3 receptor subtype, is pivotal in the regulation of IOP. We used cabergoline, as pharmacological tool, for two major reasons: first, cabergoline has well been demonstrated to drop IOP in several species; second, cabergoline is a ligand for both dopaminergic and serotonergic receptors [3]. It is noteworthy that differences exist in the effects of cabergoline in different species, both in normotensive and hypertensive eyes. For instance, cabergoline failed to significantly lower IOP in ocular normotensive Dutch-belt rabbits and ocular normotensive cats, while it is significantly effective in decreasing IOP in ocular normotensive Brown Norway rats and ocular hypertensive cynomolgus monkeys [3]. Furthermore, it is noteworthy that while $5HT_{2A}$ receptor plays a major role in IOP reduction in rats and cynomolgus monkeys [3], D_3 receptor appears to be more important in mice.

Most of dopamine and serotonin receptors are present in the eye [5], [23] and [24], but only few may be implicated in the IOP regulation. Dopamine exerts its action through five distinct GPCRs (D_{1-5} receptors), grouped in two classes, D_1-like and D_2-like receptors, that differ in their signal transduction, binding profile and physiological effects. D_1-like receptors (D_1 and D_5) are principally coupled to stimulatory Gs-proteins and enhance the

activity of adenylyl cyclase (AC), whereas D_2-like receptors (D_2, D_3, and D_4) are primarily coupled to inhibitory Gi-proteins and suppress the activity of AC [25]. The role of dopaminergic system on IOP regulation has been documented by Reitsamer and Kiel [4] who showed that dopamine modulates ciliary blood flow and aqueous production in a dose-dependent manner with a significant decrease of IOP. However, these authors did not investigate the receptor subtypes responsible for these effects.

A number of classical D_2 receptor agonists, including cabergoline, bromocriptine, lergotrile, lisuride, pergolide and cianergoline, have been shown to elicit ocular hypotension in animals and humans [26], [27], [28] and [29], while D_1 receptor agonists, such as ibopamine and fenoldopam, increases IOP in glaucomatous and ocular normotensive patients [30] and [31]. Based on the observation that phosphoinositide hydrolysis and intracellular Ca^{2+} mobilization induced by cabergoline in primary human ciliary muscle and trabecular meshwork (TM) cells are potently antagonized by a $5HT_{2A}$ selective antagonist, some authors [24], [32] and [33] suggested that $5HT_2$, particularly $5HT_{2A}$, receptor agonist activities of cabergoline may mediate the IOP reduction observed in different animal species [3]. However, these authors did not provide *in vivo* pharmacological data helping in elucidating the role of different subtype receptors in IOP regulation by cabergoline. Instead, they reported that a number of dopamine agonists do not produce significant IOP reduction in conscious cynomolgus monkeys [3]. In contrast with these data, it has been shown that 7-hydroxy-2-dipropylaminotetralin (7-OH-DPAT) a dopamine D_3-preferring receptor agonist, decreases IOP in rabbit [34]. We recently demonstrated [5] that dopamine D_3 receptor has an important role in the modulation of IOP both in physiological and pathological conditions. Topical instillation of 7-OH-DPAT is able to decrease IOP in C57BL/6J wild-type mice, on the contrary this molecule does not cause any IOP modification in C57BL/6J $D_3R^{-/-}$ mice [5]. Based on these evidence we hypothesized that the classical D_2 like receptor agonists that have been used by other groups to elicit ocular hypotension [27], [35], [36], [37], [38], [39], [40] and [41], may mostly act through dopamine D_3 receptor, with a minor contribution of other systems, such as the serotoninergic one. Among the large number of serotonin receptor subtypes, the most important for IOP regulation is the $5HT_2$ subfamily. Ciliary body and TM contain mRNAs for $5\text{-}HT_{2A\text{-}C}$ receptors, but the functionally active and pharmacologically responsive receptor is essentially the $5HT_{2A}$ [23]. This fact has generated interest regarding the role that 5-HT might have in modulating and controlling IOP. However, the exact molecular mechanism involved in the ocular hypotensive effect of $5HT_2$ receptors ligands

is not completely elucidated. It has been assumed that some non-selective compounds such as cabergoline decrease the IOP also through activation of $5HT_2$ receptors [3], even though $5HT_2$ receptor antagonists such as ketanserin decrease IOP in glaucomatous subjects [30] and [42]. Cabergoline has a higher affinity for $5HT_{1A}$ and D_2-like receptors than for $5HT_2$ [3], and it is noteworthy that $5HT_{1A}$ receptor ligands fail to significantly affect IOP [24] and [32]. Based on the above considerations and on the data generated in the present study, we believe that non-selective molecules, such as cabergoline, elicit IOP decrease through the activation of dopaminergic system rather than of serotoninergic system. The use of C57BL/6J $D_3R^{-/-}$ mice has led to the confirmation of the role of D_3 d aminergic receptor in regulation of aqueous humor outflow. Manipulating the expression levels of receptors using molecular techniques and genetic alterations represents the most specific pharmacologic strategy available today. When using a drug as an agonist or antagonist, one has to consider the probability of off-target effects; instead, when using a receptor knock out animal, one can exclude, with great degree of confidence, that an effect is mediated by the receptor product of the deleted gene [43]. Thus, C57BL/6J $D_3R^{-/-}$ mice represent an important tool for characterizing ocular hypotensive drugs [5].

The structural basis for cabergoline-mediated activation of the dopaminergic and serotonergic systems has been investigated in the present study. Particularly, an *in silico* approach was used to analyze the interaction of cabergoline with $5HT_{1A}$, $5HT_{2A-C}$, and D_3 receptors. We have previously modeled, refined and validated the human D_{2L} and D_3 receptors [8], and in the present work we have modeled and refined by all atom molecular dynamics (MD) simulations human $5HT_{1A}$ and $5HT_{2A-C}$ receptors. Because an accessory disulfide bridge within the third extracellular loop (3ECL) has been found in the crystal structure of human D_3 receptor (PDB: 3PBL) [44], we have, for the first time, modeled serotonergic receptors with both the canonical (between the 2ECL and the III helix) and the accessory disulfide bridges. Cysteine residues involved in the canonical and accessory disulfide bridges are conserved in D_3 and $5HT_{1A}$, $5HT_{2A}$, $5HT_{2B}$ and in $5HT_{2C}$ receptors. So far only two serotonergic receptors have been crystallized in complex with ergot derivatives [20] and [21] and, in these structures, the accessory disulfide bridge was experimentally found, strengthening our hypothesis that was based on sequence alignment results. We present for the first time the predicted binding data of cabergoline for serotonergic and dopaminergic receptors, because until now the binding of cabergoline was modeled only for the adenosine A2A receptor [45]. Our *in silico* approach predicts the binding mode of cabergoline at serotonergic $5HT_{2A-C}$ receptors, showing high similarity

with the experimental structure of $5HT_{2B}$-ergotamine complex, in fact the ergoline moiety of cabergoline interacts with the same key residues as the one of ergotamine in 4IB4. In comparison to the other serotonergic receptors, cabergoline binds $5HT_{1A}$ in a different mode, but the high predicted score is coherent with the high affinity of cabergoline for this receptor. In fact, beside the good prediction of the best scored poses and high correlation with experimental results, here, we infer, from the DSX-score, that the better desolvation energy associated to cabergoline binding into D_3 and $5HT_{1A}$ receptors is a crucial contribution for its higher affinity for these receptors over the $5HT_2$ subfamily. In fact, cabergoline binding to $5HT_2$ receptor subfamily does not form strong hydrophilic interaction with the V helix, as in the D_3 receptor. The phylogenetic trees, based on percentage of homology and identity, are different in terms of clustering. In the percentage identity dendrogram the D_3R clusters with $5HT_{2A-C}$ receptors, sharing the similarity of the binding mode of cabergoline. In the percentage homology tree the D_3R clusters with $5HT_{1A-B}$ receptors, having in common the high affinity for cabergoline with $5HT_{1A}$ (K_i 2 nM) but not with $5HT_{1B}$ (K_i 478 nM) [6], with this latter D_3R shares only the binding mode of the ergot moiety (Fig. 3 E). Based on these results, we can assume that the D_3 receptor is closely related to the analyzed serotonergic receptors, which also account for the cross-pharmacological effects of compounds targeting dopaminergic and serotonergic systems. However, homology and sequence data cannot provide an *a priori* information about the pharmacological effects and involvement of both system in IOP regulation [3] and [5].

Our *in silico* data provide information about the structural features of agonist binding at receptors, confirming the *in vitro* data of cabergoline binding and may help in further medicinal chemistry studies. Our *in vivo* data are in accordance with a major contribution of D_3 receptor in the IOP-lowering effect of cabergoline, whereas $5HT_{2A}$ do not seem to be relevant in the present model, perhaps because of their small number and/or their coupling efficiency in ciliary body and TM of C57BL/6J mice. Further experiments may be needed to figure out if the effect of D_3R stimulation is related to suppression of aqueous humor inflow or to increase of its outflow.

In conclusion, the present study support the hypothesis that dopaminergic system is pivotal to regulate IOP and that D_3 is the key dopamine receptor subtype in this system. Based on the data we generated, we conclude that D_3R represents an intriguing potential target for the treatment of glaucoma. Furthermore, the structure-based computational approach adopted in the present study was able to build, refine, and validate structure models of homologous dopaminergic and serotonergic receptors that may be of interest for structure-

based drug discovery of ligands, with dopaminergic selectivity or with multi-pharmacological profile, potentially useful to treat optic neuropathies such as glaucoma. Finally, these data suggest that dopaminergic ligands may be useful in the management of IOP dysfunction, and that clinical translational studies are warranted.

Acknowledgments

References

1. B. Nemesure, R. Honkanen, A. Hennis, S.Y. Wu, M.C. Leske. Incident open-angle glaucoma and intraocular pressure. Ophthalmology, 114 (2007), pp. 1810–1815

2. C. Bucolo, S. Salomone, F. Drago, M. Reibaldi, A. Longo, M.G. Uva. Pharmacological management of ocular hypertension: current approaches and future prospective. Curr Opin Pharmacol, 13 (2013), pp. 50–55

3. N.A. Sharif, M.A. McLaughlin, C.R. Kelly, P. Katoli, C. Drace, S. Husain *et al.*Cabergoline: Pharmacology, ocular hypotensive studies in multiple species, and aqueous humor dynamic modulation in the Cynomolgus monkey eyes. Exp Eye Res, 88 (2009), pp. 386–397

4. J.W. Kiel, H.A. Reitsamer. Paradoxical effect of phentolamine on aqueous flow in the rabbit. J Ocul Pharmacol Ther, 23 (2007), pp. 21–26

5. C. Bucolo, G.M. Leggio, A. Maltese, A. Castorina, V. D'Agata, F. Drago. Dopamine-(3) receptor modulates intraocular pressure: implications for glaucoma. Biochem Pharmacol, 83 (2012), pp. 680–686

6. M.J. Millan, L. Maiofiss, D. Cussac, V. Audinot, J.A. Boutin, A. Newman-Tancredi. Differential actions of antiparkinson agents at multiple classes of monoaminergic receptor. I. A multivariate analysis of the binding profiles of 14 drugs at 21 native and cloned human receptor subtypes. J Pharmacol Exp Ther, 303 (2002), pp. 791–804.

7. A. Newman-Tancredi, D. Cussac, V. Audinot, J.P. Nicolas, F. De Ceuninck, J.A. Boutin *et al.* Differential actions of antiparkinson agents at multiple classes of monoaminergic receptor. II. Agonist and antagonist properties at subtypes of dopamine D(2)-like receptor and alpha(1)/alpha(2)-adrenoceptor. J Pharmacol Exp Ther, 303 (2002), pp. 805–814

8. C.B. Platania, S. Salomone, G.M. Leggio, F. Drago, C. Bucolo. Homology modeling of dopamine D2 and D3 receptors: molecular dynamics refinement and docking evaluation. PLoS ONE, 7 (2012), p. e44316

9. D. Accili, C.S. Fishburn, J. Drago, H. Steiner, J.E. Lachowicz, B.H. Park *et al.*A targeted mutation of the D3 dopamine receptor gene is associated with hyperactivity in mice. Proc Natl Acad Sci USA, 93 (1996), pp. 1945–1949

10. C. Bucolo, F. Drago. Carbon monoxide and the eye: implications for glaucoma therapy. Pharmacol Ther, 130 (2011), pp. 191–201

11. M. Goujon, H. McWilliam, W. Li, F. Valentin, S. Squizzato, J. Paern *et al.* A new bioinformatics analysis tools framework at EMBL-EBI. Nucleic Acids Res, 38 (2010), pp. W695–W699

12. A.M. Waterhouse, J.B. Procter, D.M. Martin, M. Clamp, G.J. Barton. Jalview Version 2–a multiple sequence alignment editor and analysis workbench. Bioinformatics, 25 (2009), pp. 1189–1191

13. J. Zhang, Y. Zhang. GPCRRD: G protein-coupled receptor spatial restraint database for 3D structure modeling and function annotation. Bioinformatics, 26 (2010), pp. 3004–3005

14. W. Humphrey, A. Dalke, K. Schulten. VMD: visual molecular dynamics. J Mol Graph, 14 (1996), pp. 33–38 27-8

15. J.C. Phillips, R. Braun, W. Wang, J. Gumbart, E. Tajkhorshid, E. Villa *et al.* Scalable molecular dynamics with NAMD. J Comput Chem, 26 (2005), pp. 1781–1802

16. R. Huey, G.M. Morris, A.J. Olson, D.S. Goodsell. A semiempirical free energy force field with charge-based desolvation. J Comput Chem, 28 (2007), pp. 1145–1152

17. G. Neudert, G. Klebe. DSX: a knowledge-based scoring function for the assessment of protein-ligand complexes. J Chem Inf Model, 51 (2011), pp. 2731–2745

18. V. Audinot, A. Newman-Tancredi, A. Gobert, J.M. Rivet, M. Brocco, F. Lejeune *et al.*A comparative in vitro and in vivo pharmacological characterization of the novel dopamine D3 receptor antagonists (+)-S 14297, nafadotride, GR 103,691 and U 99194. J Pharmacol Exp Ther, 287 (1998), pp. 187–197

19. S. Kortagere, S.Y. Cheng, T. Antonio, J. Zhen, M.E. Reith, A.K. Dutta. Interaction of novel hybrid compounds with the D3 dopamine receptor: Site-directed mutagenesis and homology modeling studies. Biochem Pharmacol, 81 (2011), pp. 157–163

20. D. Wacker, C. Wang, V. Katritch, G.W. Han, X.P. Huang, E. Vardy *et al.* Structural features for functional selectivity at serotonin receptors. Science, 340 (2013), pp. 615–619

21. C. Wang, Y. Jiang, J. Ma, H. Wu, D. Wacker, V. Katritch *et al.* Structural basis for molecular recognition at serotonin receptors. Science, 340 (2013), pp. 610–614

22. A.R. Knight, A. Misra, K. Quirk, K. Benwell, D. Revell, G. Kennett *et al.* Pharmacological characterisation of the agonist radioligand binding site of 5-HT(2A), 5-HT(2B) and 5-HT(2C) receptors. Naunyn Schmiedebergs Arch Pharmacol, 370 (2004), pp. 114–123

23. N.A. Sharif, M. Senchyna. Serotonin receptor subtype mRNA expression in human ocular tissues, determined by RT-PCR. Mol Vis, 12 (2006), pp. 1040–1047

24. N.A. Sharif, C.R. Kelly, M. McLaughlin. Human trabecular meshwork cells express functional serotonin-2A ($5HT_{2A}$) receptors: role in IOP reduction. Invest Ophthalmol Vis Sci, 47 (2006), pp. 4001–4010

25. J.M. Beaulieu, R.R. Gainetdinov. The physiology, signaling, and pharmacology of dopamine receptors. Pharmacol Rev, 63 (2011), pp. 182–217

26. D.E. Potter, D.J. Shumate. Cianergoline lowers intraocular pressure in rabbits and monkeys and inhibits contraction of the cat nictitans by suppressing sympathetic neuronal function. J Ocul Pharmacol, 3 (1987), pp. 309–321

27. Q.A. Mekki, S.M. Hassan, P. Turner. Bromocriptine lowers intraocular pressure without affecting blood pressure. Lancet, 1 (1983), pp. 1250–1251

28. D.E. Potter, J.A. Burke. Effects of ergoline derivatives on intraocular pressure and iris function in rabbits and monkeys. Curr Eye Res, 2 (1982), pp. 281–288

29. O. Geyer, D. Robinson, M. Lazar. Hypotensive effect of bromocriptine in glaucomatous eyes. J Ocul Pharmacol, 3 (1987), pp. 291–294

30. M. Virno, L. Taverniti, F. De Gregorio, L. Sedran, F. Longo. Increase in aqueous humor production following D1 receptors activation by means of ibopamine. Int Ophthalmol, 20 (1996), pp. 141–146

31. J.R. Piltz, R.A. Stone, S. Boike, D.E. Everitt, N.H. Shusterman, P. Audet *et al.* Fenoldopam, a selective dopamine-1 receptor agonist, raises intraocular pressure in males with normal intraocular pressure. J Ocul Pharmacol Ther, 14 (1998), pp. 203–216

32. J.A. May, M.A. McLaughlin, N.A. Sharif, M.R. Hellberg, T.R. Dean. Evaluation of the ocular hypotensive response of serotonin 5-HT1A and 5-HT2 receptor ligands in conscious ocular hypertensive cynomolgus monkeys. J Pharmacol Exp Ther, 306 (2003), pp. 301–309

33. N.A. Sharif, C.R. Kelly, J.Y. Crider, T.L. Davis. Serotonin-2 (5-HT2) receptor-mediated signal transduction in human ciliary muscle cells: role in ocular hypotension. J Ocul Pharmacol Ther, 22 (2006), pp. 389–401

34. E. Chu, T.C. Chu, D.E. Potter. Mechanisms and sites of ocular action of 7-hydroxy-2-dipropylaminotetralin: a dopamine(3) receptor agonist. J Pharmacol Exp Ther, 293 (2000), pp. 710–716

35. S.E. Ohia, G.L. Zhan, A.M. Leday, C.A. Opere, K.H. Kulkarni, L.C. Harris *et al.*Ocular pharmacology of bicyclic hexahydroaporphines. Methods Find Exp Clin Pharmacol, 27 (2005), pp. 87–93

36. S.L. Saha, I.N. Igbo, C.A. Opere, G.L. Zhan, J. Taniyama, S.E. Ohia *et al.* Assessment of the intraocular pressure-lowering activity of bicyclic derivatives of 1-substituted benzyloctahydroisoquinoline. J Ocul Pharmacol Ther, 17 (2001), pp. 413–420

37. D.E. Potter, M.J. Ogidigben, T.C. Chu. Lisuride acts at multiple sites to induce ocular hypotension and mydriasis. Pharmacology, 57 (1998), pp. 249–260

38. M. Ogidigben, T.C. Chu, D.E. Potter. Ocular hypotensive action of a dopaminergic (DA2) agonist, 2,10,11-trihydroxy-N-n-propylnoraporphine. J Pharmacol Exp Ther, 267 (1993), pp. 822–827

39. G.C. Chiou, Y.J. Chen. Improvement of ocular blood flow with dopamine antagonists on ocular-hypertensive rabbit eyes. Zhongguo Yao Li Xue Bao, 13 (1992), pp. 481–484

40. C.E. Crosson, J.A. Burke, M.F. Chan, D.E. Potter. Ocular effects of a N,N-disubstituted 5-OH aminotetralin (N-0437): evidence for a dual mechanism of action. Curr Eye Res, 6 (1987), pp. 1319–1326

41. G.C. Chiou, F.Y. Chiou. Dopaminergic involvement in intraocular pressure in the rabbit eye. Ophthalmic Res, 15 (1983), pp. 131–135

42. G.C. Chiou, B.H. Li. Ocular hypotensive actions of serotonin antagonist-ketanserin analogs. J Ocul Pharmacol, 8 (1992), pp. 11–21

43. S. Salomone, C. Waeber. Selectivity and specificity of sphingosine-1-phosphate receptor ligands: caveats and critical thinking in characterizing receptor-mediated effects. Front Pharmacol, 2 (2011), p. 9

44. E.Y. Chien, W. Liu, Q. Zhao, V. Katritch, G.W. Han, M.A. Hanson *et al.* Structure of the human dopamine D3 receptor in complex with a D2/D3 selective antagonist. Science, 330 (2010), pp. 1091–1095

45. V. Singh, P. Somvanshi. Homology modeling of adenosine A2A receptor and molecular docking for exploration of appropriate potent antagonists for treatment of Parkinson's disease. Curr Aging Sci, 2 (2009), pp. 127–134

Table 1. Conformational stability of simulated receptors.

DISU-1	5HT$_{1A}$	5HT$_{2A}$	5HT$_{2B}$	5HT$_{2C}$	D$_3$ *
Avarage RMSD (nm)	0.51	0.68	0.47	0.47	ND
SD	0.10	0.12	0.10	0.05	ND
DISU-2	**5HT$_{1A}$**	**5HT$_{2A}$**	**5HT$_{2B}$**	**5HT$_{2C}$**	**D$_3$ ***
Avarage RMSD (nm)	0.52	0.39	0.34	0.38	0.73
SD	0.11	0.08	0.06	0.07	0.08

*As reported in Platania et al 2012 [8]

Table 2. Hydrophilic residues in the orthosteric binding pockets.

D$_3$	5HT$_{1B}$	5HT$_{1A}$	5HT$_{2A}$	5HT$_{2B}$	5HT$_{2C}$	*CXCR4
Asp 110	Asp 129	Asp 116	Asp 155	Asp 135	Asp 134	Tyr 116
Thr 115	Thr 134	Thr 121	Thr 160	Thr 140	Thr 139	Tyr 121
Ser 192	Ser 212	Ser 199	Gly 238	Gly 221	Gly 218	His 203
Ser 193	Ser 213	Thr 200	Ser 239	Ser 222	Ser 219	Ile 204
Ser 196	Ala 216	Ala 203	Ser 242	Ala 225	Ala 222	Gly 207

*The chemokine receptor CXR4 is reported as example of non aminergic receptor.

Table 3. Hydrophilic and hydrophobic residues interacting with cabergoline.

Hydrophilic	Hydrophobic
D$_3$	
Asp 110, Cys 114, Thr 115, Ser 192, Tyr 365, Thr 329, Tyr 373, Ile 183 (peptide C=O), Ser 192	His 349, Phe 345, Trp 342, Val 107
5HT$_{1A}$	
Asp 116, Cys 120, Tyr 195, Thr 196, Ser 199, Tyr 390, Asn 386, Gln 97	Val 117, Ile 113, Phe 361, Val 364, Leu 368, Ala 365
5HT$_{2A}$	
Asp 155, Thr 160, Ser 242, Ala 290 (peptide C=O)	Val 235, Leu 229, Leu 228, Val 235
5HT$_{2B}$	
Asp 135, Tyr 370, Thr 140, Glu 363	Ala 111, Trp 131, Val 107, Lys 211, Val 366
5HT$_{2C}$	
Asp 134, Ser 138, Thr 139, Asn 331	Phe 327, Trp 324, Val 208, Ala 222

*Continued line = H-bond, dashed line = hydrophilic residues in close proximity.

Table 4. Relative contribution of desolvation to DSX score.

Score	D$_3$	5HT$_{1A}$	5HT$_{2A}$	5HT$_{2B}$	5HT$_{2C}$
TOT-score	-145	-137	-122	-110	-104
SAS	-29	-23	-9	-13	-10

Figure 1. Intraocular pressure (IOP) in ocular normotensive (panel A, B) and hypertensive (C, D) wild-type (panel A, C) and D_3 receptor knock-out (B, D) mice after topical application of cabergoline alone or with U99194A (U99) pre-treatment (30 min). * $p < 0.05$; ** $p < 0.01$ vs. vehicle (VHC) treated group.
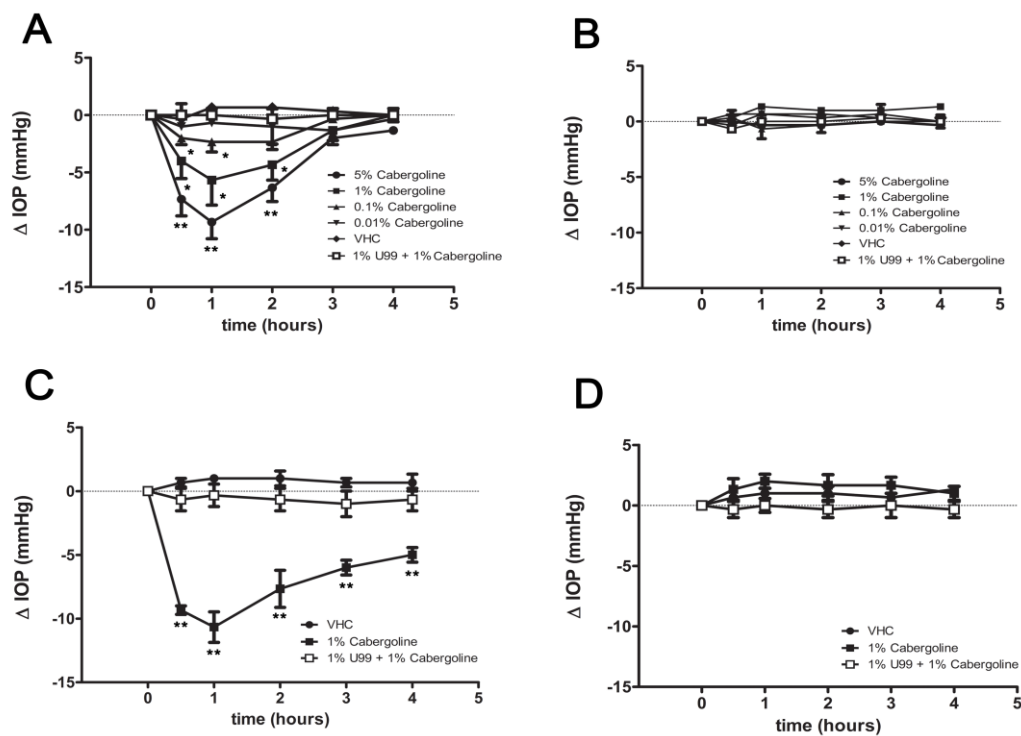
Figure 2. Sequence alignments and phylogenetic trees. Percentage identity dendrogram (A); percentage homology dendrogram (B). Alignment of the 3ECL region of analyzed receptors (C); in (D) the receptor $5HT_{1B}$ was included.
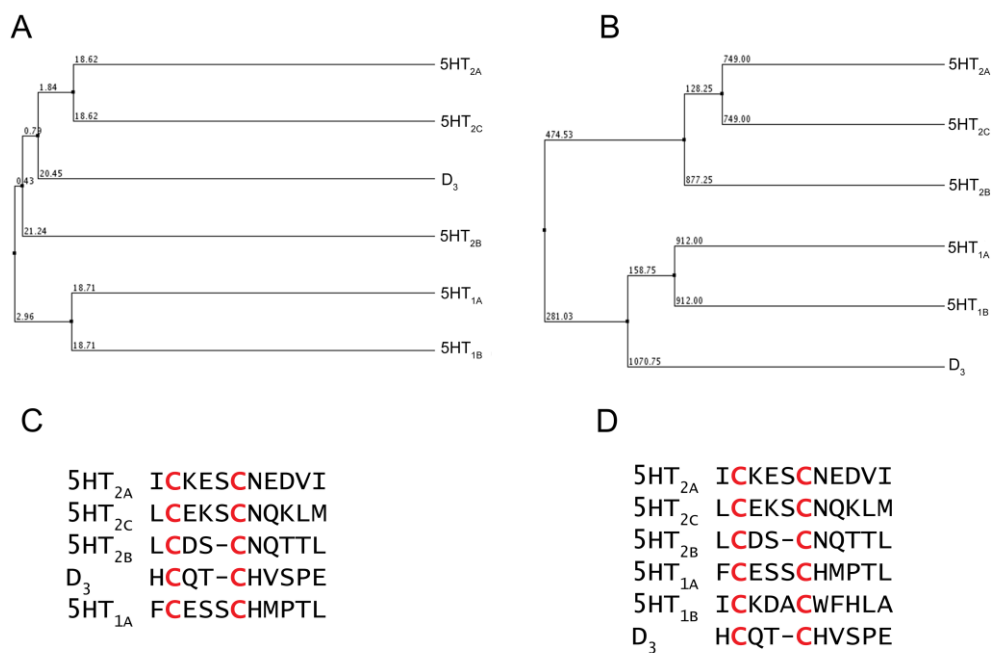
Figure 3. Binding mode of cabergoline. (A) Cabergoline docked into D_3R; (B) pose of cabergoline into $5HT_{2A}$ receptor; (C) pose of cabergoline into $5HT_{2C}$; (D) cabergoline docked into simulated $5HT_{2B}$ receptor; (E) experimental binding mode of ergotamine in the binding pocket of $5HT_{2B}$ receptor; (F) binding mode of cabergoline into the binding pocket of $5HT_{1A}$ receptor.
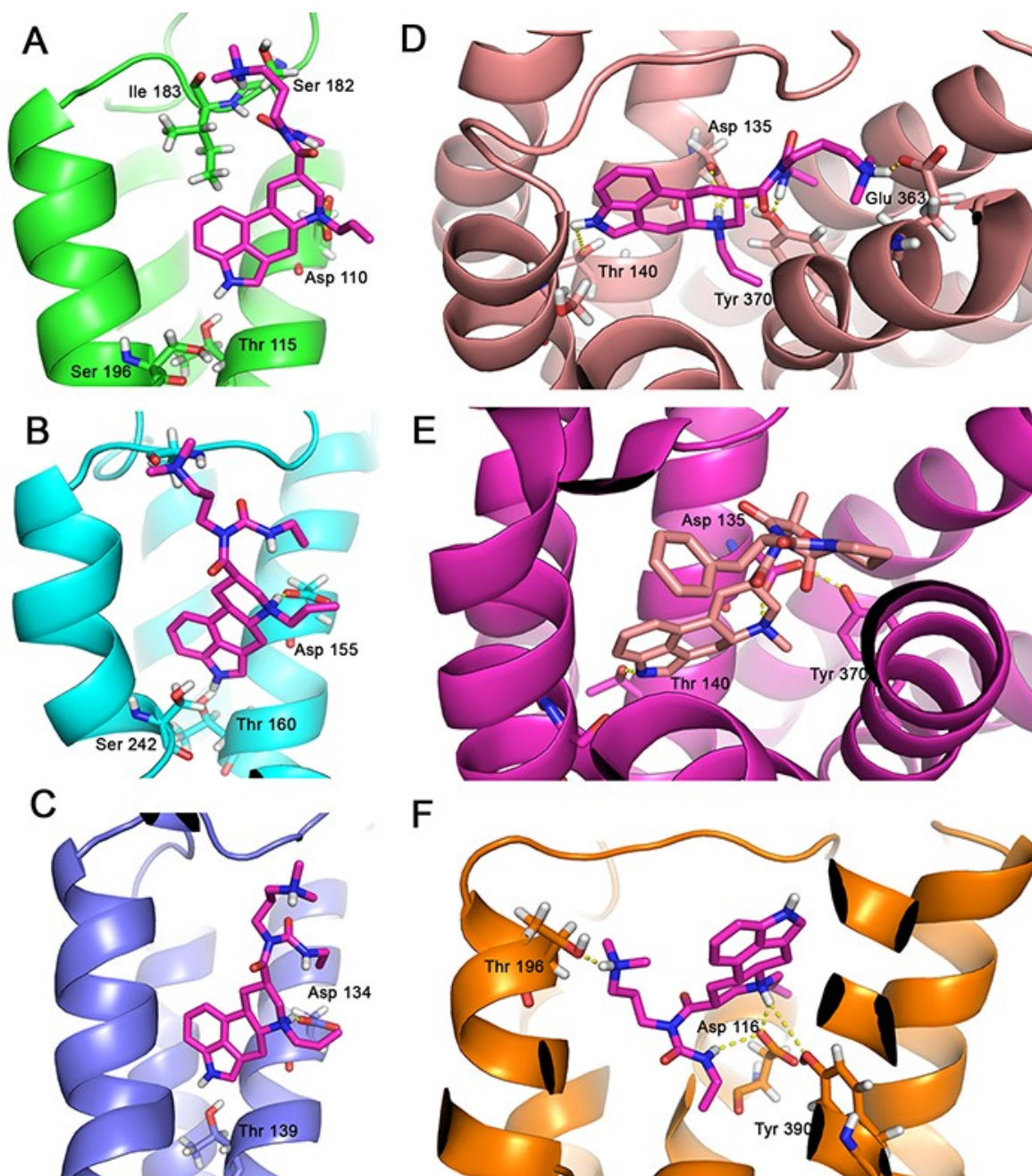
Figure 4. Correlation of predicted docking score and experimental affinity of cabergoline. AutoDock 4.2 (A) score; DSX-score (B).
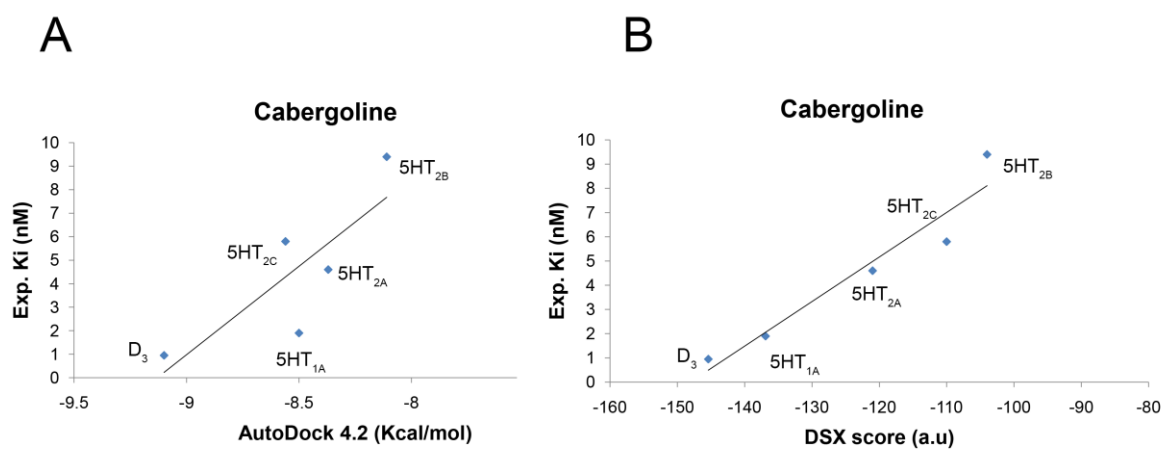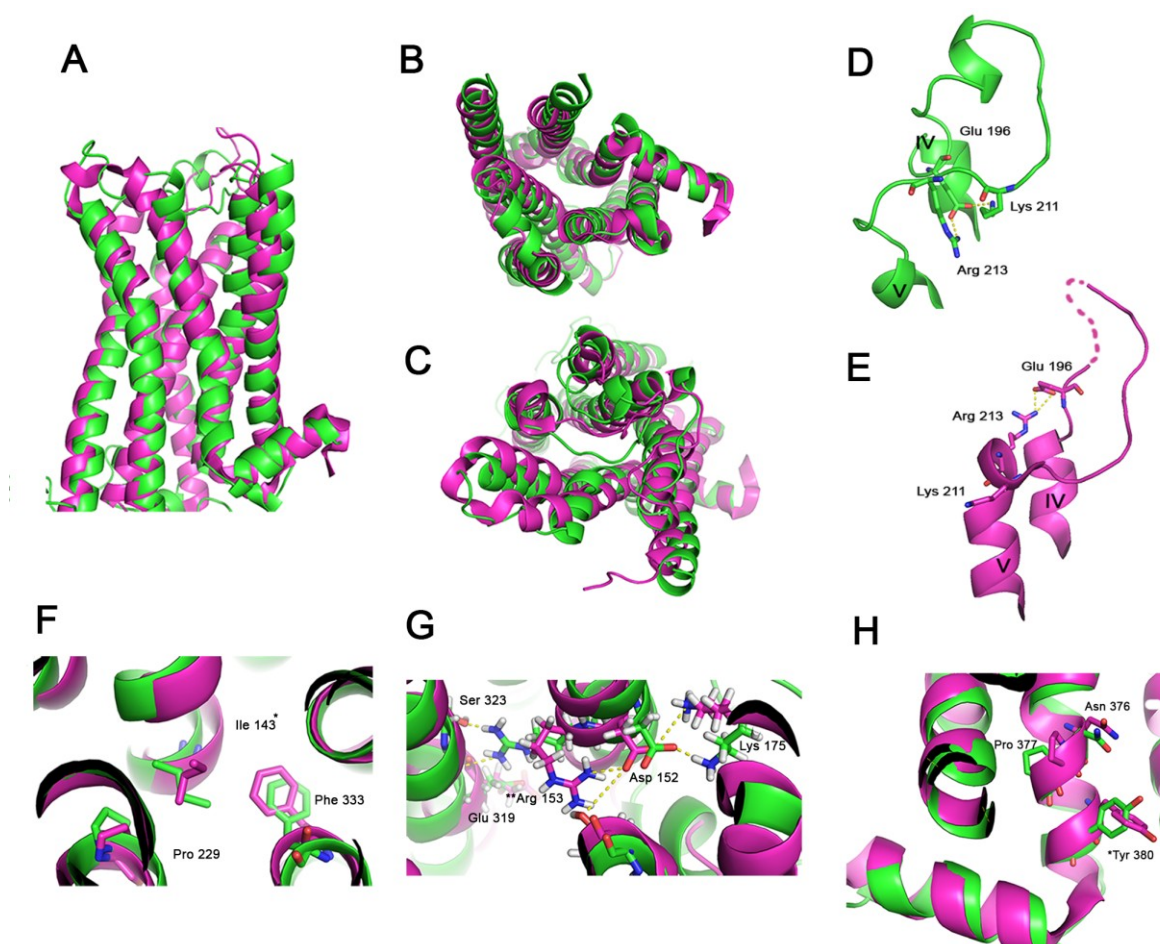
Figure 5. Binding mode of cabergoline. (A) Cabergoline docked into D₃R; (B) pose of cabergoline into 5HT$_{2A}$ receptor; (C) pose of cabergoline into 5HT$_{2C}$; (D) cabergoline docked into simulated 5HT$_{2B}$ receptor; (E) experimental binding mode of ergotamine in the binding pocket of 5HT$_{2B}$ receptor; (F) binding mode of cabergoline into the binding pocket of 5HT$_{1A}$ receptor.

DISCUSSION AND CONCLUSIONS

Looking at perspective pharmacological treatments for lowering IOP in glaucoma, there are seven GPCRs characterizing themselves as pharmacological targets: melatonin, cannabinoid, prostaglandin, adenosine, serotonergic and dopaminergic receptors. It was previously stated that GPCRs are important pharmacological targets and R&D of drugs targeting such receptors is challenging.

Human genome encode for about 800 GPCRs, which are not fully characterized in terms of function and potential GPCRs/disease combination. Although a GPCRs/disease combination could be reliable, lack of structural information is a hindrance to development of useful drugs. Even in case of divergent function, different families of GPCRs may share high sequence homology and identity, especially at binding pockets or even in binding moieties of ligands [91]; these issues make the development of selective drugs toward homologous receptors very difficult.

In the last decade an improvement in the crystallization methods of GPCRs has led to an enrichment of structural information, leading to a better understanding of issues such as: orthosteric and allosteric moieties of ligands, molecular features of active and inactive states of GPCRs and the novel perspective of biased agonism. Improvement in crystallization techniques along with computational approaches is going to pursue information useful for the R&D of drugs. Researchers will be able to exploit structural information for development of drugs with either selective or multi-pharmacological profiles and to predict set of adverse events of NCE [96]. Moreover structural information of GPCRs, either structural models and x-ray structures, could be used for repositioning of shelved drugs or de-orphanization of receptors.

Computational studies on GPCRs may involve structural modeling, and in the present thesis it has been demonstrated that molecular dynamics simulations have been useful to optimize aminergic GPCRs, leading to a set of validated structures of receptors: D_{2L}, D_3, $5HT_{1A}$, $5HT_{2A}$, $5HT_{2B}$, $5HT_{2C}$. Those optimized receptors have been successful for discrimination of selective compounds, see D_{2L} and D_3 optimized receptors (Chapter I). The main differences, between the simulations reported in chapter I carried out in 2012 and the simulations of Michino et. al. in 2013 [123], are about the dimensions of binding pockets of D_2 and D_3 receptors. In the present work of thesis it is reported a bigger and non fully compartmentalized binding pocket of D_2R in comparison to D_3R. The reason of this difference could be related to the unbound state of receptors simulated in chapter I; thus

further studies could be carried out to evaluate the role of allosteric binding site in D_2-like receptors in the unbound state, looking in example to energy of water network as reported by Michino et al. [123].

The receptor structure models reported in chapter II, optimized with MD in membrane-water environment, have been successful in the explication of binding of cabergoline, a mixed dopaminergic-serotonergic agonist with ocular hypotensive effect related to selective activation of D_3 receptor. D_3 and $5HT_{1A}$ receptors show experimental and predicted high affinity for cabergoline due to better desolvation energy of complexes in comparison to $5HT_{2A-C}$ receptors; however $5HT_{1A}$ has not been reported to have a leading role in IOP regulation [51]. In chapter II the described *in silico* studies, D_3 agonism (by cabergoline) and pharmacological blockade (by U99194A) along with D_3 gene deletion (by $D_3R^{-/-}$ mice), have confirmed the following:

- cabergoline elicited ocular hypotensive effect by means of D_3 receptor activation, at least in the glaucoma model hereby used. Moreover, the stimulation of $5HT_{2A}$ receptor does not seem to have a role on lowering IOP in mice, in contrast to the study of Sharif and coworkers [51];

- D_3 receptor when activated by different agonists, 7-OH-DPAT [55, 56] and cabergoline [91], plays a key role in lowering IOP;

- since the role of serotonergic system in regulation of IOP in comparison to dopaminergic system is still evanescent, further studies should be carried out in order to develop new ocular hypotensive drugs with high selectivity or multi-pharmacological profile.

In addition the ensemble of optimized receptor models hereby described could be exploited to study multi-pharmacological profiles not only of ocular hypotensive drugs, but also to investigate drugs for treatment of neurological and psychiatric diseases.

In consideration of pharmacological potential of biased signal of D_2-like receptors, further perspective structural studies could be carried out in order to reply to these questions:

- which are the conformational transitions induced by sensitizing (7-OH-DPAT) and no-sensitizing ligands (cis-8-OH-PBZI [130])?

- how these structural transitions influence the availability of binding pocket of hydrophilic agonists?

- how these structural changes are transmitted to molecular effectors such as $G\beta\gamma$ and β-arrestin?

Current pharmacological treatment of glaucoma, due to chronic therapy, is often characterized by sensitization and tolerance leading non-responder patients to surgical options; thus the potential to develop non-sensitizing D_3 receptor agonists is the starting point for a new scenario in R&D of hypotensive ocular drugs.

REFERENCES

[1]   King A, Azuara-Blanco A, Tuulonen A. Glaucoma. Bmj 2013;346:f3518.

[2]   Quigley HA. Open-angle glaucoma. N Engl J Med 1993;328:1097-106.

[3]   Fan BJ, Wang DY, Lam DS, Pang CP. Gene mapping for primary open angle glaucoma. Clin Biochem 2006;39:249-58.

[4]   The effectiveness of intraocular pressure reduction in the treatment of normal-tension glaucoma. Collaborative Normal-Tension Glaucoma Study Group. Am J Ophthalmol 1998;126:498-505.

[5]   Goel M, Picciani RG, Lee RK, Bhattacharya SK. Aqueous humor dynamics: a review. Open Ophthalmol J 2010;4:52-9.

[6]   Nemesure B, Honkanen R, Hennis A, Wu SY, Leske MC. Incident open-angle glaucoma and intraocular pressure. Ophthalmology 2007;114:1810-5.

[7]   Yamaguchi Y, Watanabe T, Hirakata A, Hida T. Localization and ontogeny of aquaporin-1 and -4 expression in iris and ciliary epithelial cells in rats. Cell Tissue Res 2006;325:101-9.

[8]   Krupin T, Becker B, Podos SM. Topical vanadate lowers intraocular pressure in rabbits. Invest Ophthalmol Vis Sci 1980;19:1360-63.

[9]   Maren TH. The rates of movement of Na+, Cl-, and HCO-3 from plasma to posterior chamber: effect of acetazolamide and relation to the treatment of glaucoma. Invest Ophthalmol 1976;15:356-64.

[10]   Bill A, Svedbergh B. Scanning electron microscopic studies of the trabecular meshwork and the canal of Schlemm--an attempt to localize the main resistance to outflow of aqueous humor in man. Acta Ophthalmol 1972;50:295-320.

[11]   Ethier CR, Kamm RD, Palaszewski BA, Johnson MC, Richardson TM. Calculations of flow resistance in the juxtacanalicular meshwork. Invest Ophthalmol Vis Sci 1986;27:1741-50.

[12]   Francois J. Corticosteroid glaucoma. Ann Ophthalmol 1977;9:1075-80.

[13]   Johnson DH, Bradley JM, Acott TS. The effect of dexamethasone on glycosaminoglycans of human trabecular meshwork in perfusion organ culture. Invest Ophthalmol Vis Sci 1990;31:2568-71.

[14]   Barany EH. The mode of action of miotics on outflow resistance. A study of pilocarpine in the vervet monkey Cercopithecus ethiops. Trans Ophthalmol Soc U K 1966;86:539-78.

[15]   Gabelt BT, Kaufman PL. Changes in aqueous humor dynamics with age and glaucoma. Prog Retin Eye Res 2005;24:612-37.

[16]   Toris CB, Yablonski ME, Wang YL, Camras CB. Aqueous humor dynamics in the aging human eye. Am J Ophthalmol 1999;127:407-12.

[17]   Gabelt BT, Kaufman PL. Prostaglandin F2 alpha increases uveoscleral outflow in the cynomolgus monkey. Exp Eye Res 1989;49:389-402.

[18]   Bucolo C, Salomone S, Drago F, Reibaldi M, Longo A, Uva MG. Pharmacological management of ocular hypertension: current approaches and future prospective. Curr Opin Pharmacol 2013;13:50-5.

[19]   Pfeiffer N. Dorzolamide: development and clinical application of a topical carbonic anhydrase inhibitor. Surv Ophthalmol 1997;42:137-51.

[20]   Arthur S, Cantor LB. Update on the role of alpha-agonists in glaucoma management. Exp Eye Res 2011;93:271-83.

[21] Yucel YH, Gupta N, Zhang Q, Mizisin AP, Kalichman MW, Weinreb RN. Memantine protects neurons from shrinkage in the lateral geniculate nucleus in experimental glaucoma. Arch Ophthalmol 2006;124:217-25.

[22] Fang JH, Wang XH, Xu ZR, Jiang FG. Neuroprotective effects of bis(7)-tacrine against glutamate-induced retinal ganglion cells damage. BMC Neurosci 2010;11:31.

[23] Osborne NN. Recent clinical findings with memantine should not mean that the idea of neuroprotection in glaucoma is abandoned. Acta Ophthalmol 2009;87:450-4.

[24] Russo R, Berliocchi L, Adornetto A, Amantea D, Nucci C, Tassorelli C, et al. In search of new targets for retinal neuroprotection: is there a role for autophagy? Curr Opin Pharmacol 2013;13:72-7.

[25] Borras T. Advances in glaucoma treatment and management: gene therapy. Invest Ophthalmol Vis Sci 2012;53:2506-10.

[26] Crooke A, Colligris B, Pintor J. Update in glaucoma medicinal chemistry: emerging evidence for the importance of melatonin analogues. Curr Med Chem 2012;19:3508-22.

[27] Musumeci T, Bucolo C, Carbone C, Pignatello R, Drago F, Puglisi G. Polymeric nanoparticles augment the ocular hypotensive effect of melatonin in rabbits. Int J Pharm 2013;440:135-40.

[28] Alcantara-Contreras S, Baba K, Tosini G. Removal of melatonin receptor type 1 increases intraocular pressure and retinal ganglion cells death in the mouse. Neurosci Lett 2011;494:61-4.

[29] Rauz S, Cheung CM, Wood PJ, Coca-Prados M, Walker EA, Murray PI, et al. Inhibition of 11beta-hydroxysteroid dehydrogenase type 1 lowers intraocular pressure in patients with ocular hypertension. Qjm 2003;96:481-90.

[30] Anderson S, Carreiro S, Quenzer T, Gale D, Xiang C, Gukasyan H, et al. In vivo evaluation of 11beta-hydroxysteroid dehydrogenase activity in the rabbit eye. J Ocul Pharmacol Ther 2009;25:215-22.

[31] Last JA, Pan T, Ding Y, Reilly CM, Keller K, Acott TS, et al. Elastic modulus determination of normal and glaucomatous human trabecular meshwork. Invest Ophthalmol Vis Sci 2011;52:2147-52.

[32] Sugiyama T, Shibata M, Kajiura S, Okuno T, Tonari M, Oku H, et al. Effects of fasudil, a Rho-associated protein kinase inhibitor, on optic nerve head blood flow in rabbits. Invest Ophthalmol Vis Sci 2011;52:64-9.

[33] Drago F, Bucolo C. Therapeutic potential of nitric oxide modulation in ocular diseases. Drug News Perspect 2010;23:430-7.

[34] Bucolo C, Drago F. Carbon monoxide and the eye: Implications for glaucoma therapy. Pharmacol Ther 2011;130:191-201.

[35] Kotikoski H, Vapaatalo H, Oksala O. Nitric oxide and cyclic GMP enhance aqueous humor outflow facility in rabbits. Curr Eye Res 2003;26:119-23.

[36] Giuffrida S, Bucolo C, Drago F. Topical application of a nitric oxide synthase inhibitor reduces intraocular pressure in rabbits with experimental glaucoma. J Ocul Pharmacol Ther 2003;19:527-34.

[37] Zamora DO, Kiel JW. Episcleral venous pressure responses to topical nitroprusside and N-Nitro-L-arginine methyl ester. Invest Ophthalmol Vis Sci 2010;51:1614-20.

[38] Krauss AH, Impagnatiello F, Toris CB, Gale DC, Prasanna G, Borghi V, et al. Ocular hypotensive activity of BOL-303259-X, a nitric oxide donating prostaglandin F2alpha agonist, in preclinical models. Exp Eye Res 2011;93:250-5.

[39] Privitera MG, Potenza M, Bucolo C, Leggio GM, Drago F. Hemin, an inducer of heme oxygenase-1, lowers intraocular pressure in rabbits. J Ocul Pharmacol Ther 2007;23:232-9.

[40] Kaufman PL, Rasmussen CA. Advances in glaucoma treatment and management: outflow drugs. Invest Ophthalmol Vis Sci 2012;53:2495-500.

[41] Crosson CE, Sloan CF, Yates PW. Modulation of conventional outflow facility by the adenosine A1 agonist N6-cyclohexyladenosine. Invest Ophthalmol Vis Sci 2005;46:3795-9.

[42] Li A, Banerjee J, Leung CT, Peterson-Yantorno K, Stamer WD, Civan MM. Mechanisms of ATP release, the enabling step in purinergic dynamics. Cell Physiol Biochem 2011;28:1135-44.

[43] Wang Z, Do CW, Avila MY, Peterson-Yantorno K, Stone RA, Gao ZG, et al. Nucleoside-derived antagonists to A3 adenosine receptors lower mouse intraocular pressure and act across species. Exp Eye Res 2010;90:146-54.

[44] Wan Z, Woodward DF, Stamer WD. Endogenous Bioactive Lipids and the Regulation of Conventional Outflow Facility. Expert Rev Ophthalmol 2008;3:457-70.

[45] Njie YF, Kumar A, Qiao Z, Zhong L, Song ZH. Noladin ether acts on trabecular meshwork cannabinoid (CB1) receptors to enhance aqueous humor outflow facility. Invest Ophthalmol Vis Sci 2006;47:1999-2005.

[46] Kumar A, Song ZH. CB1 cannabinoid receptor-mediated changes of trabecular meshwork cellular properties. Mol Vis 2006;12:290-7.

[47] Oltmanns MH, Samudre SS, Castillo IG, Hosseini A, Lichtman AH, Allen RC, et al. Topical WIN55212-2 alleviates intraocular hypertension in rats through a CB1 receptor mediated mechanism of action. J Ocul Pharmacol Ther 2008;24:104-15.

[48] Gagliano C, Ortisi E, Pulvirenti L, Reibaldi M, Scollo D, Amato R, et al. Ocular hypotensive effect of oral palmitoyl-ethanolamide: a clinical trial. Invest Ophthalmol Vis Sci 2011;52:6096-100.

[49] Kumar A, Qiao Z, Kumar P, Song ZH. Effects of palmitoylethanolamide on aqueous humor outflow. Invest Ophthalmol Vis Sci 2012;53:4416-25.

[50] Sharif NA, Senchyna M. Serotonin receptor subtype mRNA expression in human ocular tissues, determined by RT-PCR. Mol Vis 2006;12:1040-7.

[51] Sharif NA, McLaughlin MA, Kelly CR, Katoli P, Drace C, Husain S, et al. Cabergoline: Pharmacology, ocular hypotensive studies in multiple species, and aqueous humor dynamic modulation in the Cynomolgus monkey eyes. Exp Eye Res 2009;88:386-97.

[52] Sharif NA. Serotonin-2 receptor agonists as novel ocular hypotensive agents and their cellular and molecular mechanisms of action. Curr Drug Targets 2010;11:978-93.

[53] Tekat D, Guler C, Arici M, Topalkara A, Erdogan H. Effect of ketanserin administration on intraocular pressure. Ophthalmologica 2001;215:419-23.

[54] Chen J, Runyan SA, Robinson MR. Novel ocular antihypertensive compounds in clinical trials. Clin Ophthalmol 2011;5:667-77.

[55] Chu E, Chu TC, Potter DE. Mechanisms and sites of ocular action of 7-hydroxy-2-dipropylaminotetralin: a dopamine(3) receptor agonist. J Pharmacol Exp Ther 2000;293:710-6.

[56] Bucolo C, Leggio GM, Maltese A, Castorina A, D'Agata V, Drago F. Dopamine-(3) receptor modulates intraocular pressure: implications for glaucoma. Biochem Pharmacol 2012;83:680-6.

[57] Bouhenni RA, Dunmire J, Sewell A, Edward DP. Animal models of glaucoma. J Biomed Biotechnol 2012;2012:692609.

[58]   Gelatt KN. Animal models for glaucoma. Invest Ophthalmol Vis Sci 1977;16:592-6.

[59]   Vecino E. [Animal models in the study of the glaucoma: past, present and future]. Arch Soc Esp Oftalmol 2008;83:517-9.

[60]   Pang IH, Clark AF. Rodent models for glaucoma retinopathy and optic neuropathy. J Glaucoma 2007;16:483-505.

[61]   Clark AF, Wordinger RJ. The role of steroids in outflow resistance. Exp Eye Res 2009;88:752-9.

[62]   Kersey JP, McMullan TF, Broadway DC. Pupil block glaucoma after neodymium:YAG capsulotomy in a patient with a partially subluxated posterior chamber intraocular lens. J Cataract Refract Surg 2005;31:1452-3.

[63]   Fingert JH, Stone EM, Sheffield VC, Alward WL. Myocilin glaucoma. Surv Ophthalmol 2002;47:547-61.

[64]   Sawaguchi K, Nakamura Y, Sakai H, Sawaguchi S. Myocilin gene expression in the trabecular meshwork of rats in a steroid-induced ocular hypertension model. Ophthalmic Res 2005;37:235-42.

[65]   Daimon T, Kazama M, Miyajima Y, Nakano M. Immunocytochemical localization of thrombomodulin in the aqueous humor passage of the rat eye. Histochem Cell Biol 1997;108:121-31.

[66]   Reme C, Urner U, Aeberhard B. The development of the chamber angle in the rat eye. Morphological characteristics of developmental stages. Graefes Arch Clin Exp Ophthalmol 1983;220:139-53.

[67]   Nucci P, Tredici G, Manitto MP, Pizzini G, Brancato R. Neuron-specific enolase and embryology of the trabecular meshwork of the rat eye: an immunohistochemical study. Int J Biol Markers 1992;7:253-5.

[68]   Pang IH, Wang WH, Clark AF. Acute effects of glaucoma medications on rat intraocular pressure. Exp Eye Res 2005;80:207-14.

[69]   Senatorov V, Malyukova I, Fariss R, Wawrousek EF, Swaminathan S, Sharan SK, et al. Expression of mutated mouse myocilin induces open-angle glaucoma in transgenic mice. J Neurosci 2006;26:11903-14.

[70]   Zhou Y, Grinchuk O, Tomarev SI. Transgenic mice expressing the Tyr437His mutant of human myocilin protein develop glaucoma. Invest Ophthalmol Vis Sci 2008;49:1932-9.

[71]   Mabuchi F, Lindsey JD, Aihara M, Mackey MR, Weinreb RN. Optic nerve damage in mice with a targeted type I collagen mutation. Invest Ophthalmol Vis Sci 2004;45:1841-5.

[72]   Aihara M, Lindsey JD, Weinreb RN. Ocular hypertension in mice with a targeted type I collagen mutation. Invest Ophthalmol Vis Sci 2003;44:1581-5.

[73]   Whitlock NA, McKnight B, Corcoran KN, Rodriguez LA, Rice DS. Increased intraocular pressure in mice treated with dexamethasone. Invest Ophthalmol Vis Sci 2010;51:6496-503.

[74]   Fredriksson R, Lagerstrom MC, Lundin LG, Schioth HB. The G-protein-coupled receptors in the human genome form five main families. Phylogenetic analysis, paralogon groups, and fingerprints. Mol Pharmacol 2003;63:1256-72.

[75]   Drews J. Drug discovery: a historical perspective. Science 2000;287:1960-4.

[76]   Wise A, Gearing K, Rees S. Target validation of G-protein coupled receptors. Drug Discov Today 2002;7:235-46.

[77]   Ma P, Zemmel R. Value of novelty? Nat Rev Drug Discov 2002;1:571-2.

[78]   Overington JP, Al-Lazikani B, Hopkins AL. How many drug targets are there? Nat Rev Drug Discov 2006;5:993-6.

[79]   Garland SL. Are GPCRs still a source of new targets? J Biomol Screen 2013;18:947-66.

[80]   DeWire SM, Ahn S, Lefkowitz RJ, Shenoy SK. Beta-arrestins and cell signaling. Annu Rev Physiol 2007;69:483-510.

[81]   Luttrell LM, Gesty-Palmer D. Beyond desensitization: physiological relevance of arrestin-dependent signaling. Pharmacol Rev 2010;62:305-30.

[82]   Schmid CL, Bohn LM. Physiological and pharmacological implications of beta-arrestin regulation. Pharmacol Ther 2009;121:285-93.

[83]   Whalen EJ, Rajagopal S, Lefkowitz RJ. Therapeutic potential of beta-arrestin- and G protein-biased agonists. Trends Mol Med 2011;17:126-39.

[84]   Wacker D, Wang C, Katritch V, Han GW, Huang XP, Vardy E, et al. Structural features for functional selectivity at serotonin receptors. Science 2013;340:615-9.

[85]   Venkatakrishnan AJ, Deupi X, Lebon G, Tate CG, Schertler GF, Babu MM. Molecular signatures of G-protein-coupled receptors. Nature 2013;494:185-94.

[86]   Rasmussen SG, DeVree BT, Zou Y, Kruse AC, Chung KY, Kobilka TS, et al. Crystal structure of the beta2 adrenergic receptor-Gs protein complex. Nature 2011;477:549-55.

[87]   Dror RO, Pan AC, Arlow DH, Borhani DW, Maragakis P, Shan Y, et al. Pathway and mechanism of drug binding to G-protein-coupled receptors. Proc Natl Acad Sci U S A 2011;108:13118-23.

[88]   Manglik A, Kruse AC, Kobilka TS, Thian FS, Mathiesen JM, Sunahara RK, et al. Crystal structure of the micro-opioid receptor bound to a morphinan antagonist. Nature 2012;485:321-6.

[89]   Tarnow P, Schoneberg T, Krude H, Gruters A, Biebermann H. Mutationally induced disulfide bond formation within the third extracellular loop causes melanocortin 4 receptor inactivation in patients with obesity. J Biol Chem 2003;278:48666-73.

[90]   Platania CB, Salomone S, Leggio GM, Drago F, Bucolo C. Homology modeling of dopamine D2 and D3 receptors: molecular dynamics refinement and docking evaluation. PLoS One 2012;7:e44316.

[91]   Platania CB, Leggio GM, Drago F, Salomone S, Bucolo C. Regulation of intraocular pressure in mice: Structural analysis of dopaminergic and serotonergic systems in response to cabergoline. Biochem Pharmacol 2013;86:1347-56.

[92]   Thompson AA, Liu W, Chun E, Katritch V, Wu H, Vardy E, et al. Structure of the nociceptin/orphanin FQ receptor in complex with a peptide mimetic. Nature 2012;485:395-9.

[93]   Warne T, Serrano-Vega MJ, Baker JG, Moukhametzianov R, Edwards PC, Henderson R, et al. Structure of a beta1-adrenergic G-protein-coupled receptor. Nature 2008;454:486-91.

[94]   Valiquette M, Parent S, Loisel TP, Bouvier M. Mutation of tyrosine-141 inhibits insulin-promoted tyrosine phosphorylation and increased responsiveness of the human beta 2-adrenergic receptor. Embo J 1995;14:5542-9.

[95]   Carlsson J, Coleman RG, Setola V, Irwin JJ, Fan H, Schlessinger A, et al. Ligand discovery from a dopamine D3 receptor homology model and crystal structure. Nat Chem Biol 2011;7:769-78.

[96]   Ichikawa O, Okazaki K, Nakahira H, Maruyama M, Nagata R, Tokuda K, et al. Structural insight into receptor-selectivity for lurasidone. Neurochem Int 2012;61:1133-43.

[97]   Marti-Renom MA, Stuart AC, Fiser A, Sanchez R, Melo F, Sali A. Comparative protein structure modeling of genes and genomes. Annu Rev Biophys Biomol Struct 2000;29:291-325.

[98]   Eswar N, Webb B, Marti-Renom MA, Madhusudhan MS, Eramian D, Shen MY, et al. Comparative protein structure modeling using Modeller. Curr Protoc Bioinformatics 2006;Chapter 5:Unit 5 6.

[99]   Arnold K, Bordoli L, Kopp J, Schwede T. The SWISS-MODEL workspace: a web-based environment for protein structure homology modelling. Bioinformatics 2006;22:195-201.

[100] Xu J, Li M, Kim D, Xu Y. RAPTOR: optimal protein threading by linear programming. J Bioinform Comput Biol 2003;1:95-117.

[101] Soding J, Biegert A, Lupas AN. The HHpred interactive server for protein homology detection and structure prediction. Nucleic Acids Res 2005;33:W244-8.

[102] Zhang Y. I-TASSER server for protein 3D structure prediction. BMC Bioinformatics 2008;9:40.

[103] Zhang J, Zhang Y. GPCRRD: G protein-coupled receptor spatial restraint database for 3D structure modeling and function annotation. Bioinformatics 2010;26:3004-5.

[104] Brooks BR, Bruccoleri RE, Olafson BD, States DJ, Swaminathan S, Karplus M. CHARMM: A Program for Macromolecular Energy, Minimization, and Dynamics Calculations. J Comput Chem 1983;4:187-217.

[105] Pannuzzo M, Raudino A, Milardi D, La Rosa C, Karttunen M. alpha-helical structures drive early stages of self-assembly of amyloidogenic amyloid polypeptide aggregate formation in membranes. Sci Rep 2013;3:2781.

[106] Nygaard R, Zou Y, Dror RO, Mildorf TJ, Arlow DH, Manglik A, et al. The dynamic process of beta(2)-adrenergic receptor activation. Cell 2013;152:532-42.

[107] Dror RO, Green HF, Valant C, Borhani DW, Valcourt JR, Pan AC, et al. Structural basis for modulation of a G-protein-coupled receptor by allosteric drugs. Nature 2013;503:295-9.

[108] Shaw DE, Maragakis P, Lindorff-Larsen K, Piana S, Dror RO, Eastwood MP, et al. Atomic-level characterization of the structural dynamics of proteins. Science 2010;330:341-6.

[109] Rajamani R, Good AC. Ranking poses in structure-based lead discovery and optimization: current trends in scoring function development. Curr Opin Drug Discov Devel 2007;10:308-15.

[110] Graves AP, Shivakumar DM, Boyce SE, Jacobson MP, Case DA, Shoichet BK. Rescoring docking hit lists for model cavity sites: predictions and experimental testing. J Mol Biol 2008;377:914-34.

[111] Suenaga A, Okimoto N, Hirano Y, Fukui K. An efficient computational method for calculating ligand binding affinities. PLoS One 2012;7:e42846.

[112] Vilar S, Karpiak J, Costanzi S. Ligand and structure-based models for the prediction of ligand-receptor affinities and virtual screenings: Development and application to the beta(2)-adrenergic receptor. J Comput Chem 2010;31:707-20.

[113] Varady J, Wu X, Fang X, Min J, Hu Z, Levant B, et al. Molecular modeling of the three-dimensional structure of dopamine 3 (D3) subtype receptor: discovery of novel and potent D3 ligands through a hybrid pharmacophore- and structure-based database searching approach. J Med Chem 2003;46:4377-92.

[114] Newman AH, Grundt P, Nader MA. Dopamine D3 receptor partial agonists and antagonists as potential drug abuse therapeutic agents. J Med Chem 2005;48:3663-79.

[115] Boeckler F, Lanig H, Gmeiner P. Modeling the similarity and divergence of dopamine D2-like receptors and identification of validated ligand-receptor complexes. J Med Chem 2005;48:694-709.

[116] Ghosh B, Antonio T, Zhen J, Kharkar P, Reith ME, Dutta AK. Development of (S)-N6-(2-(4-(isoquinolin-1-yl)piperazin-1-yl)ethyl)-N6-propyl-4,5,6,7-tetrahydro

benzo[d]-thiazole-2,6-diamine and its analogue as a D3 receptor preferring agonist: potent in vivo activity in Parkinson's disease animal models. J Med Chem 2010;53:1023-37.

[117] Wang Q, Mach RH, Luedtke RR, Reichert DE. Subtype selectivity of dopamine receptor ligands: insights from structure and ligand-based methods. J Chem Inf Model 2010;50:1970-85.

[118] Tschammer N, Elsner J, Goetz A, Ehrlich K, Schuster S, Ruberg M, et al. Highly potent 5-aminotetrahydropyrazolopyridines: enantioselective dopamine D3 receptor binding, functional selectivity, and analysis of receptor-ligand interactions. J Med Chem 2011;54:2477-91.

[119] Li B, Li W, Du P, Yu KQ, Fu W. Molecular insights into the D1R agonist and D2R/D3R antagonist effects of the natural product (-)-stepholidine: molecular modeling and dynamics simulations. J Phys Chem B 2012;116:8121-30.

[120] Abdelfattah MA, Lehmann J, Abadi AH. Discovery of highly potent and selective D4 ligands by interactive SAR study. Bioorg Med Chem Lett 2013;23:5077-81.

[121] McRobb FM, Capuano B, Crosby IT, Chalmers DK, Yuriev E. Homology modeling and docking evaluation of aminergic G protein-coupled receptors. J Chem Inf Model 2010;50:626-37.

[122] Chien EY, Liu W, Zhao Q, Katritch V, Han GW, Hanson MA, et al. Structure of the human dopamine D3 receptor in complex with a D2/D3 selective antagonist. Science 2010;330:1091-5.

[123] Michino M, Donthamsetti P, Beuming T, Banala A, Duan L, Roux T, et al. A single glycine in extracellular loop 1 is the critical determinant for pharmacological specificity of dopamine d2 and d3 receptors. Mol Pharmacol 2013;84:854-64.

[124] Breiten B, Lockett MR, Sherman W, Fujita S, Al-Sayah M, Lange H, et al. Water networks contribute to enthalpy/entropy compensation in protein-ligand binding. J Am Chem Soc 2013;135:15579-84.

[125] Kongsamut S, Roehr JE, Cai J, Hartman HB, Weissensee P, Kerman LL, et al. Iloperidone binding to human and rat dopamine and 5-HT receptors. Eur J Pharmacol 1996;317:417-23.

[126] Hedberg MH, Linnanen T, Jansen JM, Nordvall G, Hjorth S, Unelius L, et al. 11-substituted (R)-aporphines: synthesis, pharmacology, and modeling of D2A and 5-HT1A receptor interactions. J Med Chem 1996;39:3503-13.

[127] Yap BK, Buckle MJ, Doughty SW. Homology modeling of the human 5-HT1A, 5-HT 2A, D1, and D2 receptors: model refinement with molecular dynamics simulations and docking evaluation. J Mol Model 2012;18:3639-55.

[128] Min C, Zheng M, Zhang X, Caron MG, Kim KM. Novel roles for beta-arrestins in the regulation of pharmacological sequestration to predict agonist-induced desensitization of dopamine D3 receptors. Br J Pharmacol 2013;170:1112-29.

[129] Millan MJ, Maiofiss L, Cussac D, Audinot V, Boutin JA, Newman-Tancredi A. Differential actions of antiparkinson agents at multiple classes of monoaminergic receptor. I. A multivariate analysis of the binding profiles of 14 drugs at 21 native and cloned human receptor subtypes. J Pharmacol Exp Ther 2002;303:791-804.

[130] Kuzhikandathil EV, Kortagere S. Identification and characterization of a novel class of atypical dopamine receptor agonists. Pharm Res 2012;29:2264-75.

LIST OF PUBLICATIONS AND SCIENTIFIC CONTRIBUTIONS

Publications

- PLoS One. 2012;7(9):e44316. doi: 10.1371/journal.pone.0044316. Epub 2012 Sep 6. *Homology modeling of dopamine D2 and D3 receptors: molecular dynamics refinement and docking evaluation.* Platania CB, Salomone S, Leggio GM, Drago F, Bucolo C.

- J Diabetes Res. 2013;2013:432695. doi: 10.1155/2013/432695. Epub 2013 May 23. *Fortified extract of red berry, Ginkgo biloba, and white willow bark in experimental early diabetic retinopathy.* Bucolo C, Marrazzo G, Platania CB, Drago F, Leggio GM, Salomone S.

- Eur J Pharmacol. 2013 Nov 5;719(1-3):25-33. doi: 10.1016/j.ejphar.2013.07.022. Epub 2013 Jul 18. *Dopamine D3 receptor as a new pharmacological target for the treatment of depression.* Leggio GM, Salomone S, Bucolo C, Platania C, Micale V, Caraci F, Drago F.

- Biochem Pharmacol. 2013 Nov 1;86(9):1347-56. doi: 10.1016/j.bcp.2013.08.010. Epub 2013 Aug 17. *Regulation of intraocular pressure in mice: structural analysis of dopaminergic and serotonergic systems in response to cabergoline.* Platania CB, Leggio GM, Drago F, Salomone S, Bucolo C.

Conference procedeedings

- Poster: "*Regulation of intraocular pressure: structural analysis of dopaminergic and serotonergic systems*". C.B.M. Platania, G.M. Leggio, F. Drago, S. Salomone, C. Bucolo. 36th Congresso Nazionale SIF 2013, Torino.

- Poster: "*Cabergoline and IOP: implications for structure-based drug discovery of selective dopaminergic ligands*". F. Drago, C.B.M. Platania, G. Marrazzo, G.M. Leggio, C. Bucolo. ARVO annual Meeting May 2013. Seattle, USA.